National Library of Canada
Bibliothèque nationale du Canada

Canadian Theses Service
Service des thèses canadiennes

Ottawa, Canada
K1A 0N4

NOTICE

The quality of this microform is heavily dependent upon the quality of the original thesis submitted for microfilming. Every effort has been made to ensure the highest quality of reproduction possible.

If pages are missing, contact the university which granted the degree.

Some pages may have indistinct print especially if the original pages were typed with a poor typewriter ribbon or if the university sent us an inferior photocopy.

Reproduction in full or in part of this microform is governed by the Canadian Copyright Act, R.S.C. 1970, c. C-30, and subsequent amendments.

AVIS

La qualité de cette microforme dépend grandement de la qualité de la thèse soumise au microfilmage. Nous avons tout fait pour assurer une qualité supérieure de reproduction.

S'il manque des pages, veuillez communiquer avec l'université qui a conféré le grade.

La qualité d'impression de certaines pages peut laisser à désirer, surtout si les pages originales ont été dactylographiées à l'aide d'un ruban usé ou si l'université nous a fait parvenir une photocopie de qualité inférieure.

La reproduction, même partielle, de cette microforme est soumise à la Loi canadienne sur le droit d'auteur, SRC 1970, c. C-30, et ses amendements subséquents.

NL-339 (r. 88/04) c

Canada

THE UNIVERSITY OF ALBERTA

OPTICAL TIME-OF-FLIGHT MULTIPLEXING

by

KEVIN JACOBSON

A THESIS

SUBMITTED TO THE FACULTY OF GRADUATE STUDIES AND RESEARCH

IN PARTIAL FULFILLMENT OF THE REQUIREMENTS FOR THE DEGREE OF

MASTER OF SCIENCE

DEPARTMENT OF ELECTRICAL ENGINEERING

EDMONTON, ALBERTA

SPRING 1990

National Library of Canada
Bibliothèque nationale du Canada

Canadian Theses Service
Service des thèses canadiennes

Ottawa, Canada
K1A 0N4

NOTICE

The quality of this microform is heavily dependent upon the quality of the original thesis submitted for microfilming. Every effort has been made to ensure the highest quality of reproduction possible.

If pages are missing, contact the university which granted the degree.

Some pages may have indistinct print especially if the original pages were typed with a poor typewriter ribbon or if the university sent us an inferior photocopy.

Reproduction in full or in part of this microform is governed by the Canadian Copyright Act, R.S.C. 1970, c. C-30, and subsequent amendments.

AVIS

La qualité de cette microforme dépend grandement de la qualité de la thèse soumise au microfilmage. Nous avons tout fait pour assurer une qualité supérieure de reproduction.

S'il manque des pages, veuillez communiquer avec l'université qui a conféré le grade.

La qualité d'impression de certaines pages peut laisser à désirer, surtout si les pages originales ont été dactylographiées à l'aide d'un ruban usé ou si l'université nous a fait parvenir une photocopie de qualité inférieure.

La reproduction, même partielle, de cette microforme est soumise à la Loi canadienne sur le droit d'auteur, SRC 1970, c. C-30, et ses amendements subséquents.

ISBN 0-315-60289-9

NL-339 (r. 88/04) c

Canada

THE UNIVERSITY OF ALBERTA

RELEASE FORM

NAME OF AUTHOR: KEVIN JACOBSON

TITLE OF THESIS: OPTICAL TIME-OF-FLIGHT MULTIPLEXING

DEGREE: MASTER OF SCIENCE

YEAR THIS DEGREE GRANTED: 1990

Permission is hereby granted to THE UNIVERSITY OF ALBERTA LIBRARY to reproduce single copies of this thesis and to lend or sell such copies for private, scholarly, or scientific research purposes only.

The author reserves other publication rights, and neither the thesis nor extensive extracts from it may be printed or otherwise reproduced without the author's written permission.

(SIGNED) Kevin Jacobson

PERMANENT ADDRESS:

158 PARKVILLE DRIVE

WINNIPEG, MANITOBA

CANADA, R2M 2J1

Date: October 27, 1989

THE UNIVERSITY OF ALBERTA

FACULTY OF GRADUATE STUDIES AND RESEARCH

The undersigned certify that they have read, and recommend to the Faculty of Graduate Studies and Research for acceptance, a thesis entitled OPTICAL TIME-OF-FLIGHT MULTIPLEXING submitted by KEVIN JACOBSON in partial fulfillment of the requirements for the degree of MASTER OF SCIENCE.

Co-supervisor

Co-supervisor

Date: October 27, 1989

ABSTRACT

This thesis discusses a multiple access addressing technique intended for high speed data transmission in an optical fibre based local area network. This technique, called Optical Time-of-Flight Multiplexing, or OTFM, employs coherent, self-heterodyne detection and thus benefits from two advantages of coherent optical systems: channel selectivity and efficient use of the large bandwidth available in optical fibre. Since it is a self-heterodyne technique, only one laser is required in each transceiver instead of the two which are required in coherent systems. This incurs a cost saving. Further, self heterodyne systems dispense with the need for mutual optical frequency stabilisation of two independent lasers, and are relatively tolerant of slow optical frequency drifts. The technique is based on the use of the difference between the propagation times of a signal through two fibre paths as an address. With the use of a frequency modulated continuous wave ranging technique, the uniquely designed propagation time differences give rise to different radio frequency carriers, upon which messages reside. Since the optical frequency of a laser may be tuned over a very wide range, typically hundreds of gigahertz, the possibility of utilising a wide transmission spectrum arises. The thesis looks at a number of system design considerations, including frequency domain phenomena, network size constraints, and topological variations, and describes an experimental system in which data transmission at a rate of 10 megabits per second was achieved.

ACKNOWLEDGEMENTS

I am obligated to Dr. R. I. MacDonald, whose idea this thesis is based upon, and to both Drs. MacDonald and G. D. Cormack for their capable supervision, and their support and encouragement. I would also like to thank the members of the examining committee, Drs. G. S. Christensen, R. Fedosejevs, and A. E. Kamal for taking time to read my thesis and to suggest improvements.

I have appreciated the contact with and help from all graduate students and staff of the Alberta Telecommunications Research Centre. In particular, I would like to acknowledge George Fraser for his many excellent suggestions, Dr. Jann Binder for much help in the laboratory and many enlightening discussions, and Sunit Lohtia, Marc Veilleux, and Brent Swekla for their helpful discussions, encouragement, and occasional distractions.

For financial assistance, I am deeply indebted to the Natural Sciences and Engineering Research Council for their post-graduate scholarship, the Alberta Telecommunications Research Centre for their fellowships, the University of Alberta for their fellowships and teaching assistantship, and Drs. R. I. MacDonald and G. D. Cormack for their grants.

I am also grateful to Herb Gans and the staff of the mechanical workshop for their fabrication of numerous mechanical devices.

Last, but not least, I owe thanks to my family for never (usually) getting too upset with me not being home when they call.

TABLE OF CONTENTS

CHAPTER PAGE

1. INTRODUCTION 1
   - 1.1 Coherent Optical Communications 1
   - 1.2 Semiconductor Lasers 6
     - 1.2.1 The Laser Spectrum 7
     - 1.2.2 Semiconductor Laser Properties 8
     - 1.2.3 Measurement of Spectral Properties of Lasers 10
   - 1.3 Self-Heterodyne Optical Communications 12
   - 1.4 Organisation of Thesis 13

2. ADDRESSING BY OPTICAL TIME-OF-FLIGHT MULTIPLEXING 14
   - 2.1 Principle of Optical Time-of-Flight Multiplexing 14
   - 2.2 Optical Frequency Modulated Continuous Wave Ranging 15
   - 2.3 OTFM Addressing Schemes 20
     - 2.3.1 Bandpass Filter Tuning 20
     - 2.3.2 External Modulator 20
     - 2.3.3 Sweep Parameter Adjustment 22
     - 2.3.4 Optical Delay Insertion 23
     - 2.3.5 Summary of Addressing Schemes 23
   - 2.4 Frequency Domain Considerations 24
     - 2.4.1 Chop-out Effect 24
     - 2.4.2 Laser Linewidth 29
     - 2.4.3 Amplitude Modulation 29
   - 2.5 Determination of Maximum Network Size 30
     - 2.5.1 Type A Systems 31
       - 2.5.1.1 Bandpass Filter Tuning and External Modulator Schemes 32
       - 2.5.1.2 Sweep Width Alteration 35
       - 2.5.1.3 Sweep Frequency Alteration 36
     - 2.5.2 Type B Systems 37
     - 2.5.3 Comparison of Schemes 40
     - 2.5.4 Delay Insertion 42
   - 2.6 Summary 42

3. TOPOLOGICAL CONSIDERATIONS 45
3.1 Survey of Network Topologies 45
3.1.1 Central Loop 45
3.1.2 Bus 47
3.1.3 Double Star 49
3.1.4 Folded Ring 51
3.1.5 Ladder 53
3.1.6 Summary 55
3.2 The Asymmetry Problem in the Central Loop and Ladder Networks 57
3.3 Power Budgets 61
3.3.1 Central Loop 64
3.3.2 Bus 65
3.3.3 Double Star 66
3.3.4 Folded Ring 66
3.3.5 Ladder 67
3.3.6 Size Comparison of Topologies 67
3.4 Summary 68

4. EXPERIMENTAL RESULTS 69
4.1 Laser Characteristics 69
4.1.1 Spectral Properties 69
4.1.2 Frequency Modulation Efficiency 86
4.2 Data Transmission Experiment 89
4.2.1 Experimental Configuration 89
4.2.2 Data Transmission 91
4.2.3 Receiver Noise Discussions 100

5. SUMMARY AND CONCLUSIONS 101

REFERENCES 103

APPENDIX A: APL FUNCTION LISTINGS 107

APPENDIX B: DEVICE DATA SHEETS 112

APPENDIX C: CIRCUIT DIAGRAMS 125

LIST OF TABLES

TABLE PAGE

1.1. Channel separation-to-bit-rate ratios for coherent optical detection..... 5

1.2. Receiver sensitivities for coherent optical detection..... 6

3.1. Summary of network topologies..... 55

3.2 Summary of network sizes..... 67

LIST OF FIGURES

FIGURE PAGE

1.1. Typical coherent system. 2

1.2. Laser mode spectrum.
(a) gain profile and resonant cavity modes
(b) multimode laser oscillation 9

2.1. Optical time-of-flight multiplexing principle. 15

2.2. FMCW- sawtooth wave case.
(a) optical frequency
(b) difference frequency 17

2.3. FMCW- triangle wave case.
(a) optical frequency
(b) difference frequency 20

2.4. Addressing by external modulator.
(a) modulator configuration
(b) triangle wave case
(c) sawtooth wave case 22

2.5. Addressing by delay insertion. 24

2.6. Construction of chopped-out signal.
(a) $f_{IF}(t)$
(b) $r(t)$
(c) $c(t)$ 26

2.7. Effect of signal chop-out. 27

2.8. Effect of signal chop-out. 29

2.9. Type A spectrum. 33

2.10. Type B spectrum. 39

2.11. Comparison of sizes of addressing schemes..... 42

3.1. Central loop topology..... 46

3.2. Bus topology..... 48

3.3. Double star topology..... 50

3.4. Folded ring topology..... 52

3.5. Ladder topology..... 54

3.6. Network efficiencies..... 56

3.7. Asymmetric network generation algorithm..... 58

3.8. An asymmetric ladder network. 60

3.9. Ladder network efficiency versus number of potentially addressable nodes..... 62

3.10. Number of addressable nodes versus number of potentially addressable nodes..... 62

3.11. Receiver configuration..... 63

4.1. Monochromator experimental configuration. 70

4.2. Mode spectra of Ortel SL300-H laser.
(a) 45 mA bias
(b) 35 mA bias..... 72

4.3. Mode spectra of Ortel SL300-H laser, coupling misaligned.
(a) 44.4 mA to 44.9 mA bias
(b) 43.8 mA to 44.3 mA bias..... 73
(c) 43.2 mA to 43.7 mA bias 74

4.4. Random mode jumping..... 75

4.5. Isolator configuration..... 76

4.6. Mode spectra of Ortel SL300-H laser, after insertion of optical isolator.
(a) 42.5 mA to 45.0 mA bias
(b) 39.5 mA to 42.0 mA bias 77

4.7. Mode spectra of Sharp LTO15MF laser, no isolator.
(a) 76.0 mA to 86.0 mA bias
(b) 64.0 mA to 74.0 mA bias 78
(c) 62.0 mA to 52.0 mA bias 79

4.8. Mode spectra of Sharp LTO15MF laser, with isolator.
(a) 76.0 mA to 86.0 mA bias
(b) 64.0 mA to 74.0 mA bias 80
(c) 62.0 mA to 52.0 mA bias 81

4.9. Self-homodyne or -heterodyne setup. 82

4.10. Linewidth of Sharp LTO15MF laser, no isolator.
(a) wide spectrum trace
(b) zoom-in trace 83

4.11. Linewidth of Sharp LTO15MF laser, with isolator.
(a) wide spectrum trace
(b) zoom-in trace 84

4.12. Effect of index-matching fluid on external cavity modes. 85

4.13. Self-heterodyne signals, square wave modulation. 87

4.14. Self-heterodyne IF spectrum..... 88

4.15. Data transmission experimental configuration. 90

4.16. PIN receiver..... 92

4.17. Received IF spectrum..... 93

4.18. Received IF oscilloscope signal, unfiltered (horizontal scale: 50 ns/div., vertical scales: 1 V/div.upper trace, 200 mV/div. lower trace)..... 95

4.19. Received IF oscilloscope signal, filtered with bandpass filter (horizontal scale: 50 ns/div., vertical scales: 1 V/div.upper trace, 50 mV/div. lower trace)..... 95

4.20. Demodulated data 1010... (horizontal scale: 50 ns/div., vertical scale: 50 mV/div.).
(a) using lowpass filter with 40.9 MHz cutoff frequency
(b) using lowpass filter with 17.5 MHz cutoff frequency..... 96

4.21. Demodulated data 1010... , using 40 MHz sweep, unfiltered (horizontal scale: 50 ns/div., vertical scale: 50 mV/div.)..... 97

4.22. Demodulated data 1010... , after amplification (horizontal scale: 100 ns/div., vertical scale: 200 mV/div.)..... 97

4.23. Received eye diagram, PRBS sequence of length 2^{20}-1 (horizontal scale: 50 ns/div., vertical scale: 200 mV/div.)..... 99

4.24. Received data, 1010000000000... (horizontal scale: 500 ns/div., vertical scale: 200 mV/div.)..... 99

A.1. APL function: LS2..... 108

A.2. APL function: FINDS..... 110

A.3. APL function: LSQ..... 111

B.1. Data sheets for Ortel SL 300H laser..... 113

B.2. Data sheets for Ortel PD050-OM PIN photodiode..... 119

B.3. Data sheets for Sharp LTO15MF laser..... 123

C.1. FET switch..... 126

C.2. Laser bias circuit..... 127

C.3. PIN diode circuit..... 128

C.4. Amp 4: wideband amplifier..... 129

C.5. Amp 3: wideband amplifier. 130

C.6. HP2: highpass filter, 440 MHz cutoff. 131

C.7. BP1: bandpass filter 132

C.8. Demodulator. 133

C.9. LP1: lowpass filter, 17.5 MHz cutoff. 134

C.10. LP2: lowpass filter, 40.9 MHz cutoff. 135

C.11. AGC amplifier. 136

LIST OF ACRONYMS AND ABBREVIATIONS

°K	degrees kelvin
A	ampere
AGC	automatic gain control
AM	amplitude modulation
APL	A Programming Language
ASK	amplitude shift keying
BER	bit error rate
BP	bandpass
BT&D	British Telecom and DuPont
dB	decibel
dBm	decibels referred to milliwatts
dc	direct current
FET	field effect transistor
FM	frequency modulation
FMCW	frequency modulated continuous wave
FP	Fabry Perot
FSK	frequency shift keying
Gb/s	gigabits per second
GHz	gigahertz
GRIN	graded index
HP	Hewlett-Packard
Hz	hertz
IF	intermediate frequency
IM/DD	intensity modulation/direct detection
J	joule
kHz	kilohertz
km	kilometer
LAN	local area network
LO	local oscillator
m	meter
mA	milliampere
Mb/s	megabits per second

MHz	megahertz
µm	micrometer
mV	millivolt
mV/div	millivolts per division
µW	microwatt
mW	milliwatt
nm	nanometer
NRZ	non-return-to-zero
ns	nanosecond
ns/div	nanoseconds per division
OTFM	optical time-of-flight multiplexing
PIN	p-type layer:intrinsic layer:n-type layer
PRBS	pseudo-random bit sequence
ps	picosecond
PSK	phase shift keying
Rx	receive
SIR	signal-to-interference ratio
SNR	signal-to-noise ratio
THz	terahertz
Tx	transmit
V/div	volts per division
Ω	ohm
W	watt
WDM	wavelength division multiplexing

LIST OF SYMBOLS

$(\Delta\nu)_{laser}$	laser linewidth
α	fibre loss
α	slope of frequency sweep
α	system loss
a_0	dc Fourier coefficient
$\hat{A}_1$	unit vector giving field direction for path 1 signal
$\hat{A}_2$	unit vector giving field direction for path 2 signal
$\hat{A}_k$	unit vector giving field direction for k^{th} channel
$a_k(t)$	ASK modulating signal of k^{th} channel
$\hat{A}_{LO}$	unit vector giving field direction for local oscillator laser
a_n	n^{th} Fourier coefficient
BW	message bandwidth
c	speed of light in vacuum
C(f)	Fourier transform of c(t)
c(t)	sinusoidal function
d	Fabry-Perot cavity length
d	fibre distance
d_a	fibre distance in ladder network
d_b	fibre distance in ladder network
Δf	width of optical sweep
$\Delta\phi(t)$	time varying phase difference between path 1 and path 2 fields
Δf_{min}	minimum required sweep width
Δi	peak-to-peak amplitude of current waveform
$\Delta\nu$	three dB spectral width of laser emission
Δt	relative time delay
Δt_{max}	maximum tolerable relative time delay
$\Delta t_{max,wc}$	maximum tolerable relative time delay, worst case
Δt_{min}	minimum resolvable relative time delay
Δx_{min}	minimum resolvable distance
E	energy gap
ϵ	dielectric permittivity
E_0	electric field amplitude

E_1	electric field amplitude in path 1
E_2	electric field amplitude in path 2
$\overline{E}_k(t)$	electric field of k^{th} channel
E_{LO}	electric field amplitude of local oscillator laser
$\overline{E}_{LO}(t)$	electric field of local oscillator laser
erfc(.)	complementary error function
$\overline{E}_{total}$	total received electric field
f_+	frequency of 'plus' component of chop-out spectrum
f_-	frequency of 'minus' component of chop-out spectrum
$f_1(t)$	optical frequency of path 1 field
$\phi_1(t)$	time varying phase in path 1 field
$f_2(t)$	optical frequency of path 2 field
$\phi_2(t)$	time varying phase in path 2 field
$f_d(t)$	difference frequency waveform
f_{fb}	'flyback' frequency
f_{IF}	intermediate frequency
$f_{IF}(t)$	intermediate frequency waveform
f_{IF1}	downshifted intermediate frequency
f_{IF2}	upshifted intermediate frequency
f_k	optical frequency of k^{th} channel
$\phi_k(t)$	FSK or PSK modulating signal of k^{th} channel
f_{LO}	optical frequency of local oscillator laser
f_{max}	maximum electrical frequency
f_{mod}	external modulator modulating frequency
$f_{opt}(t)$	optical frequency waveform
f_s	sweep frequency
$f_{s,max}$	maximum required sweep frequency
$f_{s,min}$	minimum required sweep frequency
$\gamma(\nu)$	laser gain function
$g(\nu)$	Lorentzian laser lineshape function
g_b	largest tolerable time delay, as a fraction of bit period
g_m	FET transconductance
g_s	largest tolerable time delay, as a fraction of sweep period
η	network efficiency
h	Planck's constant
i	integer index

$i_d(t)$	detector current
k	Boltzmann's constant
k	integer index
k_{am}	differential amplitude modulation efficiency
k_f	frequency modulation efficiency of a laser
L_{cr}	fibre to photodiode coupling loss at receiver
L_{ct}	laser to fibre coupling loss at transmitter
L_{ex}	coupler excess loss
L_{sw}	loss in optical switch
M	system margin
m	integer index
μ	magnetic permeability
M(t)	intensity modulation factor
m_b	constant relating sweep frequency to bit rate
$m_k(t)$	message of k^{th} channel
N	network size
n	integer index
n	refractive index
ν_0	centre frequency of Lorentzian lineshape function
N_1	population of lower laser level
N_2	population of upper laser level
n_f	refractive index of fibre
ν_m	frequency of m^{th} Fabry-Perot cavity mode
N_{max}	maximum network size
P	electrical signal power
P	power emitted from laser
p	position of a node in a network
P(t)	time varying optical power
P_0	dc optical power
P_1	path 1 received optical power
$P_{1,dB}$	path 1 received optical power, in dB units
P_2	path 2 received optical power
$P_{2,dB}$	path 2 received optical power, in dB units
P_{dB}	electrical signal power, in dB units
P_n	power at n^{th} harmonic
$P_{opt}(t)$	average optical power

P_r	total received optical power
$P_{r,dB}$	total received optical power, in dB units
P_{sens}	receiver power sensitivity
$P_{t,dB}$	transmitted optical power, in dB units
P_{th}	thermal noise power
θ	angle between unit vectors $\hat{A}_1$ and $\hat{A}_2$
q	position of a node in a network
θ_k	angle between local oscillator and k^{th} channel field directions
θ_{ki}	angle between k^{th} and i^{th} channel field directions
R	detector responsivity
r	coupling efficiency
R(f)	Fourier transform of r(t)
r(t)	rectangular function
R_b	bit rate
R_{bias}	biassing resistance
R_{load}	load resistance
r_{opt}	optimum coupling ratio
R_p	power reflectivity of Fabry-Perot mirrors
s	channel separation constant
S(f)	Fourier transform of $f_{IF}(t)$
S_k	asymmetric network series coefficients
SNR	signal-to-noise ratio
T	temperature
t	constant relating bit rate to channel bandwidth
τ	lifetime of atomic state producing the laser radiation
t	time
t_1	propagation time for signal 1
t_2	propagation time for signal 2
T_b	bit period
T_d	added delay in folded ring topology
τ_d	relative time delay
T_{net}	network delay in folded ring topology
T_s	sweep period
t_{spont}	spontaneous emission lifetime
u(t)	unit step function

V_{bias}	bias voltage
v_{noise}	voltage amplitude of noise
v_{signal}	voltage amplitude of signal
Ψ	arbitrary phase in local oscillator laser electric field

CHAPTER 1

INTRODUCTION

The purpose of this chapter is to describe the basics of coherent optical communications, present some laser fundamentals relevant to discussions in this thesis, and to explain the motivation behind the study of a self-heterodyne addressing and multiplexing technique such as optical time-of-flight multiplexing (OTFM).

1.1 Coherent Optical Communications

The deployment of fibre optic communication systems has been on the rise for many years. This tendency is due to advantages afforded by fibre systems over metallic systems, some of which are: reduced size and weight of the transmission medium, radio frequency interference immunity, increased message capacity, and increased security. Fibre systems presently being deployed are primarily of the intensity modulation/direct detection (IM/DD) type. In these systems, the intensity of light emitted from a light emitting diode or laser is modulated with a message or subcarrier signal and subsequently detected at the far end of a fibre with a photodetector. Although IM/DD has achieved widespread use, a more elegant technique, coherent optical detection [1]-[6], promises some further advantages.

Coherent detection is the optical analogue of heterodyne detection in radio. In coherent systems, a message is impressed on the amplitude, frequency, or phase of the transmitting laser's optical field, and is demodulated at the receiver with a local oscillator (LO) laser whose optical frequency is equal or near to the frequency of the transmitting laser. Many such channels can be accommodated on a single optical fibre by ensuring that the optical frequency of each channel is unique. Since a laser's optical frequency can be easily changed over a wide range, typically a few hundred gigahertz (GHz), a wide transmission spectrum is provided.

A typical multichannel coherent system is represented in Figure 1.1. There are N laser transmitters whose optical frequencies are f_1, f_2, ..., f_N. Each channel's laser is modulated with its corresponding message signal, $m_1(t)$, $m_2(t)$, ..., or $m_N(t)$, with an external modulator. The type of modulator depends on whether amplitude shift keying (ASK), frequency shift keying (FSK), or phase shift keying (PSK) is employed. Direct

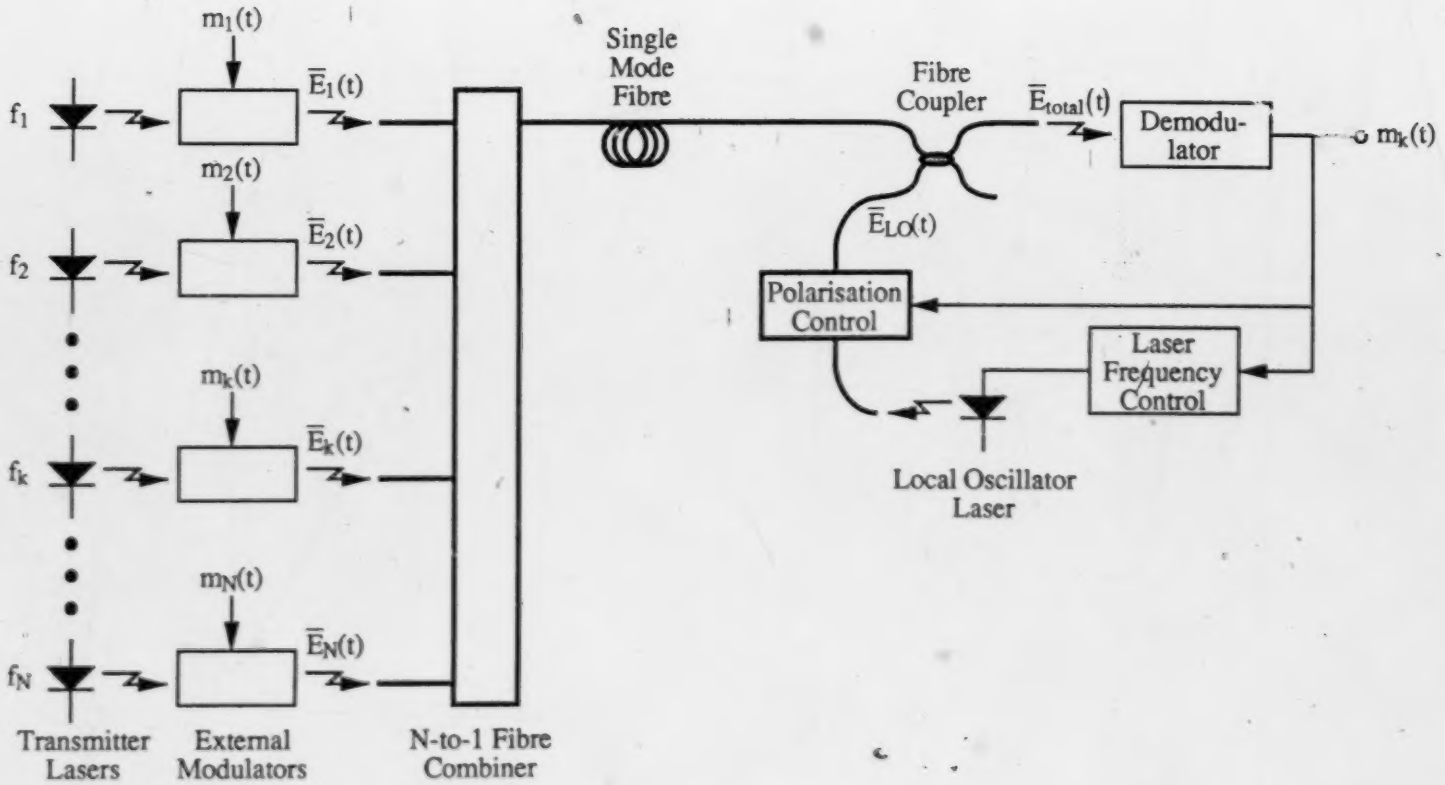

Figure 1.1. Typical coherent system.

laser modulation by modulating the drive current is also possible, but this can produce unwanted frequency or intensity variation in addition to the desired signal. Laser structures that suppress intensity variation while allowing frequency modulation, and vice versa, are being investigated [7], but are not as yet readily available. The derivations below apply to both external and direct modulation schemes.

The electric field from the k^{th} modulated laser in the system of Figure 1.1 is given by

$$\overline{E}_k(t) = E_0 \cdot a_k(t) \cdot \exp\left\{j\left[2\pi \cdot f_k \cdot t + \phi_k(t)\right]\right\} \cdot \hat{A}_k \tag{1.1}$$

where E_0 is the field amplitude, f_k is the optical frequency, $\hat{A}_k$ is a unit vector giving the direction of the electric field vector, $a_k(t)$ is the modulating signal for ASK, and $\phi_k(t)$ is the modulating signal for FSK or PSK.

The modulated light beams are combined into one single-mode transmission fibre with a N-to-one coupler. At the receiver, the light is combined with LO laser light using a fibre coupler. The electric field of the LO light is given by

$$\overline{E}_{LO}(t) = E_{LO} \cdot \exp\left\{j\left[2\pi \cdot f_{LO} \cdot t + \psi\right]\right\} \cdot \hat{A}_{LO} \tag{1.2}$$

where E_{LO} is the field amplitude, f_{LO} is the LO frequency, ψ is an arbitrary phase, and $\hat{A}_{LO}$ gives the direction of the electric field vector.

The total field at the photodetector is

$$\overline{E}_{total}(t) = \frac{E_{LO}}{\sqrt{2}} \cdot \exp\left\{j\left[2\pi \cdot f_{LO} \cdot t + \psi - \frac{\pi}{2}\right]\right\} \cdot \hat{A}_{LO} + \frac{\alpha \cdot E_0}{\sqrt{2}} \cdot \sum_{k=1}^{N} a_k(t) \cdot \exp\left\{j\left[2\pi \cdot f_k \cdot t + \phi_k(t)\right]\right\} \cdot \hat{A}_k \tag{1.3}$$

where α accounts for all losses between the transmitter and the detector, except for the final coupling loss. Note that the coupler imparts a loss of $1/\sqrt{2}$ in both LO and received light fields and a $\pi/2$ phase shift in the LO field.

The power averaged over an optical cycle is given by [8]

$$P_{opt}(t) = \frac{1}{2}\sqrt{\frac{\varepsilon}{\mu}} \cdot \left[\overline{E}_{total}(t) \cdot \overline{E}^{*}_{total}(t)\right] \tag{1.4}$$

where μ is the permeability of the photodetector material and ε is the permittivity. Using (1.3) in (1.4) and the fact that the photodetector current is proportional to the optical power, the current is obtained as

$$i_d(t) = \frac{R}{2}\cdot\sqrt{\frac{\varepsilon}{\mu}}\cdot\left\langle\frac{E_{LO}^2}{2}+\frac{\alpha\cdot E_0\cdot E_{LO}}{2}\cdot\sum_{k=1}^{N}a_k(t)\cdot\exp\left\{j\left[2\pi\cdot(f_{LO}-f_k)\cdot t-\phi_k+\psi-\frac{\pi}{2}\right]\right\}\cdot\cos\ \theta_k\right\rangle$$
$$+\frac{R}{2}\cdot\sqrt{\frac{\varepsilon}{\mu}}\cdot\frac{\alpha^2\cdot E_0^2}{2}\cdot\sum_{k=1}^{N}\sum_{i=1}^{N}a_k(t)\cdot a_i(t)\cdot\exp\left\{j\left[2\pi\cdot(f_k-f_i)\cdot t+\phi_k(t)-\phi_i(t)\right]\right\}\cdot\cos\ \theta_{ki} \qquad (1.5)$$

where R is the responsivity of the photodetector (in amperes/watt), and θ_k and θ_{ki} are the angles between the field vectors and are given by

$$\cos\theta_k = \hat{A}_{LO}\cdot\hat{A}_k$$
$$\cos\theta_{ki} = \hat{A}_k\cdot\hat{A}_i,\ k = 1, 2, ..., N, \text{ and } i = 1, 2, ..., N\ . \qquad (1.6)$$

Note that $\hat{A}_{LO}$ and $\hat{A}_k$ must be in the same direction to maximise the signal power, which implies the need for light polarisation control. Fibre that preserves the polarisation of light is available, but expensive. Alternatively, ordinary fibre may be used in conjunction with continuous polarisation matching techniques at the receiver [9]. In one of these techniques [10], polarisation is dynamically controlled by inducing stress in the fibre until the signal power is maximum.

Equation (1.5) contains intermediate frequency (IF) terms arising from beating between the LO and the message carrier frequencies (second term), cross terms due to beating between message carrier frequencies (third term), and a dc term (first term). Normally one expects that

$$E_{LO} >> \alpha^2\cdot E_0 \qquad (1.7)$$

so that the cross term signals are weak compared to the IF signals containing the channel messages. If the photodetector signal is passed through a filter whose bandwidth is just wide enough to pass one channel message, then channel selectivity is obtained by tuning f_{LO} until the desired signal falls within the filter's passband.

Channel selectivity is one advantage of coherent detection over IM/DD. Although optical carriers of different frequency may be used in IM/DD (this is called wavelength

division multiplexing or WDM), optical filters do not have sharp cutoffs between passband and stopband, and thus wide wavelength separations are required in order to minimise crosstalk between channels. In a coherent system, channel selectivity is achieved using electronic filters which can be made much sharper than their optical equivalents, and thus channels may be closer together. Typical IM/DD WDM channel spacing is on the order of 100 GHz, while spacing for a coherent system is on the order of a few hundred MHz for 45 Mb/s data rates. The effect of this separation reduction is a more efficient use of the fibre bandwidth. Table 1.1 summarises the channel separation-to-bit-rate ratios required for a signal-to-crosstalk ratio of 30 dB for various multichannel coherent schemes [5].

Modulation Scheme	Channel separation/Bit rate[0]
Heterodyne ASK	9.5
Heterodyne FSK	3.8
Heterodyne PSK	12.4
Homodyne ASK	7.5
Homodyne PSK	10.5

Table 1.1. Channel separation-to-bit rate ratios for coherent optical detection.

Another advantage that coherent affords over IM/DD is receiver sensitivity. Note from (1.5) that the received signal level is proportional to the product of the signal and LO field amplitudes. This implies that the received signal level can be increased by increasing the LO power, providing optical gain prior to signal detection. Thus, if the signal level is raised sufficiently high, the signal-to-noise ratio is limited by shot noise in the detector due to high LO power instead of thermal noise in the subsequent amplifiers. IM/DD systems cannot benefit from this heterodyne gain, and are thus less sensitive than coherent systems. Table 1.2 gives the theoretical number of photons required at the receiver to achieve a bit error rate (BER) of 10^{-9} for various coherent modulation schemes [3].

---

0 The required channel separation is actually dependent on a number of parameters, such as laser linewidth, coding scheme, frequency deviation (for FSK and PSK), and IF-to-bandwidth ratio. See [5] for details pertaining to the figures given here.

Modulation Scheme	Sensitivity, photons/bit
Heterodyne ASK	36
Heterodyne FSK	36
Heterodyne PSK	18
Homodyne ASK	18
Homodyne PSK	9

Table 1.2. Receiver sensitivities for coherent optical detection.

Practical IM/DD systems have achieved sensitivities of approximately 500 to 1000 photons per bit while experimental coherent systems have achieved sensitivities as low as 45 photons per bit [3]. The impact of this increased sensitivity is to allow longer fibre spans between repeaters. Up to 290 kilometer spans have been reported [3] for coherent systems, while IM/DD spans are typically limited to about 200 kilometers.

Coherent systems are unfortunately much more expensive to implement than are IM/DD systems, and this is true for several reasons. First, not only are lasers required in both transmitter and receiver, but they must be of a type that emit light in a single, stable longitudinal mode with a narrow linewidth. Gas lasers fit into this category, but are bulky and difficult to modulate at high frequencies. Semiconductor lasers are much more attractive due to their tiny dimensions and the possibility of integration with other electronics. Unfortunately they are more difficult to build with the desired frequency characteristics. Devices such as distributed feedback, distributed Bragg reflector, and external cavity lasers [11], [12] have achieved single mode and narrow linewidth operation, but remain somewhat expensive and suffer from a limited frequency tuning range. A second disadvantage in coherent systems is the sensitivity of laser frequency to temperature and optical feedback. Temperature stabilisers and optical isolators must be used, which further add to the cost of transmitter and receiver. The above problems may be somewhat alleviated with the use of the novel system studied in this thesis.

1.2 Semiconductor Lasers

The purpose of this section is to provide an overview of laser spectral properties and measurements pertinent to the discussions in this thesis.

1.2.1 The Laser Spectrum

The elemental components of a Fabry-Perot (FP) laser are the resonant optical cavity (called the FP cavity), and the gain medium. The FP cavity consists of two parallel, partially transmitting mirrors separated by some distance, d. Within this cavity, there is a medium whose purpose is to provide optical gain by stimulated emission. In a semiconductor laser, the gain medium is a semiconductor crystal, such as GaAlAs or InGaAsP, and the mirrors are the cleaved end facets of the crystal.

Laser oscillation has a frequency spectrum that is determined by the resonant mode pattern of the cavity and the gain profile of the medium. The resonant cavity modes are a result of standing waves occurring inside the cavity. The expression for the frequencies of these modes is [13]

$$\nu_m = \frac{m \cdot c}{2 \cdot n \cdot d} \tag{1.8}$$

where c is the speed of light in a vacuum, n is the refractive index of the laser medium, d is the length of the cavity, and m is any positive integer. The gain, $\gamma(\nu)$, in a semiconductor laser medium is a function of frequency [13]

$$\gamma(\nu) = (N_2 - N_1) \cdot \frac{c^2}{8\pi \cdot n^2 \cdot \nu^2 \cdot t_{spont}} \cdot g(\nu) \tag{1.9}$$

where N_2 and N_1 are the populations of the upper and lower laser levels, respectively, c is the speed of light, n is the refractive index of the semiconductor, and t_{spont} is the spontaneous emission lifetime. $g(\nu)$ is the lineshape shape function which is a Lorentzian function of frequency [13]

$$g(\nu) = \frac{\Delta\nu}{2\pi\left[(\nu - \bar{\nu}_0)^2 + \left(\frac{\Delta\nu}{2}\right)^2\right]} \tag{1.10}$$

where $\Delta\nu$ gives the 3 dB spectral width of the electronic states in the gain medium, and ν_0 is the centre frequency. $\Delta\nu$ is determined by the lifetime, τ, of the atomic state producing the radiation [13]

$$\Delta\nu = \frac{1}{\pi \cdot \tau} \tag{1.11}$$

and ν_0 is determined by the energy difference, E, between the two laser transition levels

$$\nu_0 = \frac{E}{h} \tag{1.12}$$

where h is Planck's constant.

Figure 1.2(a) shows a representation of expressions (1.8) and (1.10), with a horizontal line representing the loss in the laser cavity. Loss is due to scattering and absorption of photons, and the light escaping through the semi-transmitting mirrors. In 1.2(b), oscillation is shown to occur at mode frequencies where gain exceeds the laser cavity loss.

Since there is more than one cavity mode appearing in the above spectrum, this oscillation is termed 'multimode.' A laser can be made to oscillate in a single longitudinal mode by shortening the cavity, thereby ensuring that the mode separation is wide compared to the gain profile and that only one cavity mode has enough gain to exceed the cavity loss. (There are also several other phenomena that affect the modal properties of a laser [14]-[16], but these are too involved to discuss here.)

It is important to note that since FP laser oscillation depends on optical feedback from a reflective surface, it is expected that reflections from other surfaces, such as the end of an optical fibre, will affect the laser oscillation frequency [17], [18]. Thus, for stable and predictable operation, one must ensure that external reflections are not coupled back into the laser. This is usually accomplished through the use of an optical isolator, which is a device that lets light pass unimpeded in the forward direction, but attenuated in the reverse direction.

1.2.2 Semiconductor Laser Properties

A laser property important in coherent systems is the laser's frequency tunability by injection current modulation. From (1.8), it is noted that the mode spectrum of a laser cavity depends on the refractive index of the gain medium. Refractive index is dependent on both temperature and carrier density in the gain medium, which are in turn affected by the magnitude of the laser injection current. Thus, the frequency modulation (FM)

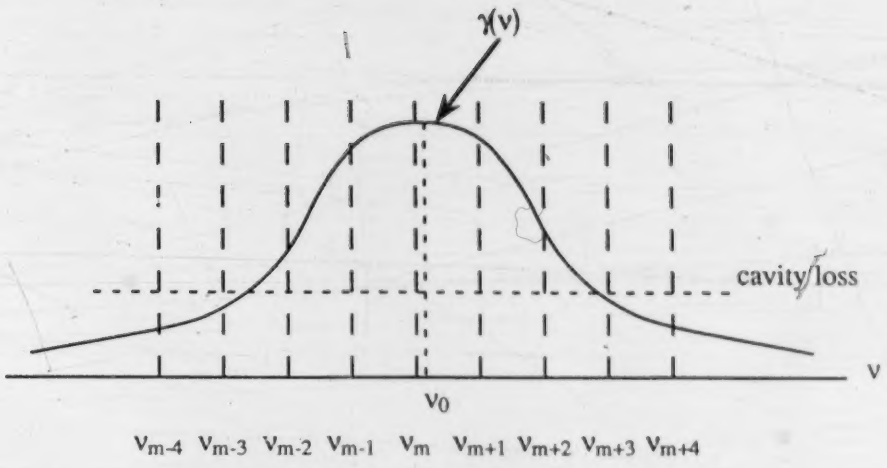

(a) gain profile and resonant cavity modes

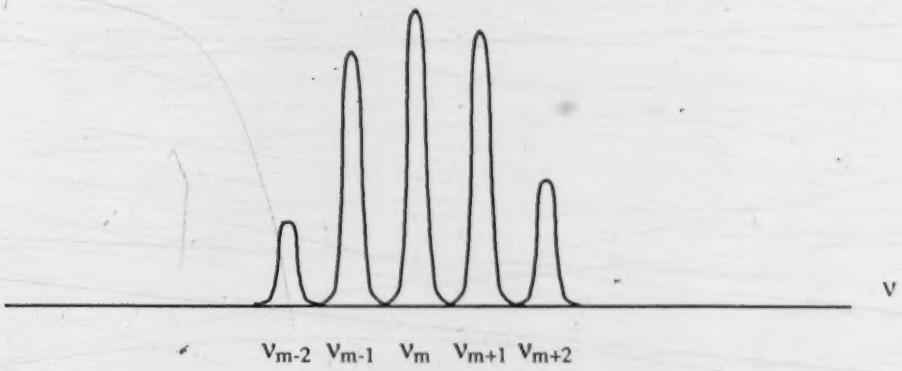

(b) multimode laser oscillation

Figure 1.2. Laser mode spectrum.

efficiency of a laser, which is the change in frequency for a given change in current, is dependent on the mechanical structure of the laser as well as the characteristics of the semiconductor gain medium. It is important to know the FM efficiency characteristic of a laser prior to its incorporation into a coherent system.

Linewidth is another important laser property, and is defined as the 3 dB width of the laser output spectrum. Measurement of this characteristic is necessary as it is often a dominant noise factor in coherent systems. The linewidth is given by [13]

$$(\Delta\nu)_{laser} = \frac{2\pi \cdot h \cdot \nu_0}{P} \cdot \frac{N_2}{N_2 - N_1} \cdot \left(\frac{c}{2\pi \cdot n \cdot d} \cdot \frac{1 - R_p}{\sqrt{R_p}} \right)^2 \tag{1.13}$$

where ν_0 is the oscillation frequency, P is the total power emitted, d is the cavity length, and R_p is the power reflectivity of the cavity mirrors.

An important property related to linewidth is the coherence time of a laser. This value can be thought of as the average time over which the phase of the laser field remains constant, and is given by [13]

$$\tau_c = \frac{1}{\pi \cdot (\Delta\nu)_{laser}} \tag{1.14}$$

1.2.3 Measurement of Spectral Properties of Lasers

The analysis of the spectral properties of lasers is of primary importance in coherent systems. There are three devices or techniques commonly employed in measuring the spectral properties of a laser: the scanning monochromator, Fabry-Perot etalon, and self-heterodyne or -homodyne techniques.

1) Scanning monochromator [19]: This device is a tunable bandpass optical filter which consists of a diffraction grating followed by a narrow slit. Light is dispersed by the grating which can be rotated in order to shift the resulting diffraction pattern across the slit. The slit allows a portion of the pattern, and thus a narrow wavelength band, to pass through to a broad spectrum photodetector. A plot of detector output against grating position is representative of the spectral content of the incident light.

Monochromators typically have a wavelength resolution of a few tenths of an angstrom to several angstroms and a tuning range of several micrometers (μm). They are

useful for analysing the mode spectrum of a laser, but do not have adequate resolution for determining laser linewidth.

(2) Fabry-Perot Etalon [13]: A Fabry-Perot (FP) etalon is another type of optical bandpass filter, and it consists of two parallel partially transmitting mirrors. Light is fully transmitted only when the wavelength is such that constructive interference between the multiple optical paths occurs. Since this transmission wavelength depends on the distance between the mirrors, the filtering wavelength may be tuned by scanning the position of one mirror with respect to the other.

The FP etalon typically has a resolution of a few hundredths of an angstrom, and a scanning range (referred to as free spectral range) of several angstroms. The range is not sufficient to display the mode spectrum, nor the resolution adequate to determine the linewidth, but the FP etalon is able to observe dynamic changes in the laser spectrum. This capability is useful in measuring the FM efficiency of a laser.

(3) Self-heterodyne or -homodyne technique [20], [21]: This technique is useful when it has been determined that the laser operates in a single mode. Self-heterodyne is a technique whereby the light from a laser is split, sent through two separate paths, and then recombined. Mixing of the two light beams at a photodetector converts the optical signal to an electrical signal which may be seen on an ordinary spectrum analyser. The frequency content of the electrical signal depends on the frequency content of the optical carrier, and thus contains information about the optical spectrum. In fact, the width of the electrical spectrum is twice the laser linewidth under the condition that the time delay difference between the two paths is greater than the coherence time of the laser. The resolution of this technique, as given by [21], is

$$\Delta = \frac{1}{2 \cdot \tau_d} \tag{1.15}$$

where τ_d is the time delay difference between the paths.

If the electrical signal is centred at dc, then the technique is called self-homodyne. Often an acoustooptic modulator is inserted into one path in order to shift the signal away from dc (self-heterodyne) so that 1/f noise is avoided.

All of the above techniques were used in this thesis in order to select an appropriate laser. The FP etalon that was available for the experiments in this thesis contained mirrors

that were optimised for a wavelength of 1300 nanometers (nm), and thus, since lasers with a wavelength of 830 nm were used, gave terrible resolution. These FP results will be omitted in this thesis. A modified version of self-heterodyne was employed, and will be described in Chapter 4.

1.3 Self-Heterodyne Optical Communications

Optical time-of-flight multiplexing (OTFM) has been proposed [22] as a coherent, self-heterodyne technique intended for multiplexing and addressing signals in a fibre optic local area network (LAN). Similar techniques have been used to multiplex fibre-optic sensors [23]-[25], and to transmit binary data [26], but the technique has not been fully investigated for communication purposes. This thesis attempts to address some of the issues involved in designing an OTFM communication system, and describes the results of an experiment which demonstrates the OTFM principle. This section explains the basis for investigating a self-heterodyne system, and sets the stage for the in-depth description of the OTFM principle which appears in Chapter 2.

In a self-heterodyne system, an IF signal is produced when light from a transmitting laser is combined with itself, rather than with a LO beam. There are two main advantages that a self-heterodyne system affords over a LO-type of system:

(1) the need for a LO laser is eliminated, significantly reducing receiver cost and complexity, and

(2) the detrimental effect of slow optical frequency drift due to local temperature variations at the laser is reduced.

Most coherent experiments have used long wavelength (1300 or 1550 nm) lasers to take advantage of the dispersion and loss minima of silica fibre. The experiments conducted for this thesis made use of a short-wavelength (836 nm) single-mode device of the type found in compact disk players. There are four reasons that this type of laser was chosen:

(1) they can be made to emit in a single longitudinal mode even with a simple Fabry-Perot cavity structure [14], [15],

(2) they tend to have narrower linewidths than long wavelength lasers even without the use of narrowing techniques [27],

(3) they may be tuned over a wide optical frequency range while remaining in one mode [25], and

(4) they are relatively inexpensive.

The main disadvantage in using a short-wavelength laser is the increase in fibre dispersion and loss; silica fibres have dispersion and loss minima at approximately 1300 and 1550 nm, respectively. Thus, the use of short wavelengths may be limited to short-reach applications such as local area networks. In fact, the use of a self-heterodyne technique is already limited to a short-reach network: not only is the advantage of optical gain by heterodyning, as described in Section 1.1, lost in self-heterodyne systems, but the requirement for two paths from each node to another precludes long-haul applications of such a technique. The benefit of channel selectivity is retained, however, and, as a bonus, addressing capability is gained by using OTFM. This capability will be described in the next chapter when the OTFM technique is fully explained.

1.4 Organisation of Thesis

The purpose of this thesis is to assess the feasibility of implementation of a system using the OTFM principle. Theoretical considerations in such a system are examined, and the data transmission capability of OTFM is proved via the construction of an experimental system.

Chapter 2 describes the multiplexing and addressing capability of OTFM. Several different schemes of addressing that may be employed in an OTFM system are presented and reviewed, various frequency domain implications are discussed, and the maximum addressable sizes imposed by the various addressing schemes are determined.

In Chapter 3, issues pertaining to network topology, or layout, are discussed. First, several different topologies that provide the required dual paths are introduced and assessed. Next, a problem specific to two of the topologies is analysed, and a solution proposed. In the final section of this chapter, the power budgets of the various topologies are derived.

The experimental portion of the thesis appears in Chapter 4. Here is described the experiments in which various lasers were tested for suitability in an OTFM system, and the experimental configuration which demonstrated the transmission of digital data.

Chapter 5 contains a summary of the discussions in this thesis and some suggestions for future work on the OTFM principle.

CHAPTER 2

ADDRESSING BY OPTICAL TIME-OF-FLIGHT MULTIPLEXING

In this chapter the principle of optical time-of-flight multiplexing (OTFM) [22] is explained, various addressing schemes that may be employed in OTFM are presented, frequency domain considerations are discussed, and the maximum network size constraints imposed by the various addressing schemes are derived.

2.1 Principle of Optical Time-of-Flight Multiplexing

As the name implies, multiplexing is achieved by measuring the relative 'time-of-flight' of a signal travelling through two unequal length paths in a network. A network such as that shown in Figure 2.1 is constructed to provide two signal paths between every pair of nodes. Node p launches a signal into both paths and node q sees the signal twice, one signal being delayed with respect to the other by Δt, which is given by

$$\Delta t = |t_1 - t_2| \tag{2.1}$$

where t_1 and t_2 are the signal propagation times in the two paths. If the network is arranged so that the signal propagation time difference between the p^{th} node and each of the other nodes is unique, then these time delays may be considered as unique addresses.

There are a number of network topologies other than the simple ring of Figure 2.1 that provide the required dual paths, each of which has advantages and disadvantages. Several topologies will be studied in detail in Chapter 3.

Since two signal paths are required in this technique, OTFM would be most cost effective for short haul applications such as a local area network, or LAN. Normally the use of long wavelengths (1300 nm or 1550 nm) is preferred due to the dispersion and loss minima of optical fibre at such wavelengths, but since the use of OTFM is limited to short haul systems, one may consider short wavelength lasers as sources. As stated in Section 1.3, short wavelength lasers have several properties desirable for this application.

In order to perform addressing, there must be a means of measuring the relative time delays in the network. The method employed in the experiments for this thesis was optical frequency modulated continuous wave (FMCW) ranging. This technique is described in the following section.

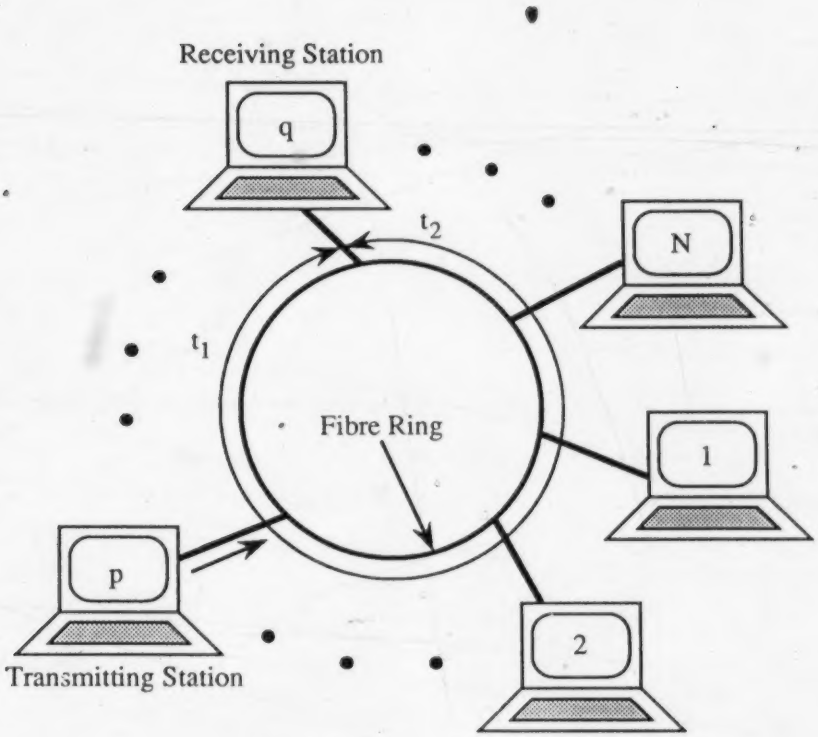

Figure 2.1. Optical time-of-flight multiplexing principle.

2.2 Optical Frequency Modulated Continuous Wave Ranging

Frequency modulated continuous wave (FMCW) ranging is a technique that has been used in radar for many years [28]. In this technique, a radio transmitter sends a signal whose frequency is linearly swept. The echo from a distant object is received and mixed with a portion of the transmitted swept carrier, creating a signal whose frequency is the difference between the frequencies of the echo and transmitted signals. This signal frequency is constant and proportional to the distance to the object.

In optical FMCW ranging, the optical frequency of a laser is swept by modulating the laser injection current, and the light is sent down the two fibre paths of an OTFM network. If a sawtooth-type frequency sweep is used, then the two signals appearing at the receiving node have the optical frequency waveforms shown in Figure 2.2(a).

The frequency $f_1(t)$ is the optical frequency of the short path signal and is given by

$$f_1(t) = f_0 + \sum_{n=0}^{\infty} \alpha \cdot (t - n \cdot T_s) \cdot u(t - n \cdot T_s) \cdot u\left[(n+1) \cdot T_s - t\right] \tag{2.2}$$

where f_0 is the quiescent frequency in Hz, α is the slope in Hz/second, and T_s is the repetition period in seconds.

The long path signal frequency is given by

$$f_2(t) = f_1(t - \Delta t) \tag{2.3}$$

where Δt is the time delay difference from (2.1).

The two signals are combined in a fibre coupler and detected with a photodetector such as a PIN diode or avalanche photodiode. The current in the detector is calculated in a manner similar to that for the general coherent case of the previous chapter. The electric fields for the two paths are

$$\bar{E}_1(t) = E_1 \cdot M(t) \cdot \exp\left\{j \cdot \phi_1(t)\right\} \cdot \hat{A}_1$$

and

$$\bar{E}_2(t) = E_2 \cdot M(t - \Delta t) \cdot \exp\left\{j \cdot \phi_1(t - \Delta t)\right\} \cdot \hat{A}_2 \tag{2.4}$$

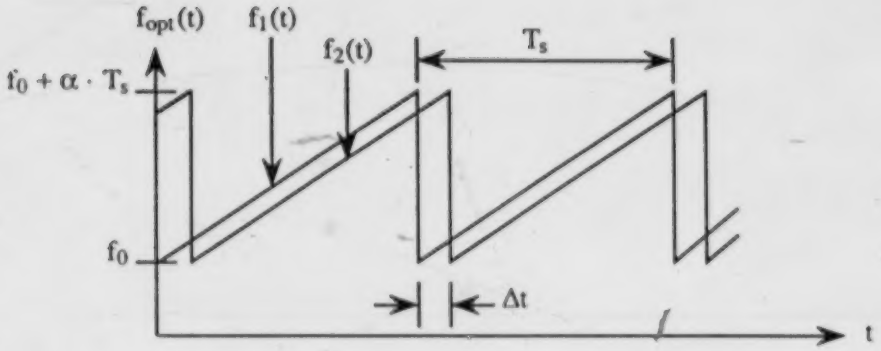

(a) optical frequency

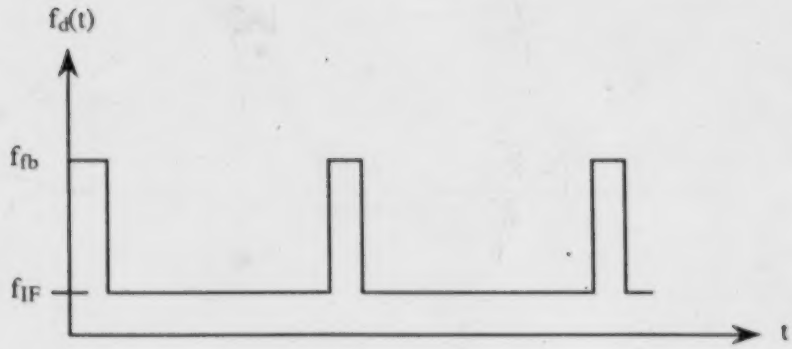

(b) difference frequency

Figure 2.2. FMCW- sawtooth wave case.

where E_1 and E_2 are the field amplitudes, M(t) is an amplitude factor describing unwanted intensity modulation, $\hat{A}_1$ and $\hat{A}_2$ are unit vectors giving the directions of the fields, and $\phi_1(t)$ is the time-varying phase

$$\phi_1(t) = 2\pi \cdot \int_0^t f_1(\tau)\, d\tau$$

$$= 2\pi \cdot f_0 \cdot t + 2\pi \cdot \alpha \cdot t \cdot \sum_{n=0}^{\infty} \left(\frac{1}{2} \cdot t - n \cdot T_s\right) \cdot u(t - n \cdot T_s) \cdot u[(n+1) \cdot T_s - t] \tag{2.5}$$

Summing expressions (2.4) and substituting into (1.4), the detector current is obtained as

$$i_d(t) = \frac{R}{2} \cdot \sqrt{\frac{\varepsilon}{\mu}} \cdot \left\{ \frac{E_1^2 \cdot M^2(t) + E_2^2 \cdot M^2(t-\Delta t)}{2} + E_1 \cdot E_2 \cdot M(t) \cdot M(t-\Delta t) \cdot \cos\left[\Delta\phi(t) + \frac{\pi}{2}\right] \cdot \cos\,\theta \right\} \tag{2.6}$$

where R is the responsivity of the detector,

$$\cos\theta = \hat{A}_1 \cdot \hat{A}_2 , \tag{2.7}$$

and

$$\Delta\phi(t) = \phi_1(t - \Delta t) - \phi_1(t)$$
$$= -(2\pi \cdot \alpha \cdot \Delta t) \cdot t - 2\pi \cdot [f_0 - \alpha \cdot (\Delta t + n \cdot T_s)] \cdot \Delta t ,$$

for $$n \cdot T_s + \Delta t \le t < (n+1) \cdot T_s . \tag{2.8}$$

The frequency of the signal portion of (2.6) is

$$f_{IF} = \frac{1}{2\pi} \cdot \left| \frac{\partial \Delta\phi(t)}{\partial t} \right| = \alpha \cdot \Delta t = \Delta f \cdot f_s \cdot \Delta t \tag{2.9}$$

where Δf is the width of the frequency sweep, and $f_s = 1/T_s$ is the sweep rate. The frequency waveform of the detected signal is shown in Figure 2.2(b).

It is clear from (2.9) that the received frequency is proportional to the time delay difference. If Δt is small compared to T_s, then f_{IF} is constant for most of the period, and may be used as a message carrier. We stated earlier that the relative delays between nodes

can be made unique, and thus, from (2.9), the carrier frequencies are unique. With appropriate filtering, channel selectivity is achieved.

To accomplish addressing, either carrier frequency or filter centre frequency may be shifted in order to centre the signal within the receiver band. Shifting of the carrier frequencies can be done by either transmitter or receiver, while shifting of filter centre frequency can be done only by the receiver. Various modes of addressing will be discussed later in this chapter.

Note from Figure 2.2(b) that there is also a detrimental 'flyback' frequency,

$$f_{fb} = \alpha \cdot (T_s - \Delta t) \tag{2.10}$$

which occurs during the time period

$$(n \cdot T_s) \le t < (n \cdot T_s + \Delta t) . \tag{2.11}$$

If Δt is sufficiently smaller than T_s, then f_{fb} is much larger than f_{IF} and the flyback time duration small so that f_{fb} can be filtered out with a small effect on the message. The effect of this filtering is to chop out small portions of the message, the implications of which will be considered in Section 2.4.1.

The preceding analysis has dealt with an optical carrier that is swept in a sawtooth pattern. Alternatively, the laser may be swept with the triangle wave shown in Figure 2.3(a). The resulting difference frequency is shown in Figure 2.3(b). The frequencies here are

$$f_1(t) = f_0 + \sum_{n=0}^{\infty} (-1)^n \cdot \alpha \cdot \left(t - \frac{n \cdot T_s}{2}\right) \cdot u\left(t - \frac{n \cdot T_s}{2}\right) \cdot u\left[\frac{(n+1) \cdot T_s}{2} - t\right] ,$$

and,

$$f_2(t) = f_1(t - \Delta t) , \tag{2.12}$$

and (2.9) is modified to obtain the IF as

$$f_{IF} = 2 \cdot \Delta f \cdot f_s \cdot \Delta t . \tag{2.13}$$

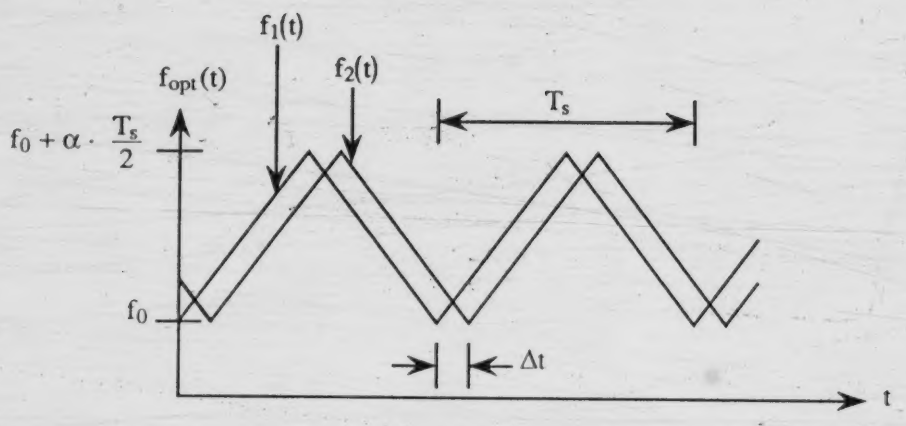

(a) optical frequency

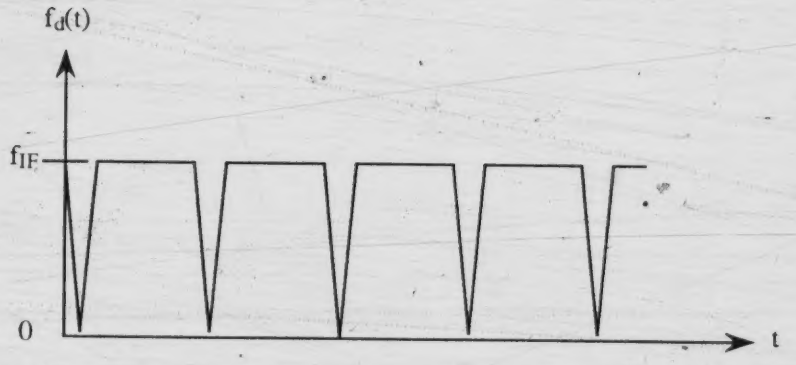

(b) difference frequency

Figure 2.3 FMCW- triangle wave case.

There are two advantages to using a triangle over a sawtooth. First, the frequency content of the triangle is lower than that of the sawtooth, which allows the laser to be swept at a higher frequency. Second, the slope of a triangle is double that of a sawtooth for the same sweep frequency, and thus f_{IF} is doubled. It is often desirable to maintain the IF much higher than the bit rate, and this doubling helps to ensure a high IF-to-bit-rate ratio.

There are a number of considerations in designing an OTFM system, such as frequency domain effects, schemes of addressing, implications of parameter choice on network size, topology variations, and power budgets. These topics will be examined in this and the following chapters.

2.3 OTFM Addressing Schemes

The previous sections have explained how multiplexing may be achieved using OTFM. To perform addressing, either transmitter or receiver must perform some operation in order to place the desired message within the receiver's bandpass filter. If addressing is performed by the receiver, then the system is of the broadcast type. Often in computer LANs, the transmitting station requires addressing control. Several receiver-controlled and transmitter-controlled addressing schemes are discussed in this section.

2.3.1 Bandpass Filter Tuning

At any receiver in an OTFM system, messages from different transmitters are seen at different IF frequencies. The receiver can thus select the appropriate message by varying the frequency position of its bandpass (BP) filter. Although this is perhaps the addressing mode most easily implemented, the usable width of the spectrum is constrained by electrical considerations, and thus the fibre bandwidth is less efficiently utilised. Also, this scheme forces receiver-controlled addressing.

2.3.2 External Modulator

Addressing can also be achieved by placing an optical frequency shifter in one of the paths, as shown in Figure 2.4(a). If the receivers' bandpass filters are fixed, the modulator may shift the quiescent frequency of one of the frequency swept signals up or down by the modulating frequency, f_{mod}, so that the appropriate IF falls within a receiver band. This modulator may be placed at either transmitter or receiver.

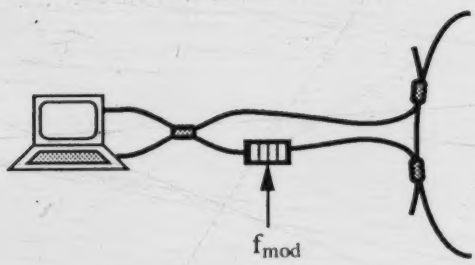

(a) modulator configuration

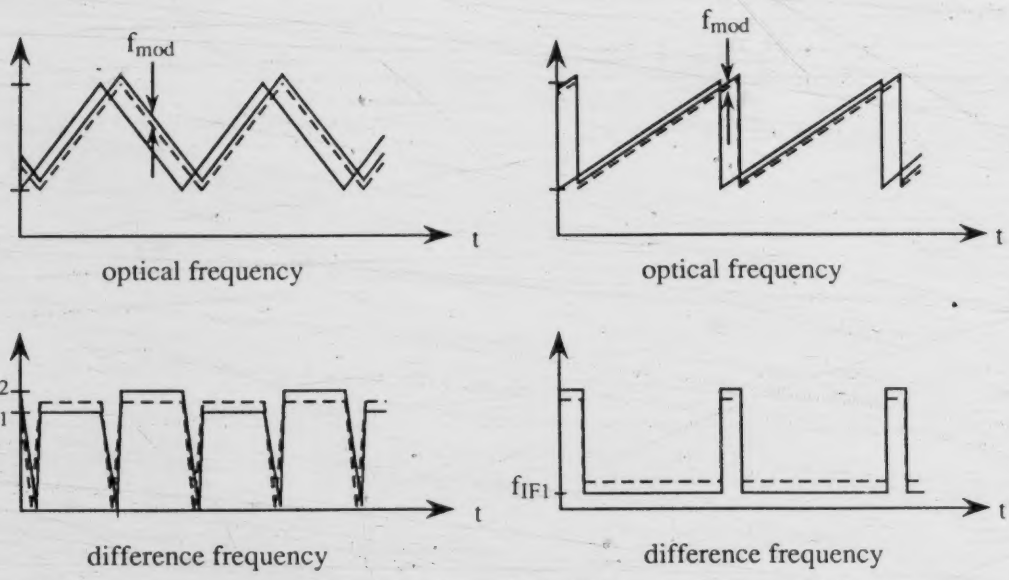

(b) triangle wave case

(c) sawtooth wave case

shifted

unshifted

Figure 2.4. Addressing by external modulator.

If a triangle sweep is used, as shown in Figure 2.4(b), f_{IF} is split into two IF signals, f_{IF1} and f_{IF2}, given by

$$f_{IF1} = f_{IF} - f_{mod}$$

and

$$f_{IF2} = f_{IF} + f_{mod} . \qquad (2.14)$$

Since one of these frequencies is filtered out, there is a 3 dB loss incurred. Also, the same pair of frequencies occur whether the optical frequency is shifted up or down, resulting in addressing ambiguities. As shown in Figure 2.4(c), these problems are not present when a sawtooth sweep is used.

The main disadvantage to this addressing scheme is that the external modulator must be driven by a high frequency electrical signal in order to perform the required shift. Thus, the width of the usable spectrum is again limited by electrical considerations. However, the external modulator scheme may be easier to implement than the BP tuning scheme for the following reason. The BP tuning receiver requires that nearly all receiver components be able to handle high frequencies, while the external modulator scheme requires only a high frequency oscillator and optical frequency shifter.

One type of external modulator that can be used is an acoustooptic modulator. However, modulation of these devices is often limited to about 200 MHz, which places a severe restriction on the number of addressable nodes.

Another type of modulator is a phase modulator, which may be used as a frequency shifter by ramping the input signal. Some devices [29] may be modulated as fast as 15 GHz, which may allow a reasonable network size.

2.3.3 Sweep Parameter Adjustment

As is apparent from expressions (2.9) and (2.13), the IF seen by a receiver depends not only on the time delay, but also on the width of the frequency sweep, Δf, and the sweep repetition frequency, f_s. Thus, variation of these parameters alters the value of the IF. If, as in the previous scheme, the receivers' filters are fixed, the transmitter may address the appropriate receiver by altering Δf or f_s to place its signal in the addressed receiver's band. This is perhaps easily accomplished (as long as the relative time delay is not zero), but, as will be seen in Section 2.5, varying these parameters puts a very severe constraint on the maximum network size.

2.3.4 Optical Delay Insertion

In this method of addressing, an optical delay is placed in the shorter of the two fibre paths, at either transmitter or receiver, in order to compensate for the relative delay in the network. This configuration is shown in Figure 2.5.

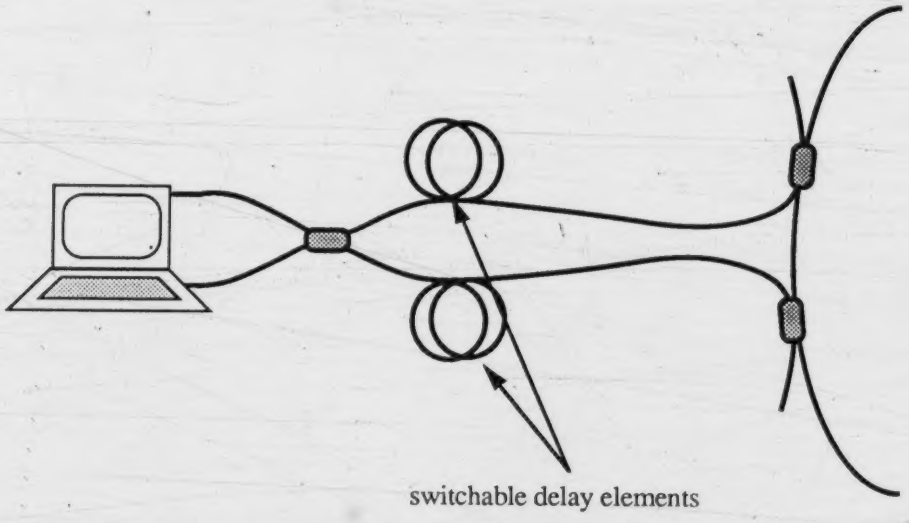

Figure 2.5. Addressing by delay insertion.

In this scheme, the over-all delay from the transmitter to the addressed receiver never changes, and can be made small so that the 'chop-out effect,' as described in the next section, is minimised. As will be seen in Section 2.5, relative time delay considerations can severely limit the size of a network. With a constant and known delay, these limitations are eliminated, and the size constraint is due only to power budget considerations. The disadvantage to this scheme is the difficulty in switching many different optical delay elements.

2.3.5 Summary of Addressing Schemes

A few conclusions can be drawn from the above discussions. Firstly, bandpass filter tuning may be used in a broadcast type of network, but requires widely tunable electrical filters. Secondly, the use of an external modulator to shift the optical frequency in one path is possible, but unfortunately requires high frequency electrical signals. The bandpass filter tuning and external modulator schemes may not utilise fibre bandwidth any more efficiently than an IM/DD system, but they still maintain an advantage since they do

not require that the laser be modulated at high frequencies. Finally, delay insertion is much preferred over sweep parameter adjustment because of the maintenance of a small relative time delay.

2.4 Frequency Domain Considerations

There are several detrimental effects that must be considered when using the OTFM technique. Among these are: the carrier 'chop-out' effect, and carrier broadening due to laser linewidth, and amplitude modulation. This section looks at the implications that these problems have on the frequency spectrum of a received carrier signal.

2.4.1 Chop-out Effect

It is apparent from Figures 2.2 and 2.3 that the signal IF is not constant over the whole sweep period. When the received IF is filtered, the frequencies that are out of band are removed, and thus the IF is periodically 'chopped out.' The resulting IF carrier is shown in Figure 2.6(a) for the sawtooth case. This waveform, denoted by $f_{IF}(t)$, can be obtained by the multiplication of a rectangular waveform, r(t) in Figure 2.6(b), by a continuous sinusoid, c(t) in Figure 2.6(c). That is

$$f_{IF}(t) = r(t) \cdot c(t) \tag{2.15}$$

where

$$r(t) = \sum_{n=0}^{\infty} u\left(t - n \cdot T_s\right) - u\left[t - (n+1) \cdot T_s + \Delta t\right]$$

and,

$$c(t) = \sin\left(2\pi \cdot f_{IF} \cdot t\right) \tag{2.16}$$

The power spectrum of the chopped out signal is the square of the convolution of the two Fourier transforms

$$S(f) = |R(f) * C(f)|^2 \tag{2.17}$$

where R(f) and C(f) are the Fourier transforms of r(t) and c(t), respectively. As shown in Figure 2.7 (note that the lines in this figure are separated by f_s), the effect on the received power spectrum is the replication of the IF signal at harmonics of the sweep frequency, f_s,

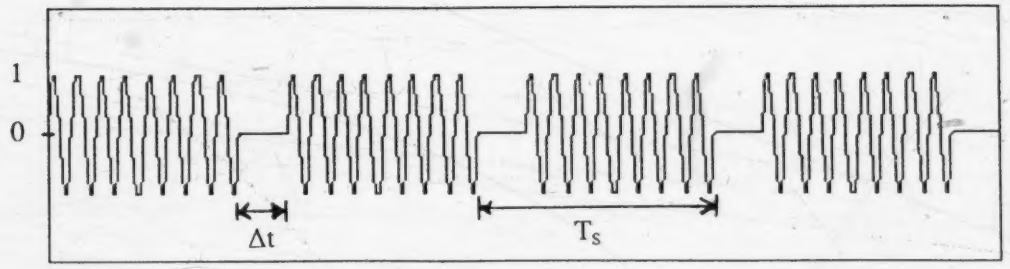

(a) $f_{IH}(t)$

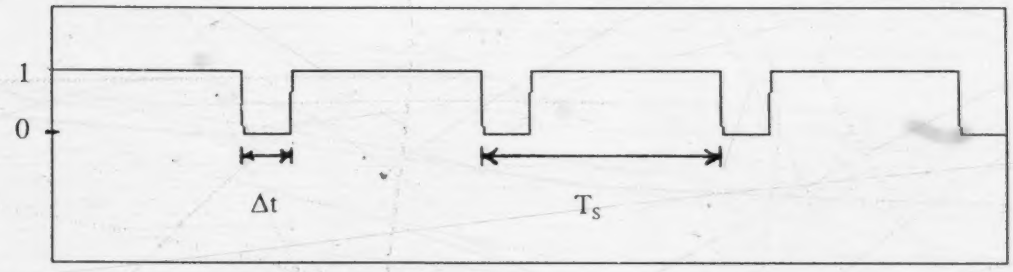

(b) r(t)

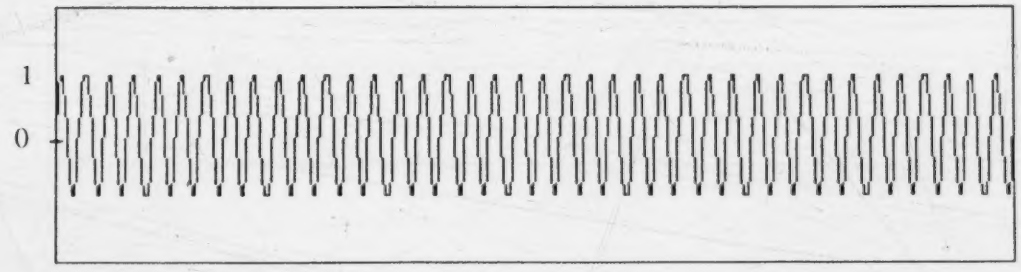

(c) c(t)

Figure 2.6. Construction of chopped out signal.

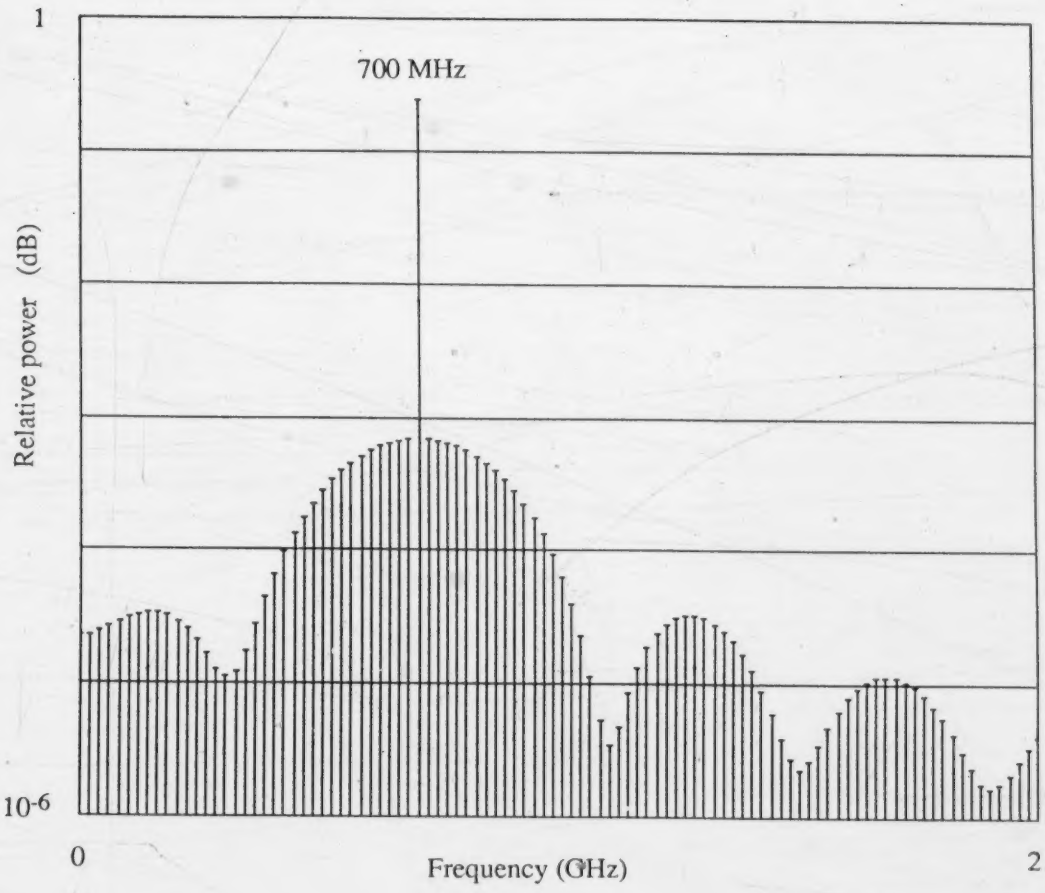

Figure 2.7. Effect of signal chop-out.

which causes interference at other nodes in the network. The shape of the spectrum, and thus the level of interference, is dependent on the relative values of Δt and T_s, which implies the imposition of an upper limit on the time delay and careful selection of channel separations.

To achieve an understanding of the level of interference caused by the chop-out effect, a simplified expression based on a Fourier series analysis [30] may be used. This analysis gives the power at the n^{th} harmonic of f_s as

$$P_n = \frac{1}{4 \cdot T_s^2} \cdot \left(\frac{1 - \cos\left[2\pi \cdot f_- \cdot (\Delta t - T_s)\right]}{(2\pi \cdot f_-)^2} + \frac{1 - \cos\left[2\pi \cdot f_+ \cdot (\Delta t - T_s)\right]}{(2\pi \cdot f_+)^2} \right),$$

where $$f_- = f_{IF} - \frac{n}{T_s}, \; f_+ = f_{IF} + \frac{n}{T_s}. \qquad (2.18)$$

Implicit in the derivation of this expression is the assumption that the signal is periodic with period T_s, which means that the phase of the carrier is assumed to be the same at the start of each period. This is, of course, an artificial situation, but the analysis is simple and gives a general picture of the severity of the chop-out effect.

Figure 2.7 was generated using the above expression along with the typical parameters f_{IF}=700 MHz, f_s=20 MHz, and Δt=2.5 ns ($\Delta t/T_s$=0.05), and shows that the components immediately on either side of f_{IF} are 25.6 dB below the level of the signal at f_{IF}, and components 10 harmonics away on either side are 29.5 dB below. Thus, for a signal-to-interference ratio (SIR) of about 30 dB, a channel separation of $10 \cdot f_s$ along with a maximum time delay of $0.05 \cdot T_s$ may be used. Further calculations show that a SIR of 20 dB results from a channel separation of f_s and a maximum time delay of $0.091 \cdot T_s$.

This seemingly stringent constraint can be somewhat alleviated in a system using the time delay insertion scheme by judicious design of Δt. Figure 2.8 shows the spectrum for $\Delta t = 0.1 \cdot T_s$. In this case, the spectrum goes to zero at frequencies which are a multiple of $10 \cdot f_s$ away from f_{IF}, and thus, if the system is designed with a channel separation of $10 \cdot f_s$, there will be little cross channel interference due the chop-out effect. Inband interference can be minimised by assuring that f_s>BW, where BW is the required message bandwidth.

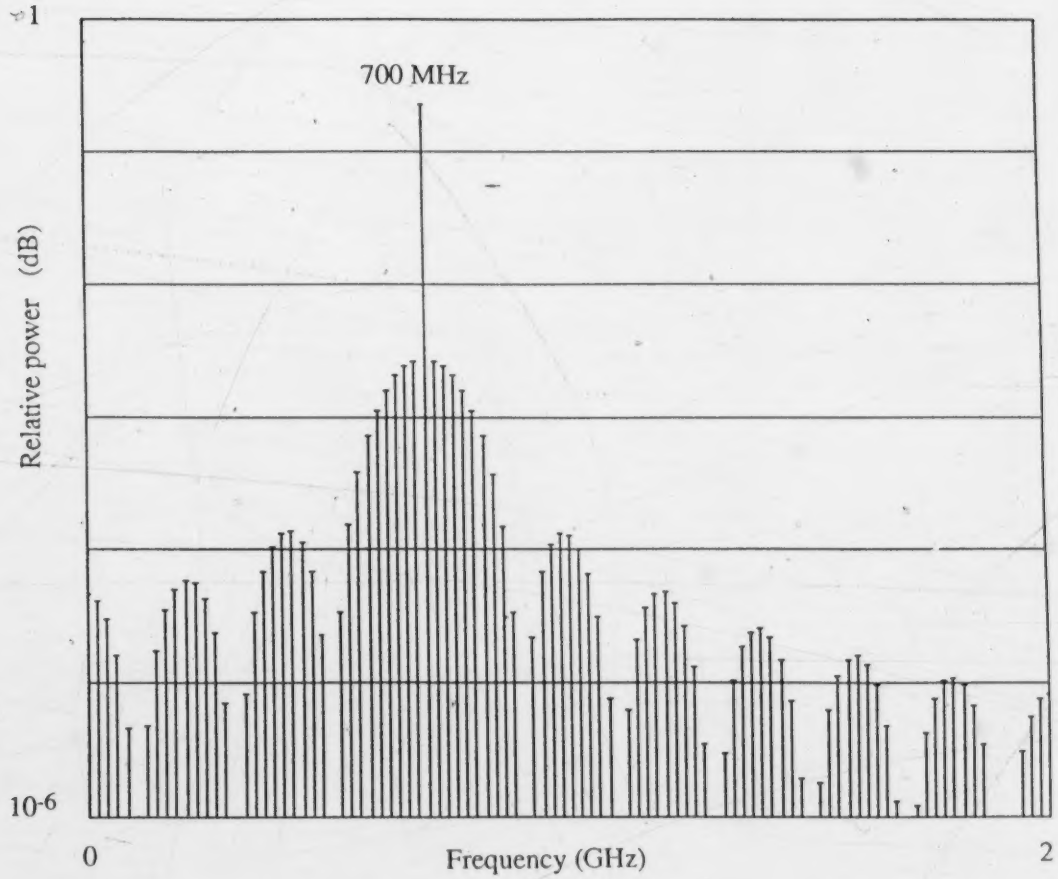

Figure 2.8. Effect of signal chop-out.

It is apparent by comparing Figures 2.2 and 2.3 that the chop-out signal for the triangle case has twice the frequency as that for the sawtooth case. The above discussions apply for the triangle if a factor of two is placed in front of f_s.

2.4.2 Laser Linewidth

A further frequency domain consideration is the broadening of the IF carrier due the laser linewidth. The dominant effect of laser linewidth is the addition of noise to the received signal, and thus the existence of a BER floor; in the absence of other noise sources, errors in the detection of the received message will still take place due to random fluctuations in the laser light. Kazovsky [31] has derived guidelines for linewidth-to-bit-rate ratios for various ASK, FSK, and differential PSK heterodyne systems. For example, a BER of 10^{-10} in a heterodyne ASK system with envelope postdetection requires a linewidth-to-bit-rate ratio of 0.18 or better.

Kikuchi and Okoshi [21] have obtained an expression describing the IF spectrum of a self-heterodyne signal due to laser linewidth. This expression reveals that the IF has a 3 dB spectral width equal to twice the laser linewidth when the relative time delay is much longer that the laser coherence time. If the relative time delay is shorter, then a narrow frequency component becomes dominant in the IF spectrum. This suggests that the use of the time delay insertion addressing scheme with a small relative time delay may result in a narrower IF, and thus a better BER.

2.4.3 Amplitude Modulation

Another mechanism causing broadening of the IF spectrum is the variation of light intensity (amplitude modulation or AM) due to modulation of the laser bias current. The effect of AM may be determined by analysing the factor, $M(t) \cdot M(t - \Delta t)$, in expression (2.6). This factor is given by

$$M(t) \cdot M(t - \Delta t) = \frac{2}{E_1 \cdot E_2} \cdot \sqrt{\frac{\mu}{\varepsilon}} \cdot \sqrt{P(t) \cdot P(t - \Delta t)} \tag{2.19}$$

where P(t) is the time varying optical power, and is given by

$$P(t) = P_0 - \frac{k_{am} \cdot \Delta i}{2} + \frac{k_{am} \cdot \Delta i}{T_s} \sum_{n=0}^{\infty} (t - n \cdot T_s) \cdot u(t - n \cdot T_s) \cdot u[(n + 1) \cdot T_s - t] \tag{2.20}$$

for the sawtooth case. In the above, P_0 is the dc light power, k_{am} is the differential AM efficiency of the laser (units of mW/mA), and Δi is the peak-to-peak amplitude of the sawtooth current waveform. The IF portion of the detector current in (2.6) is

$$i_{IF}(t) = R \cdot \sqrt{P(t) \cdot P(t - \Delta t)} \cdot \cos\left(2\pi \cdot f_{IF} \cdot t\right) \tag{2.21}$$

ignoring the constant phase terms and the polarisation mismatch factor.

Since it is difficult to find the Fourier coefficients of $i_{IF}(t)$ in this form, it is assumed that Δt is very small and can be ignored. The expression now becomes

$$i_{IF}(t) = R \cdot P(t) \cdot \cos\left(2\pi \cdot f_{IF} \cdot t\right) \tag{2.22}$$

The baseband Fourier coefficients are obtained from the Euler formulae as

$$a_0 = R \cdot P_0 ,$$

$$a_n = -\frac{R \cdot k_{am} \cdot \Delta i}{2\pi \cdot n} , \; n = 1, 2, 3, \ldots \tag{2.23}$$

Squaring these coefficients gives the relative power at harmonics of f_s. The numbers typical in the experiments of this thesis were: P_0=18 mW, R=0.45 A/W, k_{am}=0.78 mW/mA, and Δi=4.4 mA, from which

$$|a_0|^2 = 65.61 \text{ mA}^2, \text{ and } |a_n|^2 = \frac{0.05}{n^2} \text{ mA}^2$$

Thus, due to the high dc power and the relatively low AM depth, IF broadening due to unwanted AM is insignificant.

2.5 Determination of Maximum Network Size

For a network using the OTFM method there exists a maximum allowable size which depends on the particular scheme of addressing and the system parameters. This section deals with the optimum design of a system given constraints such as bit rate, channel separation, and laser frequency sweep width.

OTFM systems can be divided into two general categories according to the relationship between bit period and sweep period [22]. In what will be referred to as a type

A system, f_s is greater than or equal to the channel separation so that the harmonics of f_s are well out of band, while, in a type B system, the opposite is true and the harmonics fall within a receiver's allocated frequency band. In either case, it must be assured that the harmonics of f_s remain below some appropriate level to avoid interference between channels. The size constraints for each type are different and thus are derived separately. Derivations in this section assume that a sawtooth frequency sweep is used.

Some of the basic variables that will be used in this analysis are listed below:

f_s : sweep frequency,
T_s : sweep period ($=1/f_s$),
Δf : laser frequency sweep width,
R_b : bit rate,
T_b : bit period ($=1/R_b$),
$2 \cdot B W$: bandwidth of receiver IF filter,
Δt : time delay,
f_{IF} : intermediate frequency ,
f_{fb} : flyback frequency,
N_{max} : largest number of addressable nodes, or maximum size,
Δt_{max} : largest allowable time delay,
Δt_{min} : smallest resolvable time delay.

Some basic equations that will be used throughout are

$$BW = t \cdot R_b , \tag{2.24}$$

where t depends on the type of data modulation used,

$$f_{IF} = f_s \cdot \Delta f \cdot \Delta t , \tag{2.25}$$

for a sawtooth, and

$$N_{max} = \frac{\Delta t_{max}}{\Delta t_{min}} + 1 . \tag{2.26}$$

2.5.1 Type A Systems

In this type of system the signal at harmonics of f_s appear well out of the receiver band. This case is shown in Figure 2.9.

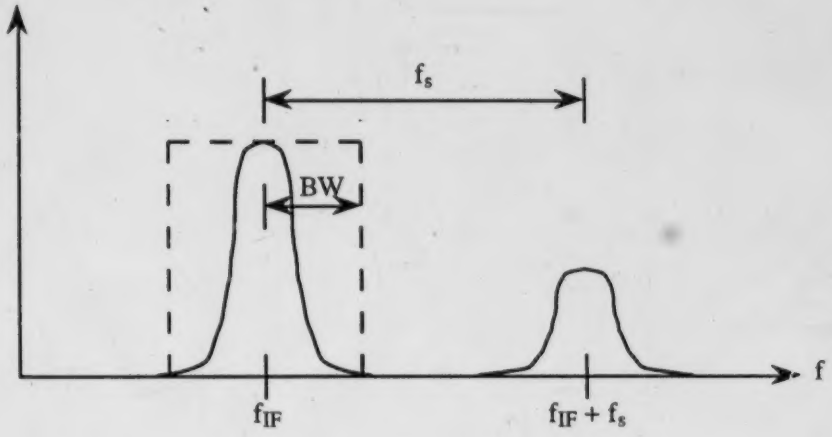

Figure 2.9. Type A spectrum.

It is clear that f_s must be at least twice the message bandwidth in order to avoid interference between adjacent channels, that is,

$$f_s \geq s \cdot BW \quad , \tag{2.27}$$

where

$$s \geq 2 \quad . \tag{2.28}$$

The derivations for maximum size differ for the various addressing schemes, and thus are divided accordingly.

2.5.1.1 Bandpass Filter Tuning and External Modulator Schemes

The minimum resolvable time delay for a type A system is that which corresponds to an IF separation of f_s, which, from expression (2.25), is given by,

$$\Delta t_{min} = \frac{f_s}{\Delta f \cdot f_s} = \frac{1}{\Delta f} \quad . \tag{2.29}$$

Maximum time delay for the bandpass filter tuning and external modulator schemes may be constrained by either electrical frequency considerations or time delay considerations. If the former is the case, then, from (2.25),

$$\Delta t_{max} = \frac{f_{max}}{\Delta f \cdot f_s}, \tag{2.30}$$

where f_{max} is the highest electrical frequency that either the receiver or external modulator is able to respond to. Using this along with (2.29) in (2.26), N_{max} becomes

$$N_{max} = \frac{f_{max}}{f_s} + 1 . \tag{2.31}$$

Obviously the size gets larger as f_s decreases. The smallest f_s for a type A system is obtained from (2.24) and (2.27) as

$$f_{s,min} = s \cdot t \cdot R_b , \tag{2.32}$$

which, when substituted into (2.31) gives

$$N_{max} = \frac{f_{max}}{s \cdot t \cdot R_b} + 1 . \tag{2.33}$$

To determine the maximum allowable time delay when time delay considerations impose the dominant constraint, refer back to Figure 2.2. It is clear that if the delay is longer than $T_s/2$, then f_{fb} becomes smaller than f_{IF}, and winds up in the same frequency slot that the difference frequency would for a particular time delay shorter than $T_s/2$. This results in an addressing ambiguity and must be avoided. Thus, the maximum time delay is given by,

$$\Delta t_{max} = g_s \cdot T_s = \frac{g_s}{f_s} \tag{2.34}$$

where

$$0 \le g_s < \frac{1}{2} \tag{2.35}$$

which, using equations (2.26), (2.29), and (2.32) gives a maximum size of,

$$N_{max} = \frac{g_s \cdot \Delta f}{f_s} + 1 = \frac{g_s \cdot \Delta f}{s \cdot t \cdot R_b} + 1 \qquad (2.36)$$

The above expression is similar to (2.33) and becomes the limiting case only when

$$f_{max} \geq g_s \cdot \Delta f \qquad (2.37)$$

Since Δf is the width of an optical sweep and can be tens to hundreds of GHz, (2.37) would not normally be true, and the size would be given by (2.33).

Another consideration is the relative delay between the two arriving message signals. It must be assured that the delay between arrivals of the same bit from the two paths is kept below some fraction, g_b, of the bit period

$$\Delta t_{max} = g_b \cdot T_b = \frac{g_b}{R_b}, \qquad (2.38)$$

where

$$0 \leq g_b < 1 \qquad (2.39)$$

With (2.26) and (2.29), this gives a maximum size of

$$N_{max} = \frac{g_b \cdot \Delta f}{R_b} + 1 \qquad (2.40)$$

which becomes the appropriate expression only when g_b is the more severe constraint. This occurs when (2.37) is true and

$$R_b > \frac{g_b}{g_s} \cdot f_s \qquad (2.41)$$

or, using (2.32),

$$g_b < \frac{g_s}{s \cdot t} \qquad (2.42)$$

The preceding discussion has been based on a sawtooth frequency sweep. If a triangle is used instead, f_{IF} doubles, which halves the minimum resolvable delay. However, Δt_{max} in equation (2.30) is also halved, leaving equations (2.31) and (2.33)

unchanged. Expressions (2.36) and (2.40) are modified to describe the triangle case by placing a factor of two in front of g_s and g_b, respectively. Note also that (2.35) becomes

$$0 \le g_s < \frac{1}{4} \tag{2.35a}$$

for the triangle wave.

2.5.1.2 Sweep Width Alteration

Maximum addressable size for the sweep width alteration scheme is derived in a manner similar to that of the previous section, but with an additional consideration. Since Δf is being altered according to receiver address, and, from (2.29), the minimum resolvable time delay is dependent on Δf, one must take into account the worst case address.

As before, the largest time delay allowed will depend on whether the system is sweep period limited or bit period limited, as decided by equation (2.41) or (2.42). First let us consider the former, in which case the maximum delay is given by (2.34).

The smallest required sweep width is, from (2.25),

$$\Delta f_{min} = \frac{f_{IF}}{\Delta t_{max} \cdot f_s} \tag{2.43}$$

Using the above and expression (2.34),

$$\Delta f_{min} = \frac{f_{IF}}{g_s} \tag{2.44}$$

From (2.26), (2.29), and (2.43), the maximum size is

$$N_{max} = \frac{f_{IF}}{f_s} + 1 \tag{2.45}$$

The intermediate frequency, f_{IF}, can be found from equations (2.25), (2.29), (2.43), and (2.44) as

$$f_{IF} = \sqrt{g_s \cdot \Delta f \cdot f_s} \tag{2.46}$$

where Δf is the largest sweep width obtainable from the laser. From this and (2.45),

$$N_{max} = \sqrt{\frac{g_s \cdot \Delta f}{f_s}} + 1 = \sqrt{\frac{g_s \cdot \Delta f}{s \cdot t \cdot R_b}} + 1 \qquad (2.47)$$

By comparing expression (2.47) with (2.36), it is apparent that the maximum size is degraded by using this type of addressing.

The derivation for the bit period limited case, where (2.42) is true, is very similar to the above, and the final result is

$$N_{max} = \sqrt{\frac{g_b \cdot \Delta f}{R_b}} + 1 \qquad (2.48)$$

Again, by comparing (2.48) to (2.40), it is found that the network size is degraded.

2.5.1.3 Sweep Frequency Alteration

As in the sweep width alteration case, addressing by sweep frequency alteration requires an additional consideration when determining the maximum network size. Since the sweep frequency is being altered, expression (2.34) must be remain true for the highest required f_s.

Assuming the system is sweep period limited, the worst case maximum time delay from (2.34) is

$$\Delta t_{max,wc} = \frac{g_s}{f_{s,max}}, \qquad (2.49)$$

where $f_{s,max}$ is the f_s required to address the receiver with the smallest time delay, and is obtained from (2.25) and (2.29) as

$$f_{s,max} = f_{IF}. \qquad (2.50)$$

The maximum size becomes, from (2.26), (2.29), (2.49), and (2.50),

$$N_{max} = \frac{g_s \cdot \Delta f}{f_{IF}} + 1 \qquad (2.51)$$

Calculation of f_{IF} is achieved by inserting the smallest sweep frequency, $f_{s,min}$, into (2.46):

$$f_{IF} = \sqrt{g_s \cdot \Delta f \cdot f_{s,min}} \quad (2.52)$$

Substitution of (2.52) into (2.51) results in

$$N_{max} = \sqrt{\frac{g_s \cdot \Delta f}{f_{s,min}}} + 1 = \sqrt{\frac{g_s \cdot \Delta f}{s \cdot t \cdot R_b}} + 1 \quad (2.53)$$

The above expression is identical to (2.47), which demonstrates the parallelism between the two sweep parameter alteration cases.

In the bit limited case of sweep frequency alteration, the maximum size is simply given by (2.40). However, a system is only bit limited when the condition (2.41) is true for $f_{s,max}$. It can be shown that (2.41) becomes

$$R_b > \frac{s \cdot t \cdot \Delta f \cdot g_b^2}{g_s} \quad (2.54)$$

Since Δf is normally very large, a sweep frequency altered system may only be bit limited for very high bit rates.

2.5.2 Type B Systems

The analyses in this section pertain only to the time delay constraints in the bandwidth tuning and external modulator addressing schemes. The derivations for sweep parameter alteration are omitted since B type systems will be shown to be inferior to type A systems.

Each channel in a type B system is allocated a frequency band that is wide compared to f_s. In other words, the replications of the message at harmonics of f_s occur within the channel allocation band, as shown in Figure 2.10.

The sweep frequency is

$$f_s < s \cdot BW \quad (2.55)$$

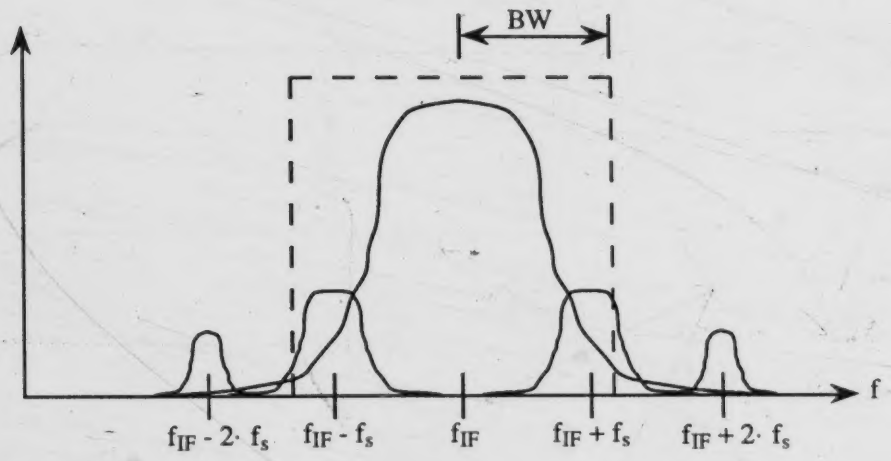

Figure 2.10. Type B spectrum.

The smallest resolvable time delay in this case is obtained from equation (2.25) and the channel separation, $s \cdot BW$, as

$$\Delta t_{min} = \frac{s \cdot BW}{\Delta f \cdot f_s} = \frac{s \cdot t \cdot R_b}{\Delta f \cdot f_s} \tag{2.56}$$

The maximum allowable time delay is determined by a procedure similar to that for type A. First, consider the bit period, which gives a constraint of

$$\Delta t_{max} = g_b \cdot T_b = \frac{g_b}{R_b} \tag{2.57}$$

where g_b is a fraction as given by (2.39). Using (2.56) and (2.57) in (2.26), the maximum size is found to be

$$N_{max} = \frac{g_b \cdot \Delta f \cdot f_s}{s \cdot t \cdot R_b^2} + 1 \tag{2.58}$$

This shows that an increase in the bit rate in the B system incurs a double penalty on the size. This can be made less severe, however, if f_s is scaled with R_b. That is, if it is assured that

$$f_s = m_b \cdot R_b \,, \quad m_b < s \cdot t \tag{2.59}$$

which gives

$$N_{max} = \frac{g_b \cdot m_b \cdot \Delta f}{s \cdot t \cdot R_b} + 1 \qquad (2.60)$$

Note that the N_{max} in this expression becomes larger as $m_b \rightarrow s \cdot t$, which is the point where the system becomes type A. At the limit, $m_b = s \cdot t$, the expression for N_{max} becomes identical to equation (2.40). This fact suggests that the bit limited B system is inferior to the bit limited A system from the point of view of network size maximisation.

As in the type A system, the sweep limited case must also be considered. The time delay constraint is again some fraction, g_s, of T_s

$$\Delta t_{max} = g_s \cdot T_s = \frac{g_s}{f_s} . \qquad (2.61)$$

This gives the maximum size as,

$$N_{max} = \frac{g_s \cdot \Delta f}{s \cdot t \cdot R_b} + 1 \qquad (2.62)$$

which is identical to expression (2.36).

Expression (2.62) becomes the limiting case when

$$R_b < \frac{g_b}{g_s} \cdot f_s . \qquad (2.63)$$

If the type B system is sweep limited, there exists the possibility of a size advantage over the type A system. Since signal replications due to the chop-out effect appear with a separation smaller than the channel separation, cross-channel interference is less severe. In fact, if the adjacent channels appear at spectral zeros, the cross-channel interference is very small. In type A systems, the first harmonic away from f_{IF} is in the band of the adjacent channel, while in type B systems, it appears in between channels as long as

$$BW < f_s \leq (s - 1) \cdot B W . \qquad (2.64)$$

Since the first harmonic away does not occur in the receiver band, the constraint on the value of g_s may be less severe than in the type A system. To determine the conditions for

remaining sweep limited while taking advantage of the relaxation of g_s, expression (2.63) is applied. For maximum bit rate, f_s must be at its largest value, which is given by (2.64) as $f_s = (s - 1) \cdot BW$. Using this and expressions (2.63) and (2.24) it is found that the condition for a sweep limited system is

$$g_b > \frac{g_s}{(s - 1) \cdot t} \tag{2.65}$$

Since s is typically fairly large (see Table 1.1), this will likely hold true for even for large values of g_s.

The next logical question is how much can g_s be relaxed. Knowing that the component falling into the adjacent channel band might now be the second harmonic away from f_{IF}, the largest allowable Δt must be found such that cross-channel interference is acceptable. The criterion for acceptable interference is chosen to be a SIR of 20 dB. The spectrum was calculated using (2.18) for various values of g_s, and it was found that g_s=0.095 met the above criterion. In Section 2.4.1, it was determined that g_s=0.091 resulted in a SIR of 20 dB when the first harmonic away was considered. In light of these results, it can be stated that the size improvement is in fact small.

The analyses in this section have shown that the type B system affords little or no size advantage over the type A system. The only problem with the type A system is the practical problem of generating a high frequency triangle or sawtooth wave. This problem may ultimately limit the bit rate obtainable with an OTFM system.

2.5.3 Comparison of Schemes

Plots of expressions (2.33), (2.36), and (2.53) appear in Figure 2.11 for $s \cdot t$=10, g_s=0.1, f_{max}=3 GHz and 15 GHz, and Δf=40 GHz and 200 GHz. The separation of 10 was chosen upon consideration of the channel separation guidelines introduced in Section 1.1. Since the signal at the receiver appears as an ASK signal, the separation of $9.5 \cdot R_b$ applies, and it was decided to exceed that guideline slightly for a safety margin. With this separation and the g_s of 0.1, expression (2.42) is likely to be false (g_b would have to be smaller than 0.01, which is unlikely), and thus the system is sweep limited. The f_{max} of 15 GHz is applicable to the external modulator scheme when using one of the BT&D phase modulators [29] whose modulation bandwidths are 15 GHz.

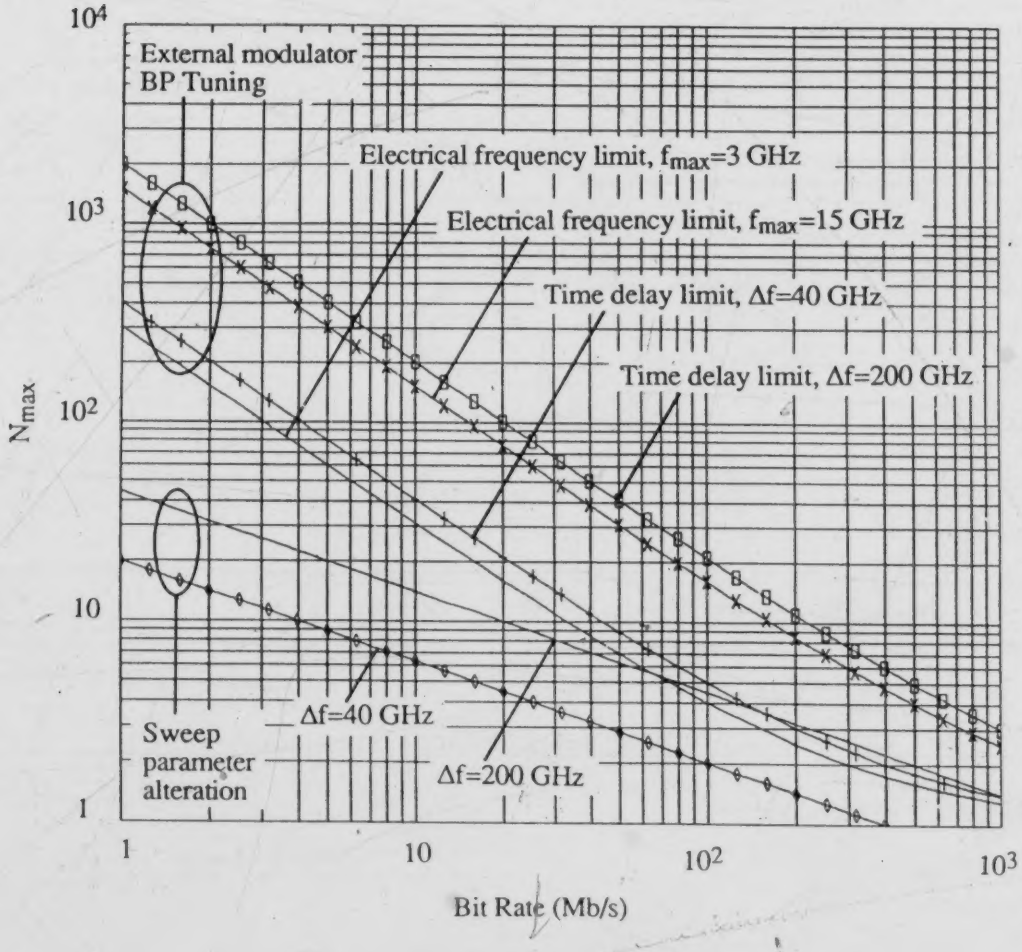

Figure 2.11. Comparison of sizes of addressing schemes.

Note from the figure that the bandpass filter tuning and external modulator schemes are more likely to be limited by electrical frequency constraints than by the time delay constraints. Note also that the sweep parameter alteration schemes allow smaller sizes at lower bit rates, but become better than the others at approximately 65 Mb/s. This occurs because the size for sweep parameter alteration is proportional to $1/\sqrt{R_b}$, while the other sizes are proportional to $1/R_b$.

2.5.4 Delay Insertion

If time delay insertion is used, then the relative delay between the two signal arrivals is constant, and the network is constrained by neither sweep nor bit period. Instead, network size is limited by either fibre dispersion or power budget considerations.

A quick calculation can determine the severity of dispersion. The fibre dispersion parameter for short wavelengths is typically 100 ps/nm/km. First of all, linewidths of the lasers used in this thesis are much less than 0.001 nm, so this gives an rms pulse spread of less than 0.1 ps/km. The second thing to consider is the shift in wavelength due to the frequency sweep. A sweep width of 20 GHz is a shift in wavelength of approximately 0.05 nm for 840 nm lasers. This sweep width corresponds to a minimum resolvable time difference of 50 ps, and a pulse spread of 5 ps/km. Given that this application is a LAN and will have a reach of a few kilometers at most, it is expected that dispersion will not be a limiting factor.

Power budget calculations depend heavily on the particular choice of network topology, and so this topic is reserved for Chapter 3 after topological considerations are discussed.

2.6 Summary

In summary, OTFM uses propagation time differences between dual network paths as addresses. To detect these differences, optical FMCW ranging is employed, which produces a message carrier whose frequency is proportional to the relative delay between transmitting and receiving nodes. Since optical frequencies are typically on the order of hundreds of terahertz (359 THz for 836 nm) and can be swept over a large frequency range (hundreds of GHz), IFs may be very high. Thus, OTFM offers more efficient utilisation of the wide bandwidth available with optical fibre. Since the received signal may be in the electrical frequency regime, very sharp electrical filters may be used, providing channel selectivity.

Section 2.3 discussed several addressing alternatives in the implementation of an OTFM system. It was pointed out that the optical delay insertion scheme may be the best alternative, but may also be the most difficult of the schemes to implement.

Three deleterious frequency domain effects were discussed in Section 2.4. It is believed that IF spectrum broadening due to laser linewidth, which limits the BER achievable, is a more severe problem than either the chop-out effect or amplitude modulation, which can both be controlled by appropriate system design.

In Section 2.5, it was found that an A type system generally allows a size advantage over the B type system. We also found that addressing by sweep parameter adjustment causes network size reduction as compared to either the bandpass filter tuning or external modulator schemes, but only for low bit rates. Finally, it was stated that a network using addressing by delay insertion has a size limit imposed only by power budget considerations.

CHAPTER 3

TOPOLOGICAL CONSIDERATIONS

Issues relating to the network layout, or topology, are discussed in this chapter. Several topological variations are presented along with their advantages and disadvantages, and the problem of addressing ambiguities in two of these topologies is discussed. Finally, power budgets for the various topologies are analysed.

3.1 Survey of Network Topologies

There are numerous ways of providing the dual signal paths in a network employing the OTFM method [22]. This section reviews the advantages and disadvantages of a number of the possible network topologies. Throughout this section, reference will be made to a quantity called 'network efficiency.' Network efficiency, η, is defined as the number of uniquely addressable nodes, N, divided by the potential network size, N_{max}, as defined by expression (2.26) in Section 2.5

$$\eta = \frac{N}{N_{max}} \cdot 100\% \qquad (3.1)$$

The value of η is different for each topology, and is one measure of the desirability of the topology.

3.1.1 Central Loop

The central loop topology is possibly the most obvious of network configurations. This topology, shown in Figure 3.1, consists of a ring of fibre with signals tapped off from each direction using couplers with a coupling ratio of r. A 3 dB coupler serves to combine the two signals into the receiver, and divide the signal from the transmitter. The time delay difference is given by

$$\Delta t = |t_1 - t_2| \qquad (3.2)$$

where t_1 and t_2 are the propagation times in paths 1 and 2, respectively.

The advantage of this topology is that the received signal power is constant irrespective of the relative positions of the transmitting and receiving nodes (this will become apparent in Section 3.3 when the power budget for this topology is analysed).

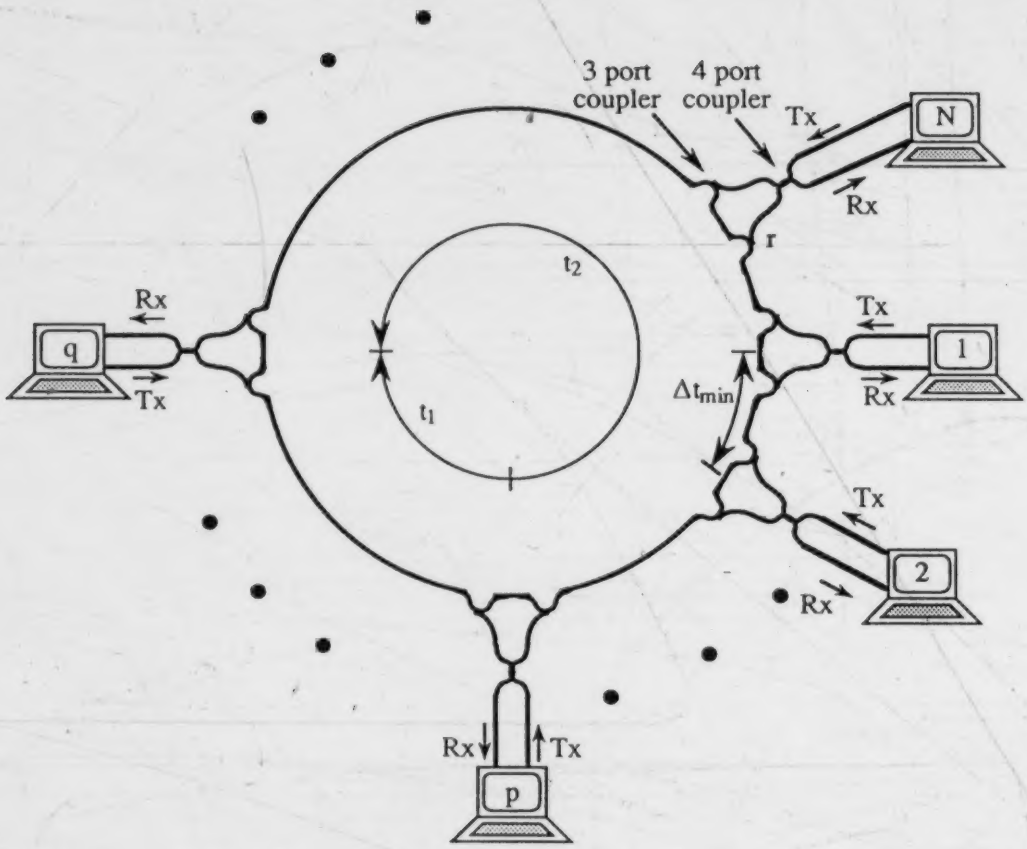

Figure 3.1. Central loop topology.

Constant signal power level is desirable in a communication system since signal-to-noise ratios remain the same for all received signals.

The disadvantages inherent in this topology are unfortunately numerous. First, light launched into the loop circulates around indefinitely, which adds to the noise at each receiver. This problem, however, may not be too serious since the 'second-time-around' signals will have experienced considerable network loss, and thus may be sufficiently extinguished.

Second, there exist addressing ambiguities in a central loop network. These occur at receivers that are equidistant in either direction from the transmitting node. Since the detection process produces an IF equal to the absolute value of the difference between the two signal frequencies, the receiver at each of these equidistant points sees an identical signal, and may be erroneously addressed. As will be shown in Section 3.2, this problem reduces the number of addressable nodes in a central loop network, thus decreasing the network efficiency.

A third disadvantage is that a central unit containing the central addressing loop may be required. Since the distances between adjacent stations must be carefully selected to control channel separation, and the actual node separations may be required to be much larger than these distances, it may be advantageous to contain the addressing unit at a central location and run arbitrarily long lines to each node. More fibre is thus required to connect all nodes to this central unit. On the other hand, this may be favorable since the addressing unit may be made secure so that, in the event of a broken fibre, only one node is out of service instead of the whole system.

3.1.2 Bus

A topology that is related to the central loop is the bus, shown in Figure 3.2. It consists of two fibre loops, one of which contains delay elements between nodes. One signal is coupled onto each of the loops, and they propagate in the same direction. One unit of delay is added to one signal as the signals pass each node, and the relative time delay difference for transmission from node p to node q is

$$\Delta t_{p \to q} = (q - p) \cdot \Delta t_{min} \quad , 1 \leq p < q \leq N, \tag{3.3}$$

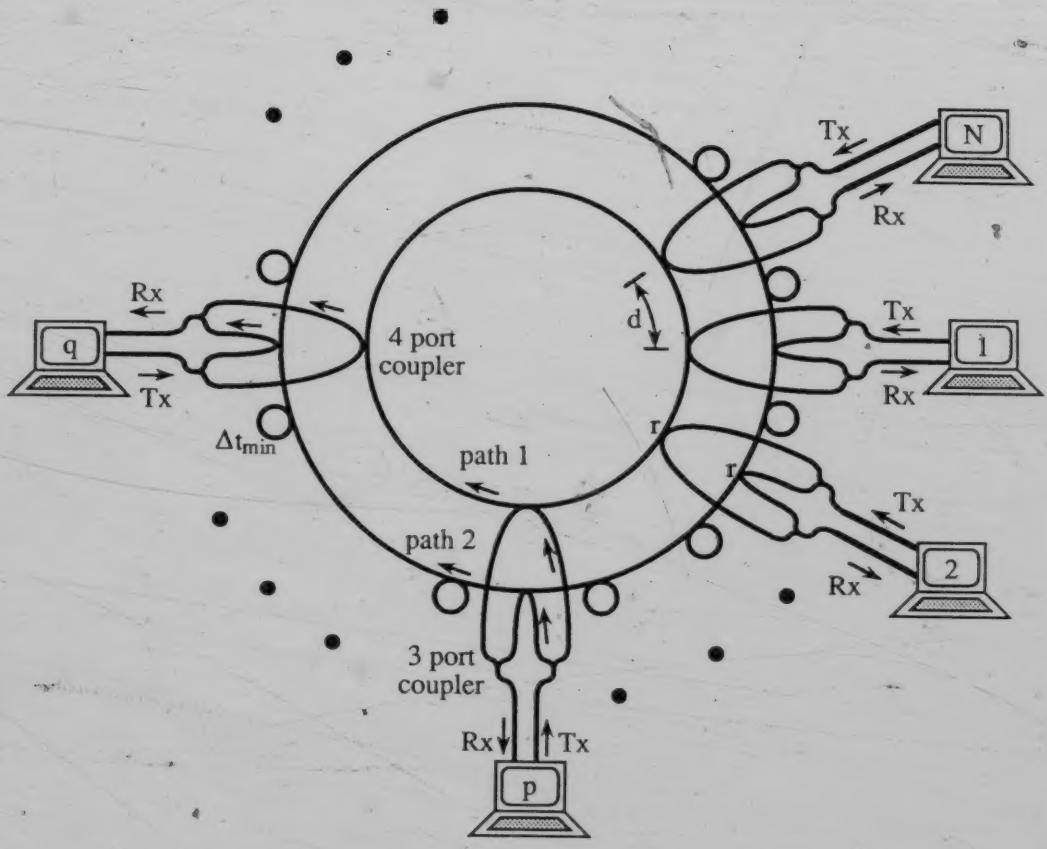

Figure 3.2. Bus topology.

where p is the position of the transmitting station, q is the position of the receiving station, N is the number of nodes in the network, and Δt_{min} is the minimum resolvable time delay as given by (2.29). If the roles of p and q are interchanged, that is q transmits and p receives, then Δt becomes

$$\Delta t_{q \to p} = (N - q + p) \cdot \Delta t_{min} \quad (3.4)$$

The primary advantage of this layout is that addressing ambiguities are eliminated, which means most efficient use of addressable space. In fact, since the number of addressable nodes is equal to the potential size, the network efficiency is 100%.

A second advantage is that, although signals do repropagate around the two loops, relative delay accumulates with each complete circulation so that interfering signals become higher and higher in frequency, and thus are not seen by any receiver.

Thirdly, no central addressing unit is required since the delay elements can be located at each node, and the two lines between nodes may be as long as necessary, providing they are of identical length. If, in this case, a fibre is cut at any point, not all one way communications are interrupted, but two way communications are. The bus may be made more robust by placing the addressing loop in a central secure unit.

There are a couple of problems inherent in this topology. Signals accumulate loss as they propagate around the loop which means signal levels depend on the relative positions of transmitter and receiver. Secondly, more fibre and couplers are required than in certain other topologies, which increases cost.

3.1.3 Double Star

The double star is constructed by 'piggy-backing' two star couplers as shown in Figure 3.3. One star coupler splits the light into a set of equal length reference paths, and the other splits the light into paths containing various delays. Delays range from 0 to $(N-1)\cdot\Delta t_{min}$. Here, Δt for communication between nodes p and q is

$$\Delta t = (p + q - 2) \cdot \Delta t_{min} \quad (3.5)$$

This topology has these advantages: no addressing ambiguities, equal signal power at all receivers, and no signal repropagation problem.

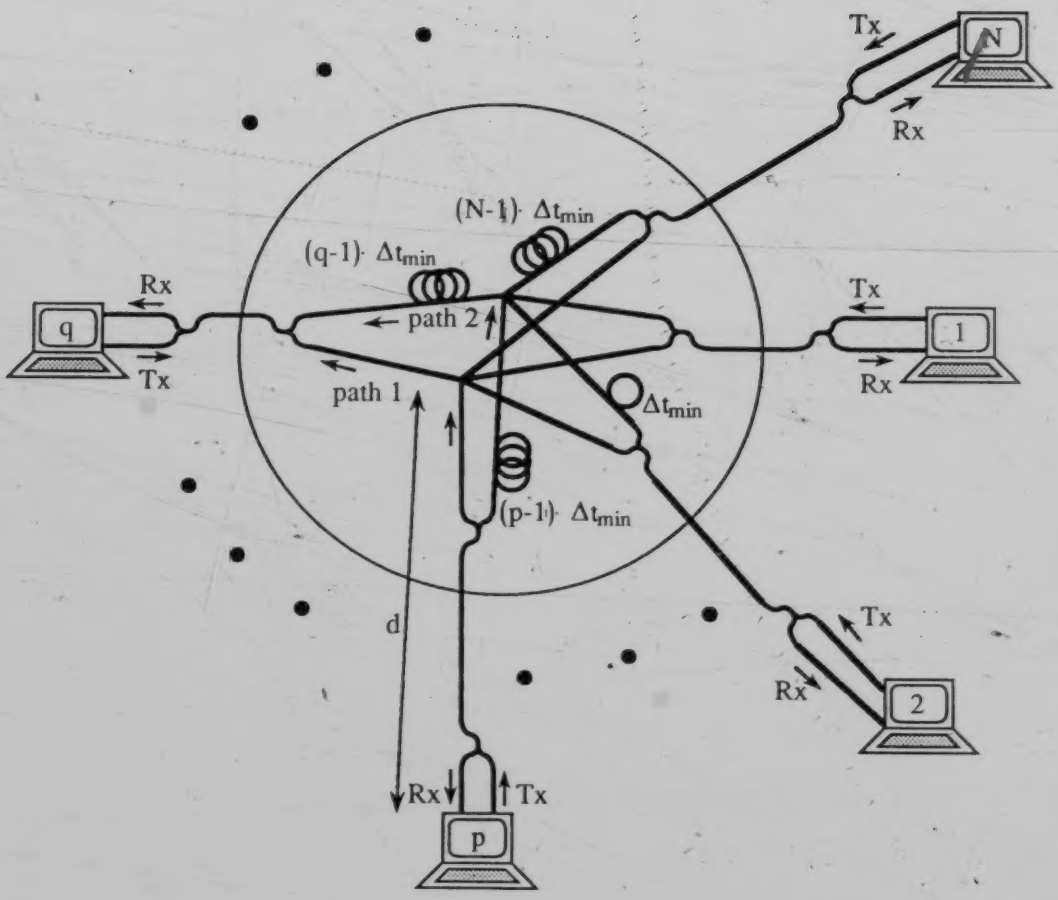

Figure 3.3. Double star topology.

Network efficiency of the double star is a function of the number of nodes in the network. For a network having N nodes, the largest time delay is that corresponding to communication between the N^{th} and $(N-1)^{th}$ nodes, and is equal to

$$\Delta t_{max} = [N + (N - 1) - 2] \cdot \Delta t_{min} = (2 \cdot N - 3) \cdot \Delta t_{min} \qquad (3.6)$$

where Δt_{min} is the minimum resolvable time delay as discussed in Chapter 2. The maximum size as given by (2.26) is thus

$$N_{max} = 2 \cdot N - 2 \qquad (3.7)$$

and the network efficiency is

$$\eta = \frac{N}{2 \cdot N - 2} \cdot 100\% \qquad (3.8)$$

Note that this quantity decreases to 50% as the network becomes increasingly large. The efficiency of the double star network is higher than that for the central loop topology for large networks, but decreases quickly to half that of the bus topology.

One disadvantage of this topology is that a central addressing unit is required and all stations require a fibre run.

3.1.4 Folded Ring

The folded ring of Figure 3.4 is a rearrangement of the central loop topology that eliminates the addressing ambiguity problem. Here, the two signals are injected into the ring at symmetric points, and travel towards each other. A delay, T_d, is added at one end in order to ensure the elimination of addressing ambiguities. T_{net} is the total network delay excluding T_d, and is given by

$$T_{net} = N \cdot \Delta t_{min} . \qquad (3.9)$$

As in the bus topology, Δt depends on the the direction of data transmission. If, in Figure 3.4, p is the transmitter and q is the receiver, then

$$\Delta t_{p \to q} = (N - q) \cdot \Delta t_{min} + T_d \qquad (3.10)$$

and

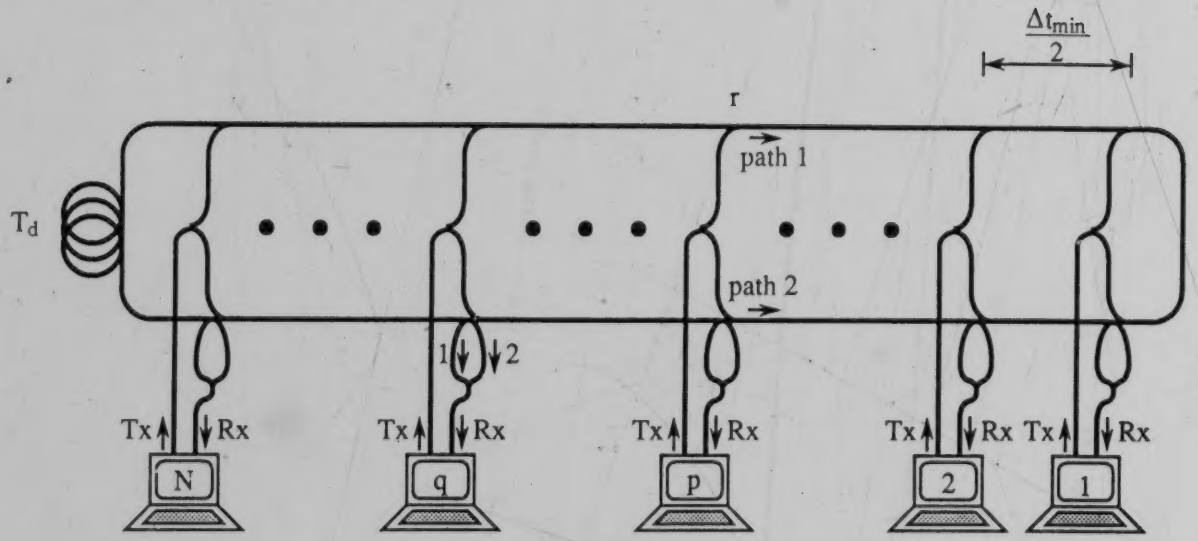

Figure 3.4. Folded ring topology.

$$\Delta t_{q \to p} = p \cdot \Delta t_{min} \qquad (3.11)$$

if their functions are reversed. Note that, in both cases, the relative time delay, and thus the address, is dependent only on the position of the intended receiver.

It is apparent from (3.10) and (3.11) that, in order for ambiguities to be avoided,

$$T_d = T_{net} = N \cdot \Delta t_{min} \qquad (3.12)$$

is the smallest allowable value for T_d. The largest time delay in the network occurs when p is transmitting to q, and q=1, and is given by (3.10) as

$$\Delta t_{max} = \left(\Delta t_{p \to q}\right)_{q=1} = \left(2 \cdot N - 1\right) \cdot \Delta t_{min} \qquad (3.13)$$

From (3.1), (2.26), and (3.13), the efficiency is found to be 50%, and independent of N.

The primary advantage of this topology is the absence of addressing ambiguities. A further advantage is the fact that the address of each node is the same regardless of the position of the transmitter. This simplifies the design of the transmitters since a node need not know its own position in the network to perform addressing.

The folded ring topology suffers from signal repropagation and must have a centralised addressing unit. As well, received signal power is not constant.

3.1.5 Ladder

The ladder network is a modification of the folded ring. In Figure 3.5, the left end of the network is terminated in a node instead of allowing the signal to repropagate around. The relative time delay for transmission between nodes p and q is

$$\Delta t = (q - p) \cdot \Delta t_{min} \quad , 1 \le p < q \le N \qquad (3.14)$$

The signal repropagation problem is eliminated in this network, but addressing ambiguities reappear. Fortunately, as will be shown in Section 3.2, the ambiguities can be more economically overcome in the ladder than in the central loop. The network efficiency is also obtained in Section 3.2.

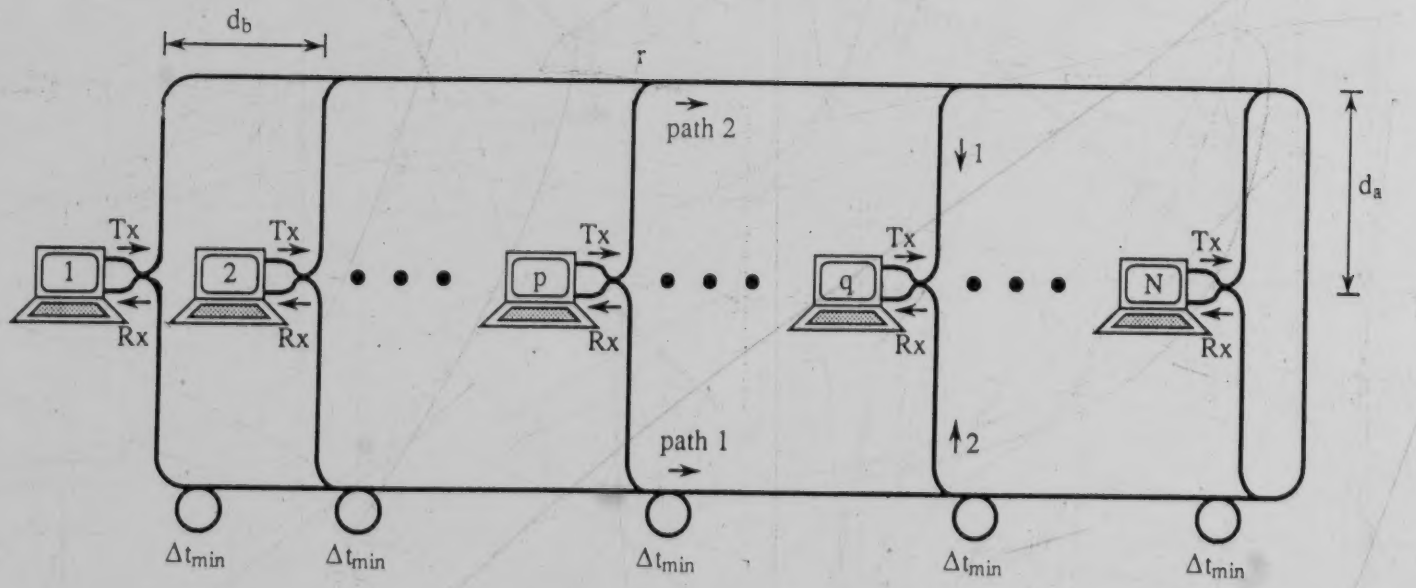

Figure 3.5. Ladder topology.

As in the bus network, no central addressing unit is required since delays may be located at each node. This network may be considered more robust than the bus since, if a fibre is broken in the ladder, only those nodes to the left (in Figure 3.5) of the break are placed out of service; those to the right may still communicate amongst themselves. The problem of non-uniform signal power is unfortunately present once more.

3.1.6 Summary

The advantages and disadvantages of various topologies were outlined in the preceding sections. Table 3.1 summarises the above discussions.

	Central Loop	Bus	Double Star	Folded Ring	Ladder
Signal Repropagation	Y	Y	N	Y	N
Constant Received Power	Y	N	Y	N	N
Addressing Ambiguities	Y	N	N	N	Y
Distributed	N	Y	N	N	Y
Network Efficiency	5	1	2	3	4
Robustness	4	3	1	3	2

Table 3.1. Summary of network topologies.

The question of distributed versus centralised networks requires some explanation. While all of these networks may be configured with a central addressing unit, only the bus and ladder networks may be distributed regardless of the value of Δt_{min}. If, however, Δt_{min} is large enough to allow practical node separation, then the central loop and folded ring networks may also be distributed. The double star can only be a centralised network.

Network efficiency of the topologies is ranked from best to worst, a rank of 1 denoting the best. The ranking is apparent from Figure 3.6, which contains plots of network efficiency versus addressable size for the double star, central loop, and ladder topologies. (Network efficiencies for the central loop and ladder networks are obtained in Section 3.2.) The central loop and ladder are more efficient than the folded ring for very

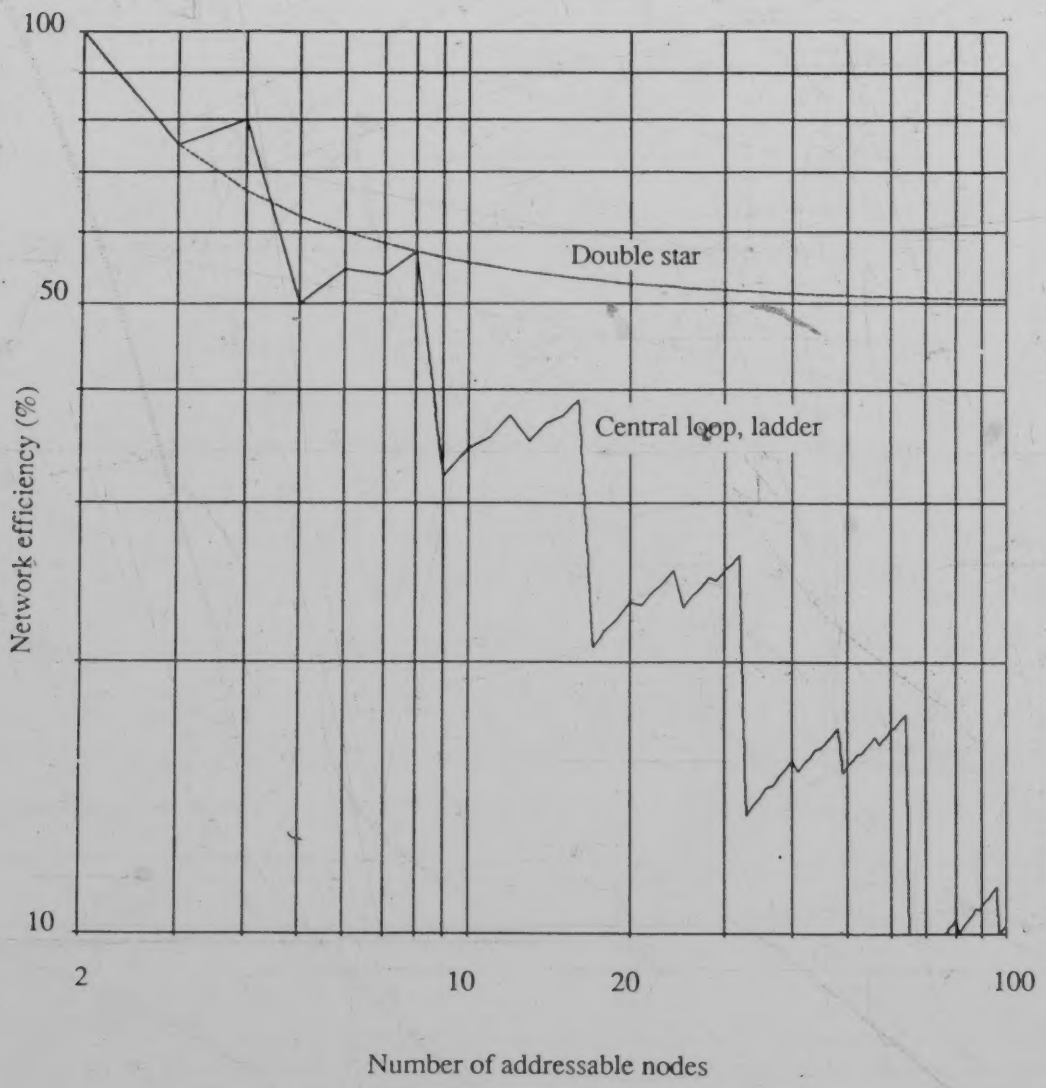

Figure 3.6. Network efficiencies.

small networks, but become highly inefficient as the network size increases. The efficiencies for central loop and ladder appear to be the same in this plot, but, as will be explained in Section 3.2, the central loop suffers addressing ambiguities at certain sizes where the ladder does not.

Another entry in Table 3.1 is the robustness of the networks, which concerns the degree to which each are affected by fibre breaks. If the networks are compared in their centralised configuration, then all are equivalent since the more vulnerable fibre lines are those emanating from the central unit, and in this case, a broken fibre affects only one node. The table, however, compares the robustness of the networks assuming they may be distributed. It is obvious that the central loop is the worst since a fibre broken in the ring brings down the whole system. The double star is ranked the best since it can in fact only be a centralised topology. In the ladder, a broken fibre still may allow two-way data transmission between certain nodes, while in both the bus and folded ring, only one-way transmission remains intact.

In light of the issues discussed in this section, it is believed that the double star topology is the best choice if the use of a network with a central addressing unit is acceptable. If, however, a central unit is to be avoided, then the bus network becomes the optimum choice.

3.2 The Asymmetry Problem in the Central Loop and Ladder Networks

A severe problem with the central loop and ladder networks is the existence of addressing ambiguities. Ambiguities occur when there are two or more nodes that have the same distance address with respect to a transmitting node. This occurs at points equidistant in either direction from the transmitting node; in other words, ambiguous addresses are symmetries about a node. To avoid an ambiguity, no node is allowed at one of the pair of symmetric points. This has the effect of reducing the number of addressable nodes in a network. This section looks at the creation of asymmetric networks, with emphasis on the ladder topology.

An asymmetric ladder can be built using an intuitive algorithm. First, start with a node, denoted by a filled circle, at the far left of the ladder, as shown in Figure 3.7. There are an infinite number of slots, denoted by open circles, (and which are separated by the minimum resolvable time delay) to the right where a second node may be placed. If a node

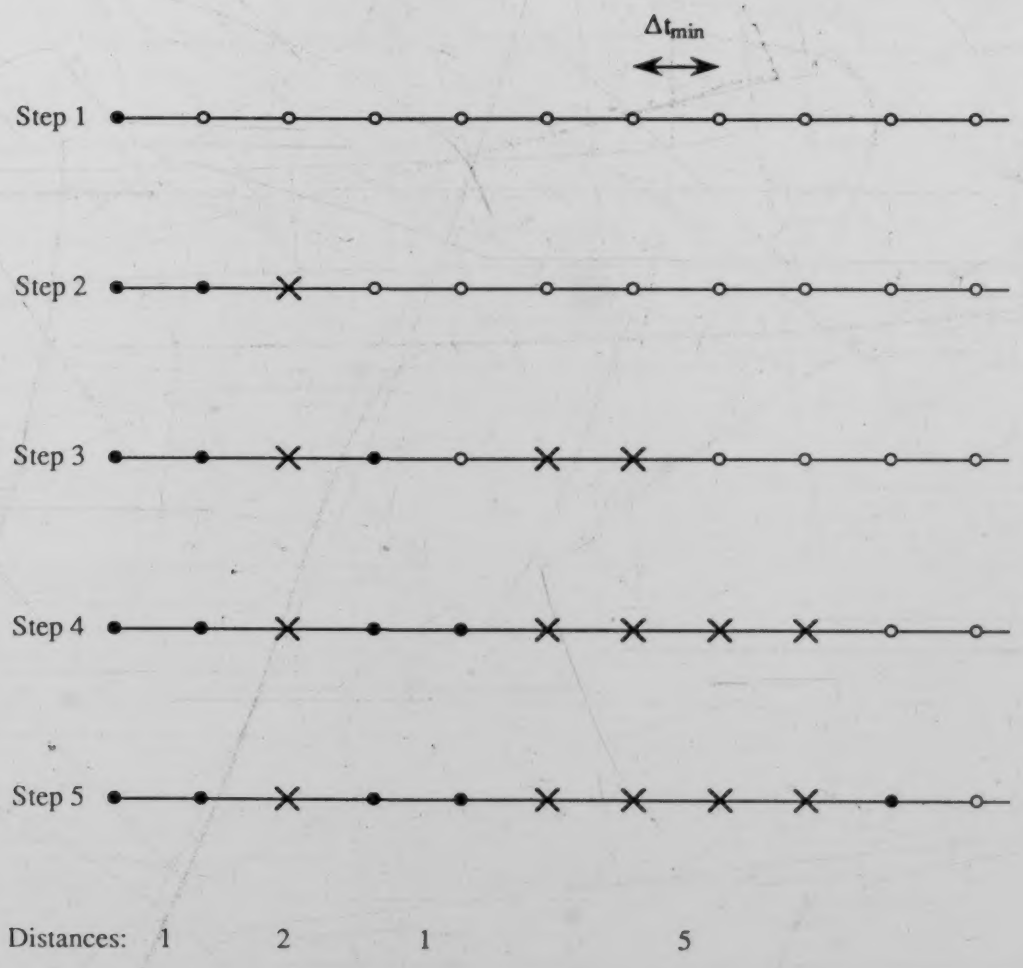

Figure 3.7. Asymmetric network generation algorithm.

is placed immediately to the right of the first one, there is a slot, denoted by the X, where a node is disallowed by symmetry. In step 3, a node is placed at the next available slot, and all symmetries to the right are disallowed. This procedure is continued until a network of the desired size is obtained. The numbers at the bottom of this figure denote the number of slots in between allowed nodes. It turns out, as one might expect, that the fields of disallowed slots become larger as the network grows. Thus, the network efficiency as defined by expression (3.1) decreases as the network size increases.

In the above example a node had always been placed at the first available slot. It is possible to obtain different networks by skipping available slots. A pair of APL functions (the listings of which appear in Appendix A) were written to create large networks, and included a variable vector (termed the 'skip vector') to define the pattern of slot-skipping. Networks were generated for many different skip vectors, but it turned out that the first network, the one for which no slot-skipping took place, always had the largest number of allowed nodes. Although it was impossible to calculate every possible asymmetric network for proof, it is believed that the non-skipped one may be the optimum.

When a large, non-skipped network was calculated, an obvious pattern arose. Such a network is shown in Figure 3.8. The numbers here represent distances between adjacent allowed nodes. The network size is 9842 and the number of allowed nodes is 512, giving a network efficiency of 5.2 %. Note that short subnetworks, such as (1 2 1), (1 2 1 5 1 2 1) and so on, are repeated after the appearance of every new number. The numbers that appear are 1, 2, 5, 14, 41, 122, 365 etc., and this is a series described by,

$$S_1 = 1,$$
$$S_k = 3 \cdot S_{k-1} - 1, \; k = 2, 3, 4, \ldots \qquad (3.15)$$

It is interesting to note that if one looks at the first appearance of a series number, the sum of all the previous distances in the network is one less than that series number. For example, the sum of all distances previous to the first appearance of 41 is 40, the sum of all distances previous to the first 122 is 121, and so on. These points are where the network becomes saturated with disallowed slots, and the next allowable slot is past the furthest symmetry of the first node.

Knowing the pattern of network generation, another APL function (listed in Appendix A) was written to create large networks very quickly. From a large network, it was possible to plot a graph of network efficiency versus number of potentially addressable

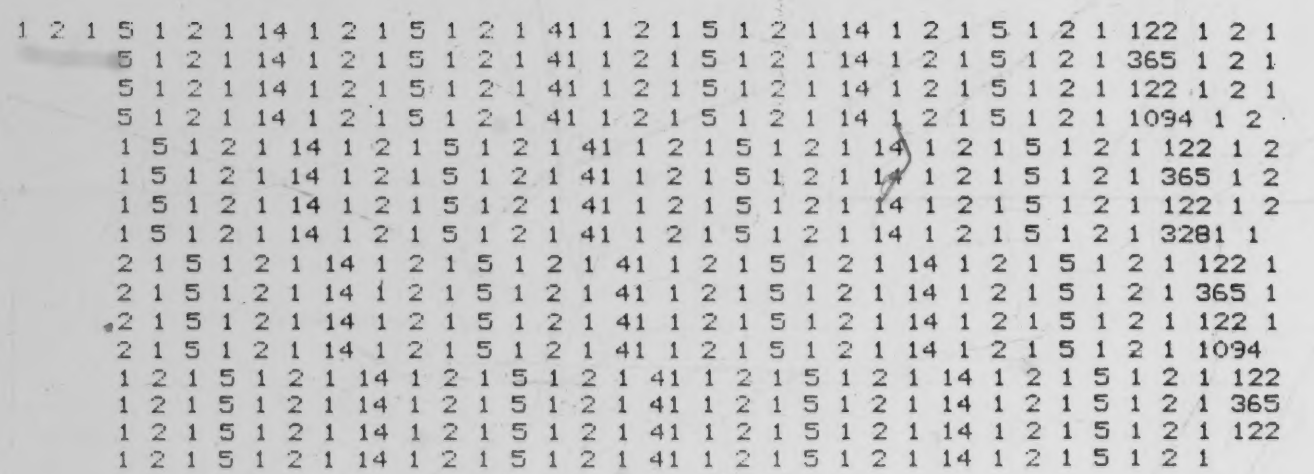

Figure 3.8. An asymmetric ladder network.

nodes. This appears in Figure 3.9. The network efficiency decreases as the size increases, and large downward slides occur when a new series number first appears. Immediately after a slide, the efficiency rises since only small distances are being added for each new node. Figure 3.10 uses the same data to show the number of addressable nodes versus number of potentially addressable nodes. It is apparent from these graphs that the address ambiguity problem severely limits network size for the ladder.

The networks generated for the ladder can also be used as central loop networks by tying the ends of the ladders together. The only time that this works, however, is just after adding a new series number. Since the efficiency is minimum at these points, it is apparent that the loop has a more severe asymmetry constraint. It would appear that, for the central loop, there are certain sizes for which no unambiguous networks exist. These sizes may be taken care of, however, by new networks generated by different skip vectors.

3.3 Power Budgets

The final topic of this chapter is the analysis of power budgets for the various topologies. Ignoring coupler loss, amplitude modulation, phase factors, and polarisation mismatch, the amplitude of the optical power at the detector is, from (2.6),

$$P_r = 2 \cdot \sqrt{P_1 \cdot P_2}$$

or, in dB units,

$$P_{r,dB} = \frac{1}{2} \cdot [P_{1,dB} + P_{2,dB}] + 3 \tag{3.16}$$

where P_1 and P_2 are the magnitudes of the average optical power in the two paths, and are given by

$$P_1 = \frac{1}{2} \cdot \sqrt{\frac{\varepsilon}{\mu}} \cdot E_1^2$$

and

$$P_2 = \frac{1}{2} \cdot \sqrt{\frac{\varepsilon}{\mu}} \cdot E_2^2 \tag{3.17}$$

With the receiver configuration shown in Figure 3.11, the signal power delivered by the field effect transitor (FET) amplifier (which has a high input impedance, a 50Ω output impedance, and a transconductance, g_m) to the matched load resistance, R_{load}=50Ω, is

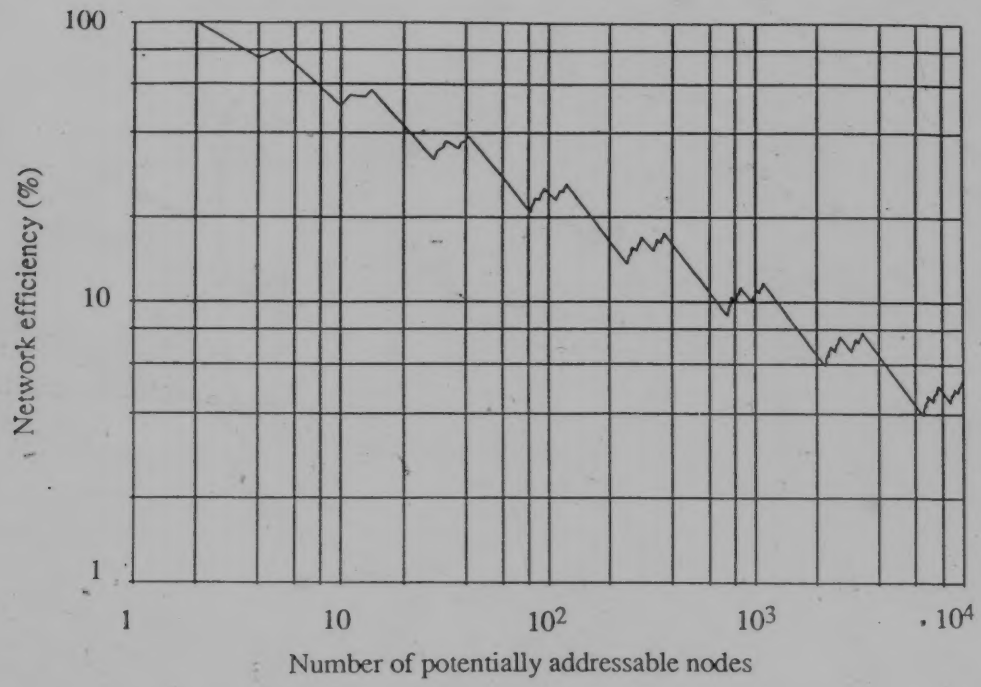

Figure 3.9. Ladder network efficiency versus number of potentially addressable nodes.

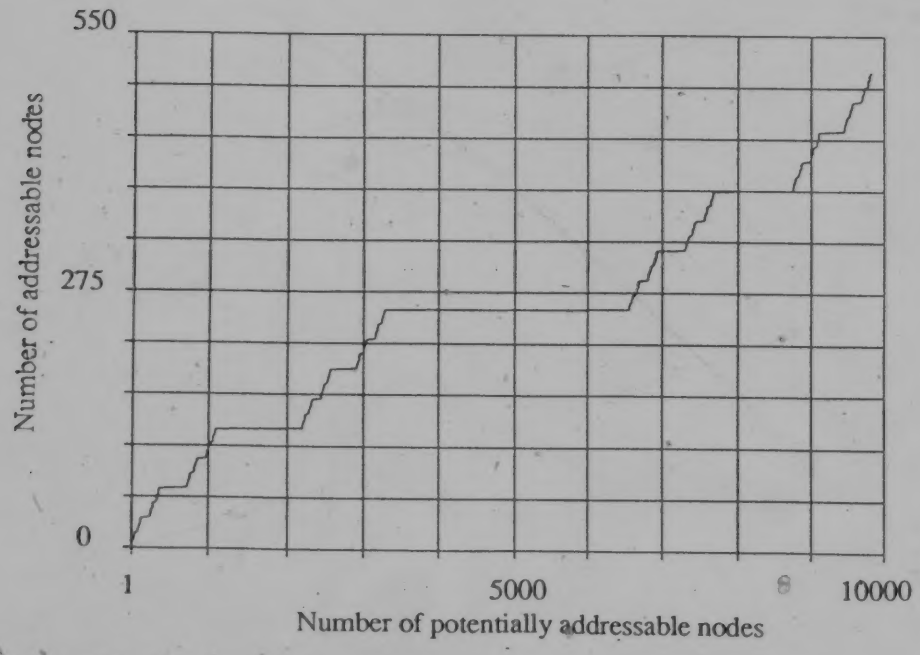

Figure 3.10. Number of addressable nodes versus number of potentially addressable nodes.

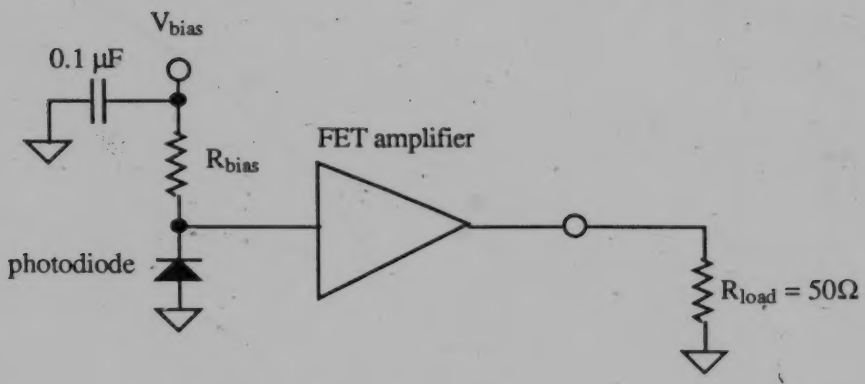

Figure 3.11. Receiver configuration.

$$P = \frac{R_{load}}{8} \cdot \left(g_m \cdot R_{bias} \cdot R \cdot P_r\right)^2 = 6.25 \cdot \left(g_m \cdot R_{bias} \cdot R \cdot P_r\right)^2$$

or, in dB units,

$$P_{dB} = 2 \cdot P_{r,dB} + 20 \cdot \log\left(g_m \cdot R_{bias} \cdot R\right) + 10 \cdot \log(6.25) \tag{3.18}$$

where R_{bias} is the photodetector biassing resistance, and R is the responsivity of the photodetector. The receiver sensitivity in dB units is

$$P_{sens} = P_{th} + SNR + M \tag{3.19}$$

where P_{th} is the thermal noise floor, SNR is the signal-to-noise ratio required for a given BER, and M is a system margin. The thermal noise power is given by the well known expression

$$P_{th} = 10 \cdot \log\left(k \cdot T \cdot B\ W\right) = 10 \cdot \log\left(k \cdot T \cdot t \cdot R_b\right) \tag{3.20}$$

where $k \approx 1.38 \cdot 10^{-23}$ J/°K is Boltzmann's constant, and T is the temperature in degrees Kelvin.

Expressions for received power as a function of the following system parameters will be derived for each topology:

N	: network size,
$P_{t,dB}$	: transmitted optical power in dB,
r	: coupling ratio as a fraction,
L_{ex}	: coupler excess loss in dB,

α : fibre loss in dB/km,

L_{ct} : laser-to-fibre coupling loss at transmitter, in dB,

L_{cr} : fibre-to-detector coupling loss at receiver, in dB,

L_{sw} : losses due to optical switches, in dB,

Δx_{min} : smallest resolvable distance, given by

$$\Delta x_{min} = \frac{c}{n_f} \cdot \Delta t_{min} \tag{3.21}$$

where c is the speed of light in a vacuum, and n_f is is the refractive index of the fibre. It will be assumed throughout this section that addressing by delay insertion is used.

3.3.1 Central Loop

If node p is transmitting to node q, one can calculate the optical power falling on the detector by tracing through the signal paths in Figure 3.1. The optical power from signal path 1 is

$$P_{1,dB} = P_{t,dB} -6+20\cdot\log(1-r)+20\cdot(q-p)\cdot\log r +\Delta x_{min}\cdot(q-p)\cdot\alpha+2\cdot(q-p+1)\cdot L_{ex} +L_{ct}+L_{cr}+L_{sw}+\Delta x_{min}\cdot(q-p-1)\cdot\alpha \tag{3.22}$$

The final term in (3.22) is the additional fibre loss due to insertion of fibre delays.

The power from path 2 is

$$P_{2,dB} = P_{t,dB} -6+20\cdot\log(1-r)+20\cdot(N-q+p-1)\cdot\log r +\Delta x_{min}\cdot(N-q+p-1)\cdot\alpha +2\cdot(N-q+p+1)\cdot L_{ex}+L_{ct}+L_{cr} \tag{3.23}$$

The total received power is found by substituting (3.22) and (3.23) into (3.16)

$$P_{r,dB} = P_{t,dB} -3+20\cdot\log(1-r)+20\cdot(N-2)\cdot\log r +\Delta x_{min}\cdot N\cdot\alpha+\frac{\Delta x_{min}}{2}\cdot(q-p-1)\cdot\alpha +2\cdot(N+2)\cdot L_{ex}+L_{ct}+L_{cr}+\frac{L_{sw}}{2} \tag{3.24}$$

Note that if the term due to the insertion of additional fibre delays were not present, then the received power would be absolutely independent of the relative positions of transmitting and receiving nodes. In fact, since Δx_{min} is typically on the order of a few centimeters, and fibre loss at 830 nm is approximately 2 dB/km, this term is negligible with respect to the other losses.

The received power is obviously dependent on the choice of coupler ratio r. The optimum choice is found by taking the derivative of (3.24) with respect to r, and setting it equal to zero. This results in a optimum coupling ratio of

$$r_{opt} = \frac{N-2}{N-1} . \tag{3.25}$$

Substitution of (3.25) into (3.24) gives

$$P_{r,dB} = P_{t,dB} -3-20\cdot(N-1)\cdot\log(N-1)+20\cdot(N-2)\cdot\log(N-2)+\Delta x_{min}\cdot N\cdot\alpha+2\cdot(N+2)\cdot L_{ex} + L_{ct}+L_{cr}+\frac{L_{sw}}{2} . \tag{3.26}$$

From this equation and the receiver sensitivity given by (3.19), the maximum size constraint due to network loss considerations can be obtained. The system parameters were assumed to have the following reasonable values:

$P_{t,dB}$ = 12.6 dBm (18 mW),
g_m = 0.05 mS,
L_{ex} = -0.1 dB,
α = -2 dB/km,
L_{ct} = -6 dB,
L_{cr} = -3 dB,
L_{sw} = -6 dB,
Δx_{min} = 2 cm,
R_{bias} = 10kΩ,
R = 0.45 A/W,
SNR = 15 dB, for BER=10^{-9},
M = 3 dB,
T = 295°K.

The maximum size was found by plotting P_{dB} against N, using expression (3.26) in (3.18), and determining the largest N that allowed the received power to remain larger than the receiver sensitivity limit given by (3.19). N_{max} was found for 1 Gb/s, 100 Mb/s, 10 Mb/s, and 1 Mb/s to be 114, 132, 151, and 171 nodes, respectively.

3.3.2 Bus

The received power for the bus topology of Figure 3.2 is

$$P_{r,dB} = P_{t,dB} + 3 - 10 \cdot N \cdot \log N + 10 \cdot (N-2) \cdot \log(N-2) + \left(d + \Delta x_{min}\right) \cdot (N-1) \cdot \alpha + \frac{\Delta x_{min}}{2} \cdot \alpha + (N+2) \cdot L_{ex} + L_{ct} + L_{cr} + \frac{L_{sw}}{2} \quad (3.27)$$

where d is the distance between nodes. The above was derived for the worst case, which is when q=N and p=1. It was also assumed that the optimum coupling ratio has been chosen.

The same system parameters as in the central loop case were used here, as well as a node separation of d=5m. The maximum sizes for 1 Gb/s, 100 Mb/s, 10 Mb/s, and 1 Mb/s, were found to be 214, 247, 282, and 318 nodes, respectively.

3.3.3 Double Star

The power equation for the double star network of Figure 3.3 is

$$P_{r,dB} = P_{t,dB} - 3 - 10 \cdot \log N + \Delta x_{min} \cdot (2 \cdot N - 4) \cdot \alpha + \left(2 \cdot d + \frac{\Delta x_{min}}{2}\right) \cdot \alpha + N \cdot L_{ex} + L_{ct} + L_{cr} + \frac{L_{sw}}{2} \quad (3.28)$$

where d is the total distance from a node to the centre of a star coupler. The worst case for this topology occurs when q=N and p=N-1. Note that it is assumed that the excess loss of a star coupler is proportional to the number of coupler ports. In fact, the actual size dependence of excess loss is a function of the exact configuration of the star. The assumption in the above equation is used in order to find an approximate network size.

The sizes for 1 Gb/s, 100 Mb/s, 10 Mb/s, and 1 Mb/s were found to be 463, 509, 555, and 601, respectively.

3.3.4 Folded Ring

From Figure 3.4, the power budget for the folded ring is found to be

$$P_{r,dB} = P_{t,dB} + 6 - 5 \cdot (3 \cdot N + 2) \cdot \log(3 \cdot N + 2) + 5 \cdot (3 \cdot N - 2) \cdot \log(3 \cdot N - 2) + \Delta x_{min} \cdot \left(\frac{3}{2} \cdot N - \frac{1}{2}\right) \cdot \alpha + 2 \cdot d \cdot \alpha + (2 \cdot N + 2) \cdot L_{ex} + L_{ct} + L_{cr} + \frac{L_{sw}}{2} \quad (3.29)$$

where d is the distance from a node to the addressing loop. For this topology, the worst case occurs when node 1 transmits to node N.

With the system parameters the same as for the previous cases and d=5m, the sizes for 1 Gb/s, 100 Mb/s, 10 Mb/s, and 1 Mb/s were calculated as 112, 131, 150, and 169, respectively.

3.3.5 Ladder

The ladder's power equation, derived from Figure 3.5, is

$$P_{r,dB} = P_{t,dB} + 3 - 10\cdot(2\cdot N-1)\cdot\log(2\cdot N-1) + 10\cdot(2\cdot N-3)\cdot\log(2\cdot N-3) + \Delta x_{min}\cdot\left(N-\frac{1}{2}\right)\cdot\alpha + \left[4\cdot d_a + (2\cdot N-1)\cdot d_b\right]\cdot\alpha + (2\cdot N+1)\cdot L_{ex} + L_{cf} + L_{cr} + \frac{L_{sw}}{2} \quad (3.30)$$

where d_a is the short length from the central couplers to the outside couplers, and d_b is the distance between nodes. These distances were assumed to be d_a=10 cm and d_b=5m. The above equation has been derived for the worst case which arises when q=2 and p=1.

Maximum sizes for 1 Gb/s, 100 Mb/s, 10 Mb/s, and 1 Mb/s were 107, 124, 141, 159 nodes, respectively.

3.3.6 Size Comparison of Topologies

The sizes generated in the previous section are summarised in Table 3.2.

Bit Rate	Central Loop	Bus	Double Star	Folded Ring	Ladder
1 Gb/s	114	214	463	112	107
100 Mb/s	132	247	509	131	124
10 Mb/s	151	282	555	150	141
1 Mb/s	171	318	601	169	159

Table 3.2. Summary of network sizes.

It is interesting to note that the central loop, folded ring, and ladder topologies have the same approximate size limitation, while the bus topology limitation is roughly double. The dominant losses are due to the coupling and excess losses in the couplers, and since

each signal passes half as many couplers in the bus network than in the others, the bus has a sensitivity advantage. The double star network seems to be the best of all networks, but one must keep in mind that the size will heavily depend on the excess loss in the star coupler. Also note that the maximum sizes are relatively insensitive to bit rate. Recall from Figure 2.11 that the best addressing scheme can handle very few nodes at high bit rates (3 nodes at 1 Gb/s, for example). This suggests that the delay insertion addressing scheme is the best alternative for high bit rates. However, it is also noteworthy that the external modulator and bandpass tuning schemes may have a size advantage over delay insertion for low bit rates (300 to 2000 nodes for 1 Mb/s).

3.4 Summary

We have seen that there are several topologies that may be considered in designing a system that employs OTFM. These topologies have been compared from many points of view. In general it seems that the double star topology is the most desirable, followed closely by the bus. Both avoid the addressing ambiguity problem and tend to allow the largest network size.

CHAPTER 4

EXPERIMENTAL RESULTS

This chapter outlines the results of two sets of experiments The purpose of the first set was to obtain the spectral characteristics of three different semiconductor lasers, and that of the second set to demonstrate the transmission of binary data using the OTFM principle.

4.1 Laser Characteristics

Three lasers made by two different manufacturers were characterised in order to assess their suitability in an OTFM system. The first two lasers were Ortel's SL300-H model, and the third was a Sharp LT015MF, and all were unstabilised FP lasers. The data sheets of these lasers appear in Appendix B. Lasers were acquired whose wavelengths were near 830 nm instead of the more common 780 nm because of the immediate availability of couplers and GRIN (graded index) lenses which were optimised for the 830 nm wavelength region.

Experiments described in this section were conducted to obtain the spectral characteristics and frequency modulation efficiencies of the lasers.

4.1.1 Spectral Properties

As mentioned in the first chapter, a laser for use in a coherent system must emit in a single longitudinal mode with a narrow linewidth. Thus, the selection of an appropriate laser device warrants the the study of its spectral properties. This section outlines experiments in which the modal behavior of all the aforementioned lasers were examined, and linewidth of only the Sharp laser was examined.

First, the McPherson 270 Scanning Monochromator was used to observe the mode spectra of the lasers. Figure 4.1 shows the experimental configuration[1]. The laser light was focussed by a GRIN lens into a single mode fibre. The light at the monochromator was modulated with a chopper wheel, and the signal from the detector was amplified with an amplifier locked to the chopping frequency. The plotter recorded the amplifier output as the grating was scanned, providing a trace of the mode spectrum of the laser.

---

1 The drawing of the monochromator is only a simplified picture; the actual optical path is more involved, but is not worth reproducing here. See [19] for more detail.

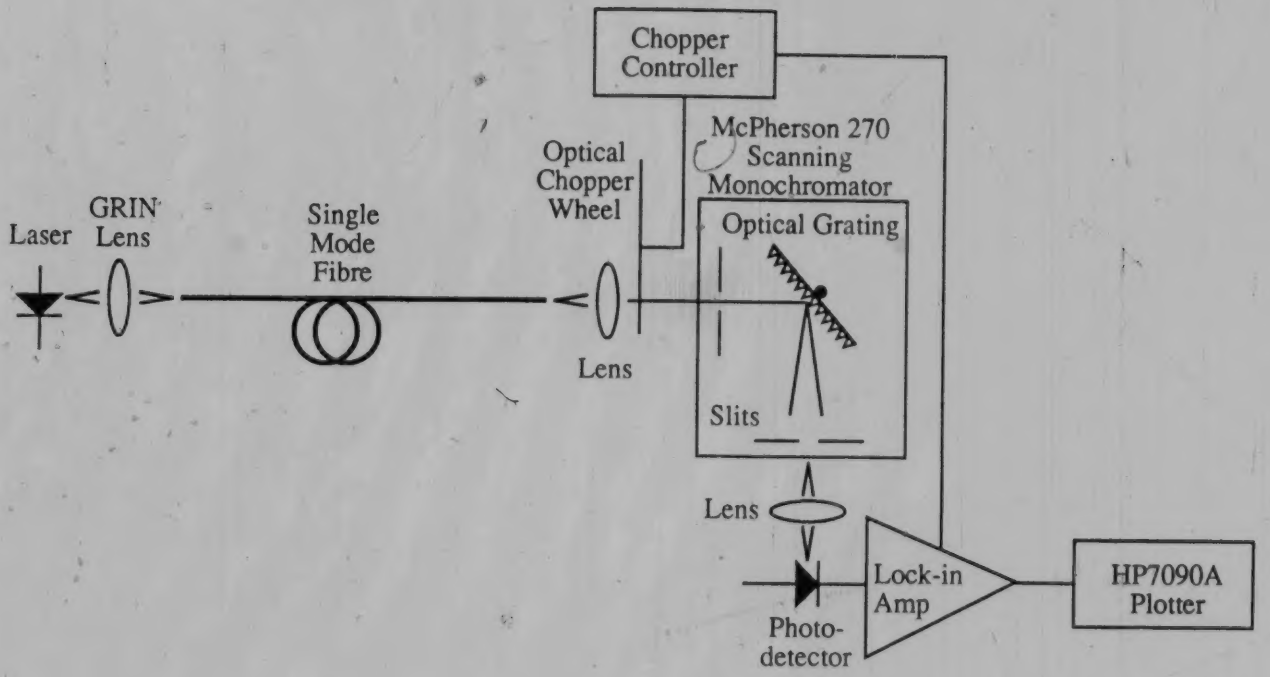

Figure 4.1. Monochromator experimental setup.

The mode spectra of the first Ortel SL300-H for bias currents of 45 mA and 35 mA appear in Figure 4.2. Since the side modes are only about 4 dB down from the main mode, this laser is not single-mode enough for a coherent system.

The reason for the multimode behavior of this laser was suspected to be the high level of optical feedback from the near and far ends of the fibre. To reduce the feedback, the fibre was misaligned axially, thus defocussing reflections back into the laser. Figure 4.3 shows that the laser has indeed become more single-mode, but its oscillation frequency seems to jump between cavity modes as the bias current is changed. This is evidence that there still may exist reflections strong enough to have a detrimental effect.

A theory to explain the seemingly random jumping between laser cavity modes is presented with the help of Figure 4.4. The tall lines represent resonant modes of the laser cavity as predicted by equation (1.8), and the short lines represent the external cavity (fibre end) modes. It is assumed here that the dominant external cavity is due to the near fibre end reflection. There is a reduction in the cavity loss at frequencies where lines of the two patterns coincide, and thus the laser may oscillate at these frequencies. Oscillation at frequencies where the mode patterns nearly overlap is also possible, but coupling into these modes is weaker, and thus the intensity weaker. As the bias current is changed, the two mode patterns shift with respect to each other and different pairs of modes overlap, causing the oscillation frequency to jump to different cavity modes. This explains the splitting of oscillation between widely separated laser cavity modes.

In order to further reduce feedback, an Optics For Research IO-5-NIR tunable optical isolator having approximately 30 dB of isolation was inserted between the laser and the fibre, as shown in Figure 4.5.

The mode spectra for this configuration appear in Figure 4.6. The traces containing sharp spikes occurred because of hopping between modes while the trace was obtained, which suggests that optical feedback is still strong enough to have an effect.

The second Ortel laser was put through the above tests, and was found to exhibit similar behavior.

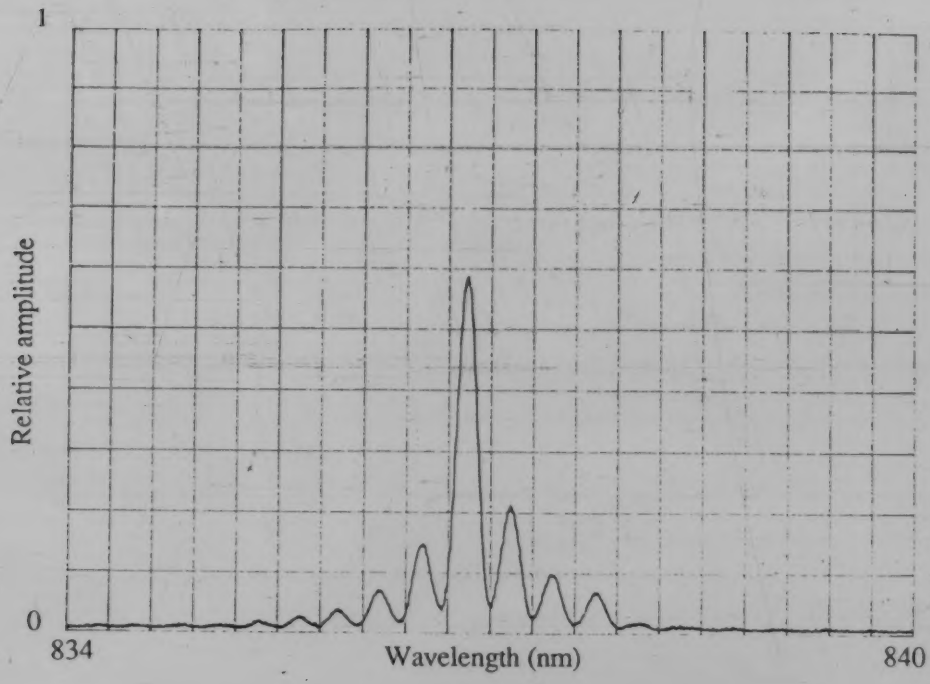

(a) 45 mA bias

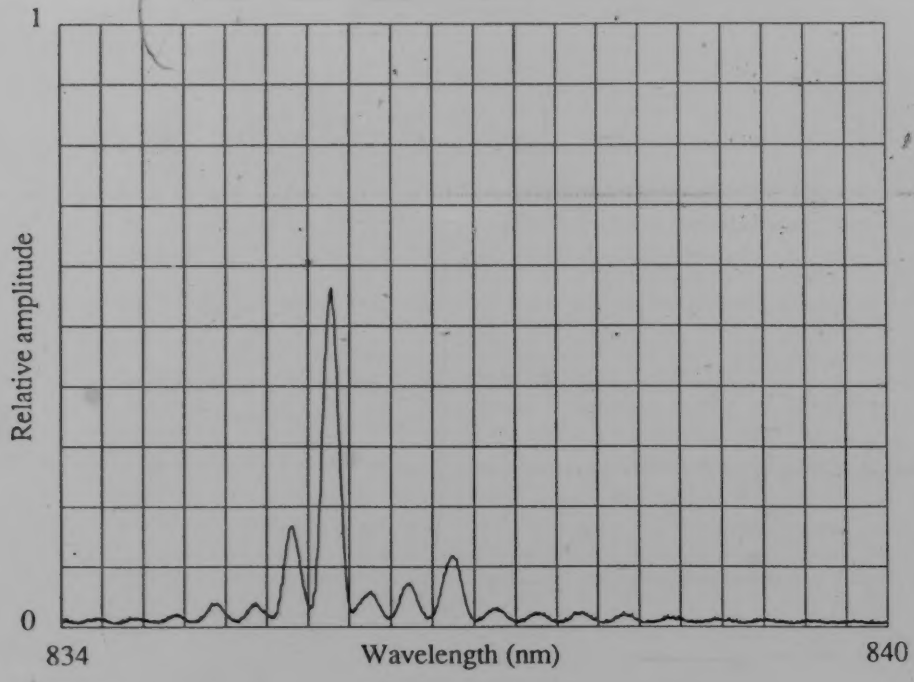

(b) 35 mA bias

Figure 4.2. Mode spectra of Ortel SL300-H laser.

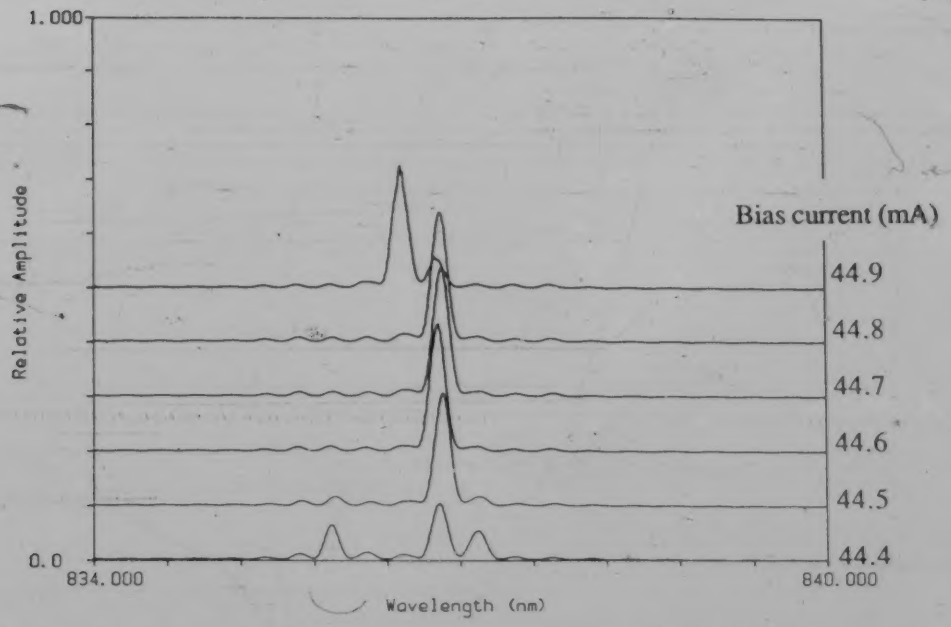

(a) 44.4 mA to 44.9 mA bias

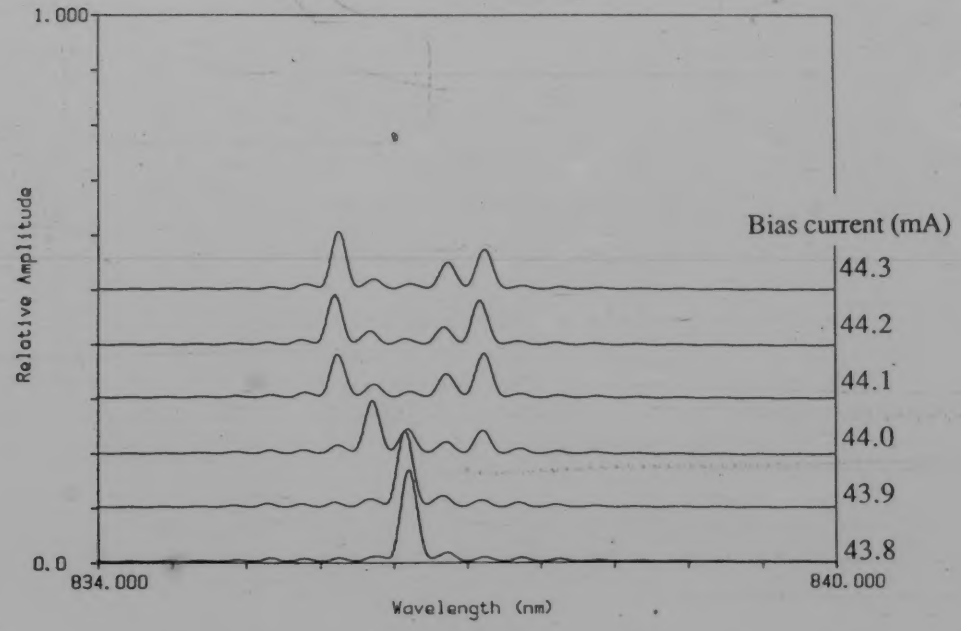

(b) 43.8 mA to 44.3 mA bias

Figure 4.3. Mode spectra of Ortel SL300-H laser, coupling misaligned.

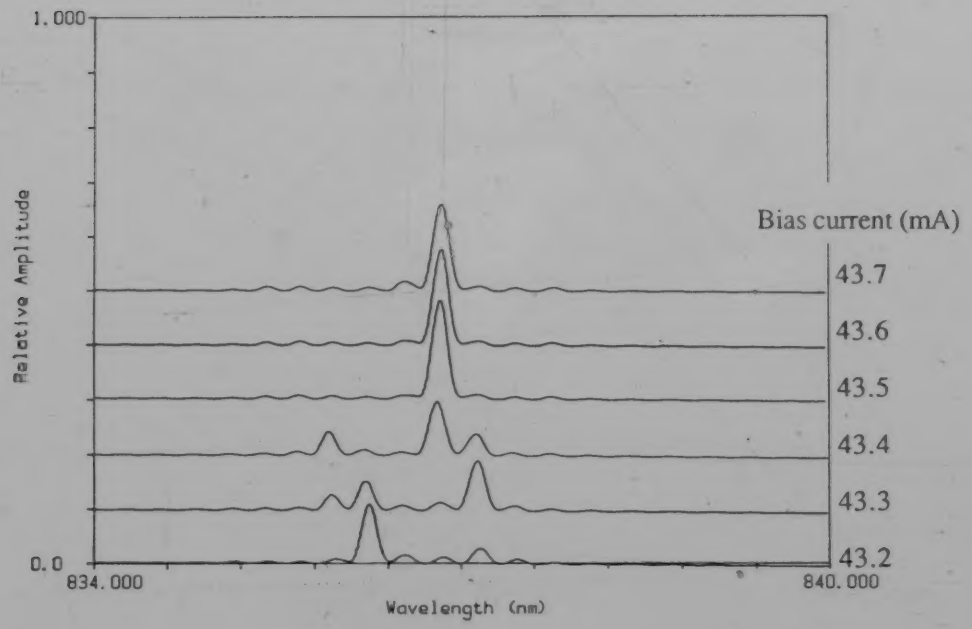

(c) 43.2 mA to 43.7 mA bias

Figure 4.3. Mode spectra of Ortel SL300-H laser, coupling misaligned.

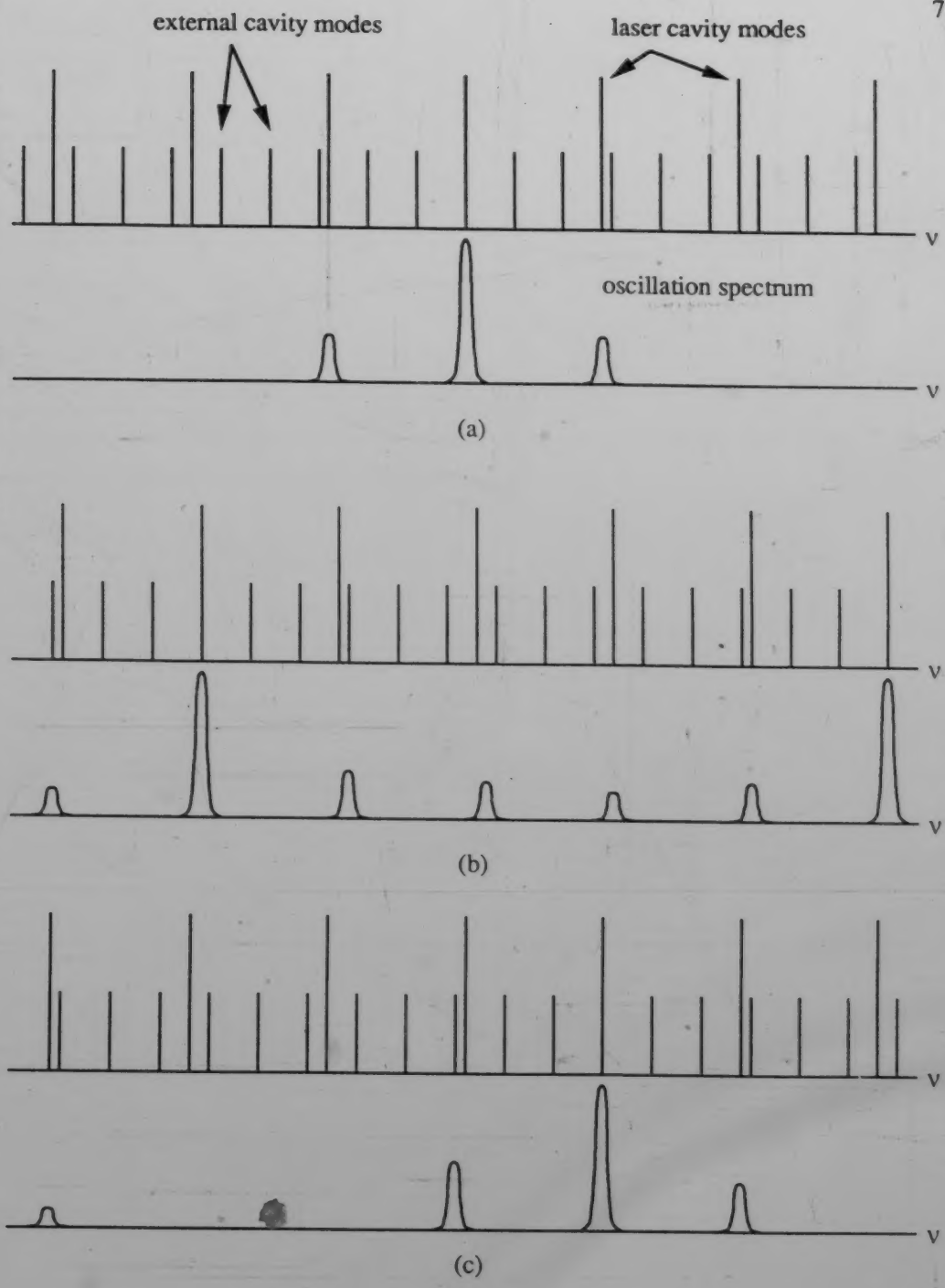

Figure 4.4. Random mode jumping.

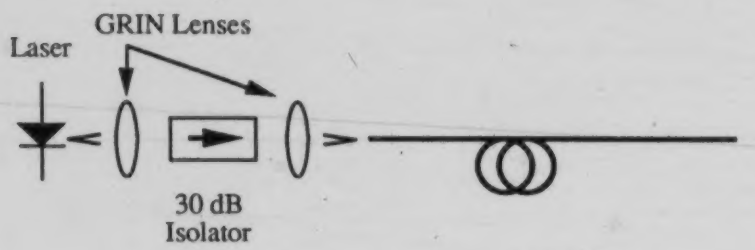

Figure 4.5. Isolator configuration.

The Sharp LT015MF was the last laser to be examined. Figure 4.7 shows its mode spectra without having inserted the optical isolator. It is obviously very multimode due to the high level of optical feedback. The spectra of the laser with the isolator in place are shown in Figure 4.8. The spectra now contain a single mode, and the laser appears to stay in one mode for bias currents ranging from 60.0 mA to 86.0 mA. Judging from the stability of the mode spectrum, this laser is a likely candidate for use in a coherent system, and is in fact the one selected for use in the data transmission experiment.

In the next experiment, the linewidth of the Sharp laser was examined using the self-homodyne technique; the experimental configuration appears in Figure 4.9. The laser light is collimated by an anti-reflection-coated, plano-convex GRIN lens, sent through the isolator and focussed into a single mode fibre. A 3 dB coupler splits the light into two fibre paths whose lengths differ by several times the coherence length of the laser. The light is recombined and focussed onto a wide bandwidth PIN photodiode, and the resulting electrical signal is amplified and sent to a high frequency spectrum analyser.

Figure 4.10 is the spectrum analyser trace obtained with the isolator removed, and a path length difference of 10 meters. From this, the linewidth is estimated to be 75 MHz. The trace obtained with the isolator reinserted and a path length difference of 1.15 kilometers appears in Figure 4.11. The linewidth now appears to be approximately 10 MHz. These results demonstrate the broadening of laser linewidth with increasing optical feedback.

In Figure 4.11(a), one can see small modes at about 650 MHz, 1.3 GHz, and so on, that were not previously visible. When a path of 1.1 meters is inserted, the modes become even more visible, as shown in the upper trace of Figure 4.12. These modes are due to the 16.5 cm external cavity between the laser and the near fibre end.

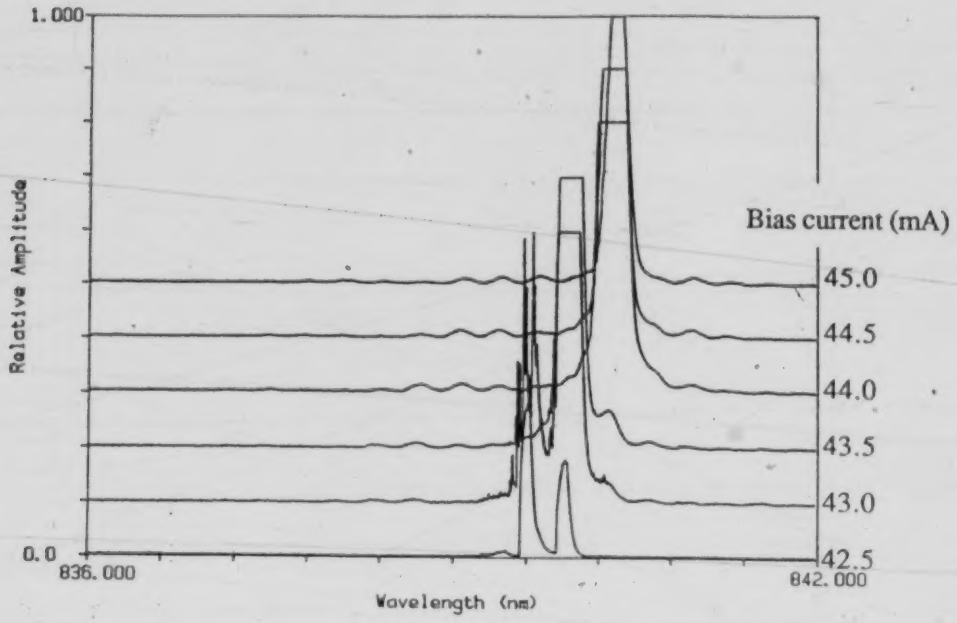

(a) 42.5 mA to 45.0 mA bias

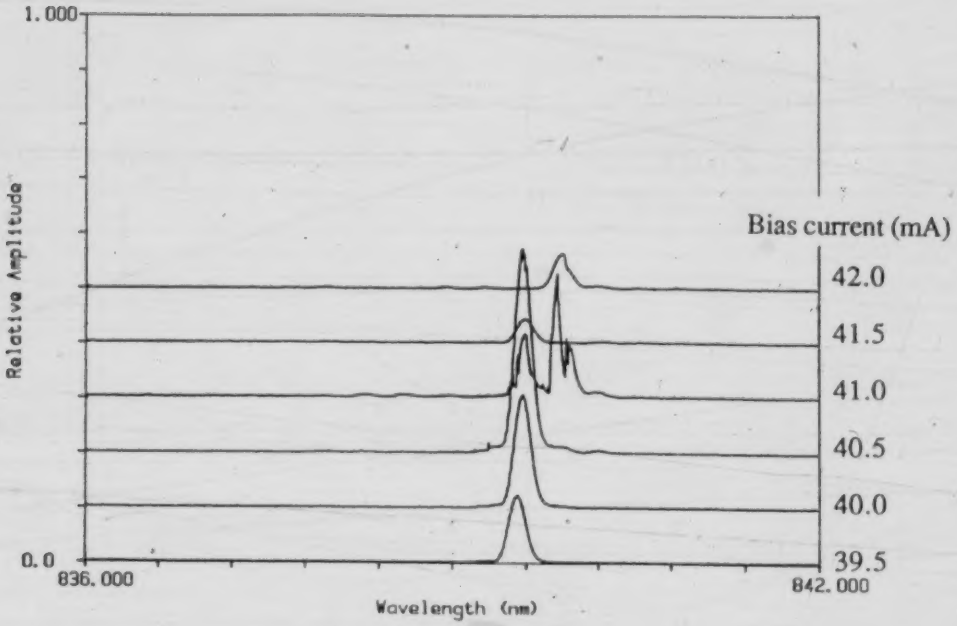

(b) 39.5 mA to 42.0 mA bias

Figure 4.6. Mode spectra of Ortel SL300-H laser, after insertion of optical isolator.

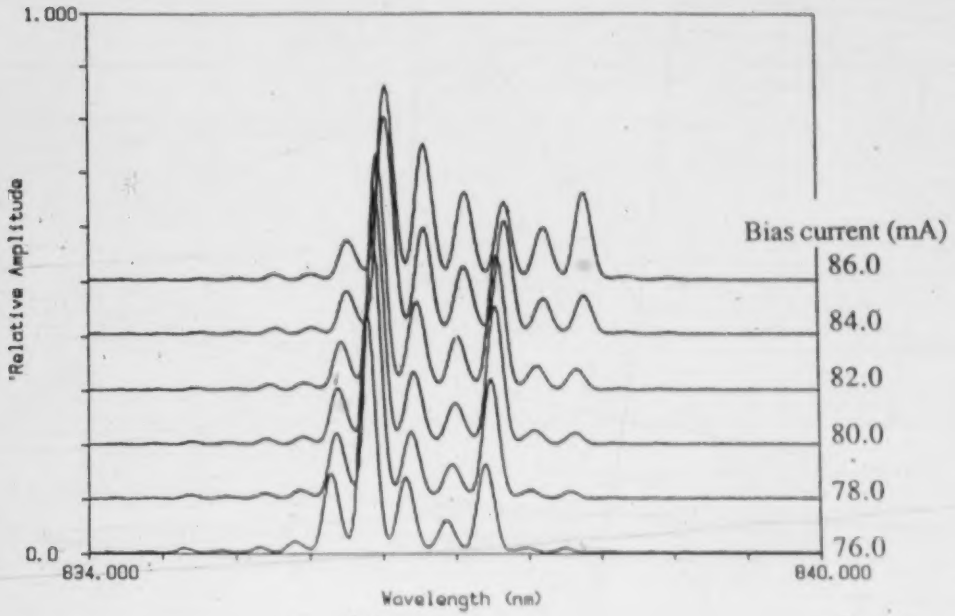

(a) 76.0 mA to 86.0 mA bias

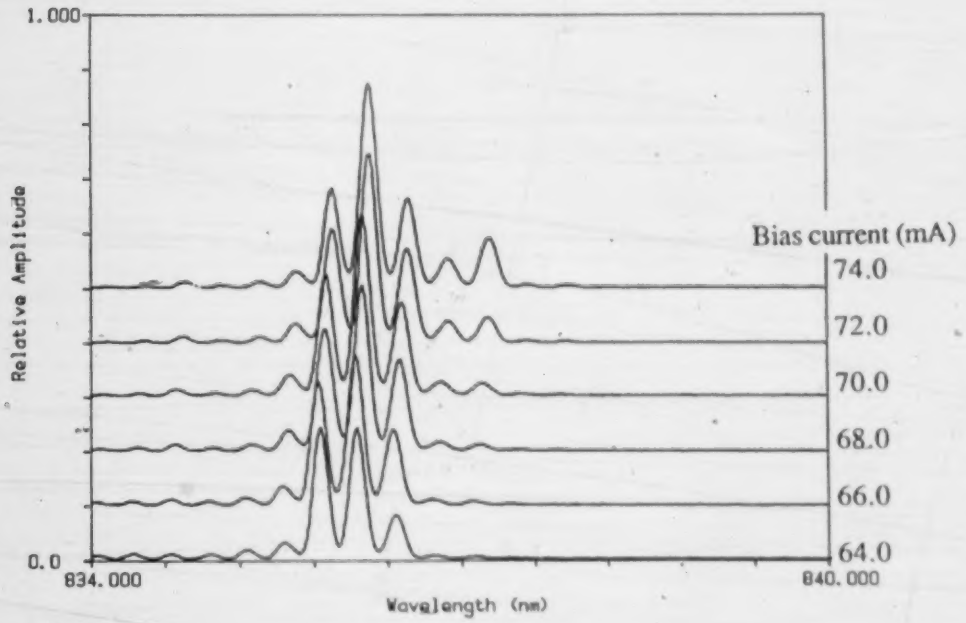

(b) 64.0 mA to 74.0 mA bias

Figure 4.7. Mode spectra of Sharp LTO15MF laser, no isolator.

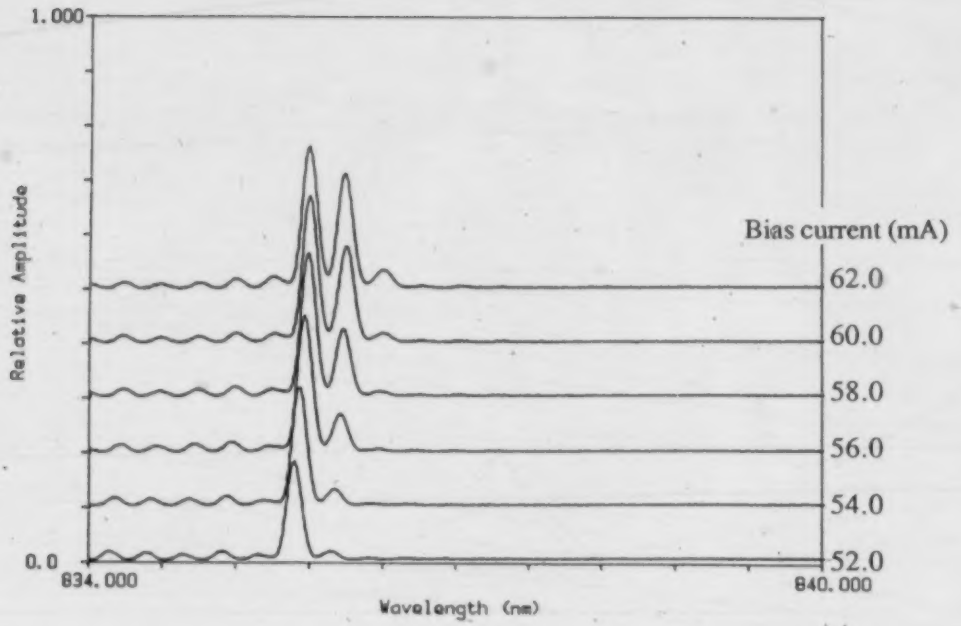

(c) 62.0 mA to 52.0 mA bias

Figure 4.7. Mode spectra of Sharp LTO15MF laser, no isolator.

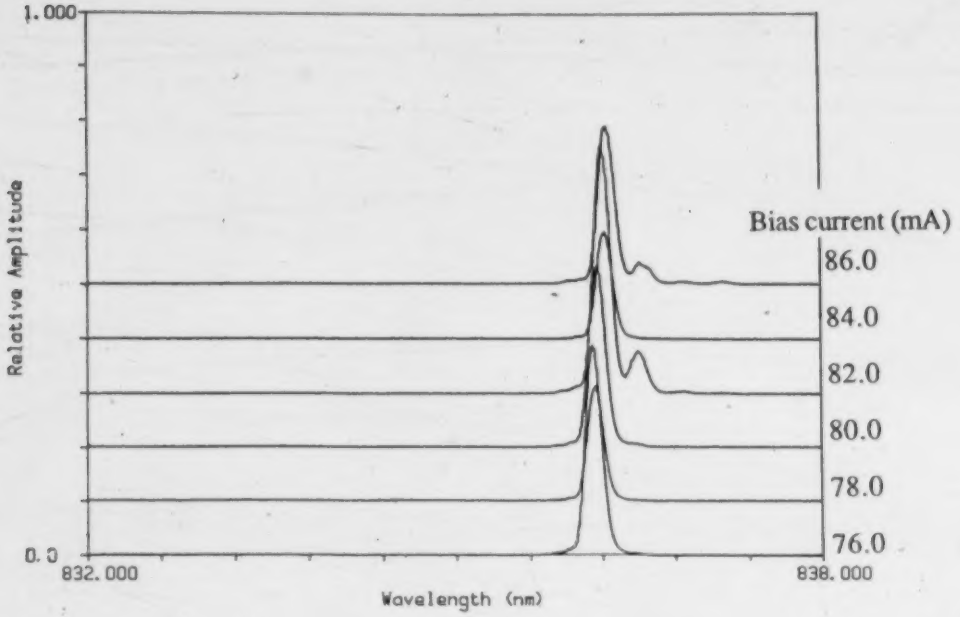

(a) 76.0 mA to 86.0 mA bias

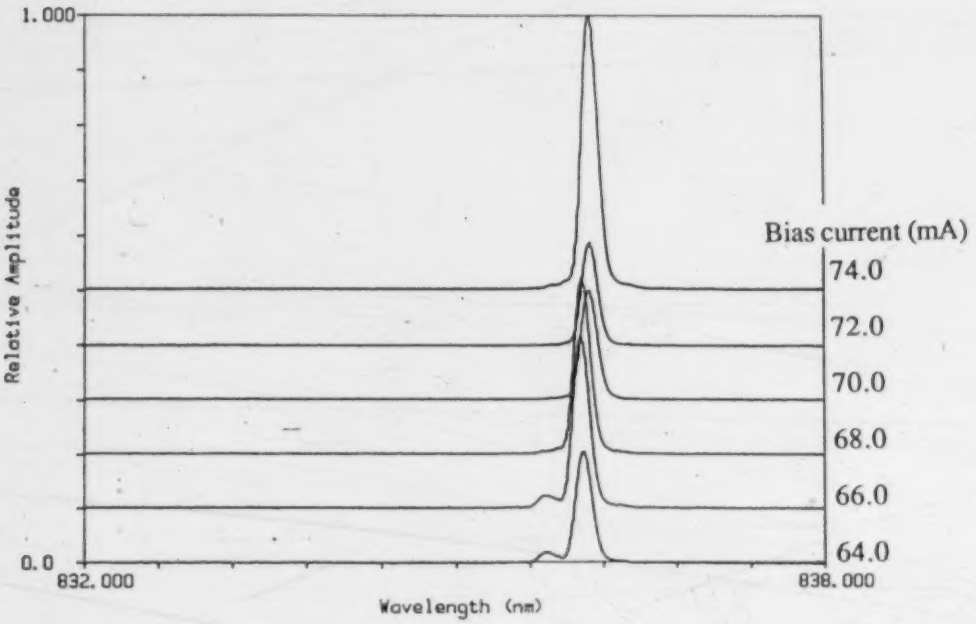

(b) 64.0 mA to 74.0 mA bias

Figure 4.8. Mode spectra of Sharp LTO15MF laser, with isolator.

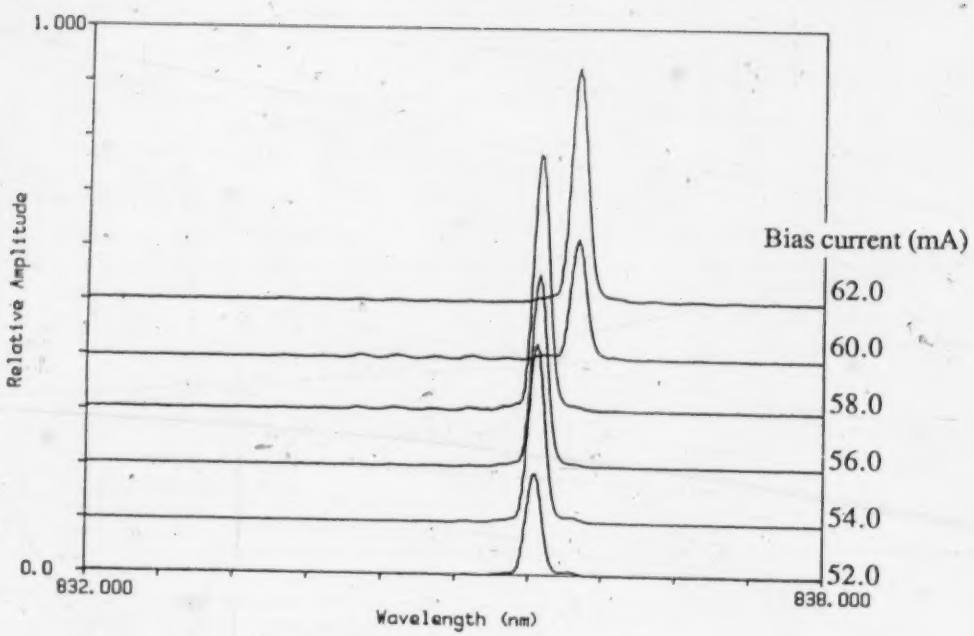

(c) 62.0 mA to 52.0 mA bias

Figure 4.8. Mode spectra of Sharp LTO15MF laser, with isolator.

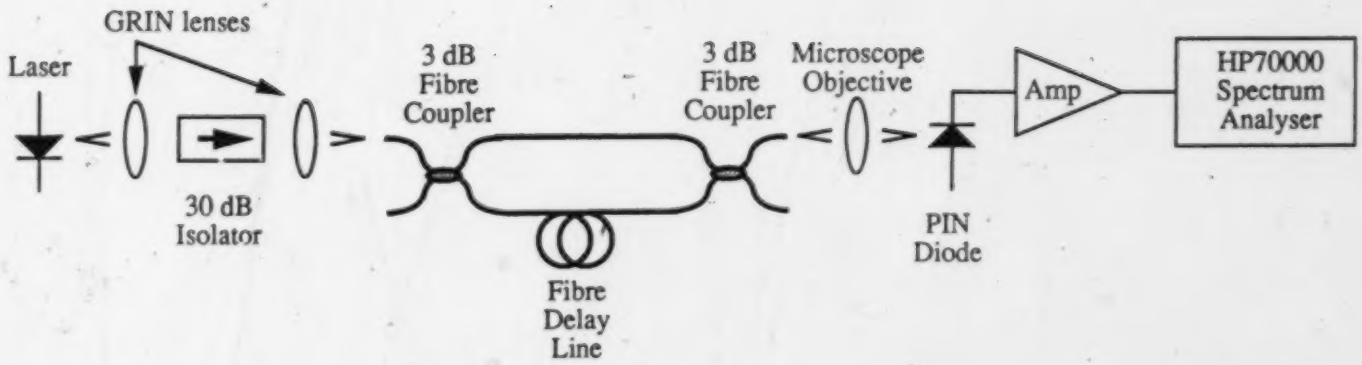

Figure 4.9. Self-homodyne or -heterodyne setup.

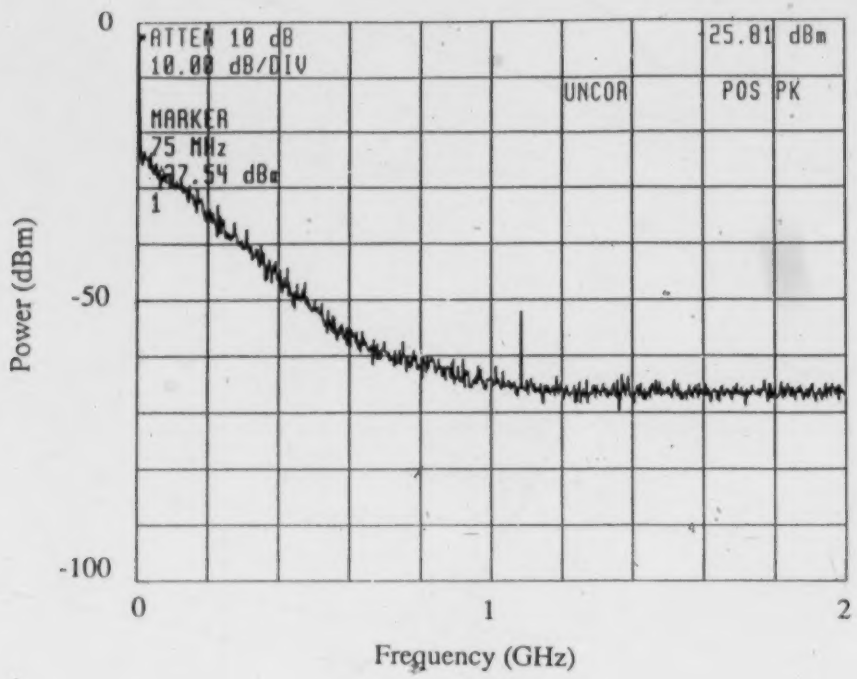

(a) wide spectrum trace

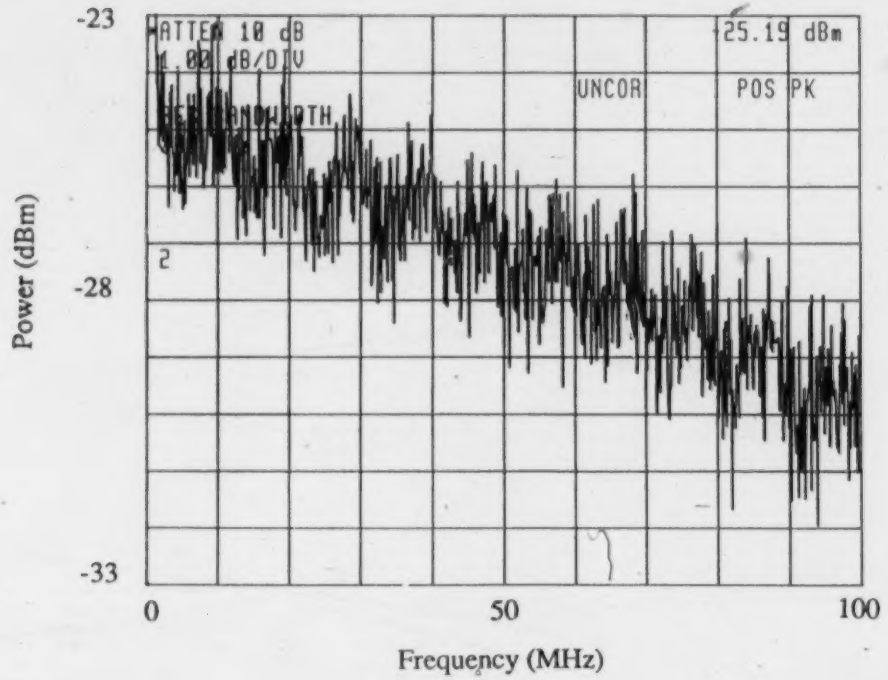

(b) zoom-in trace

Figure 4.10. Linewidth of Sharp LTO15MF laser, no isolator.

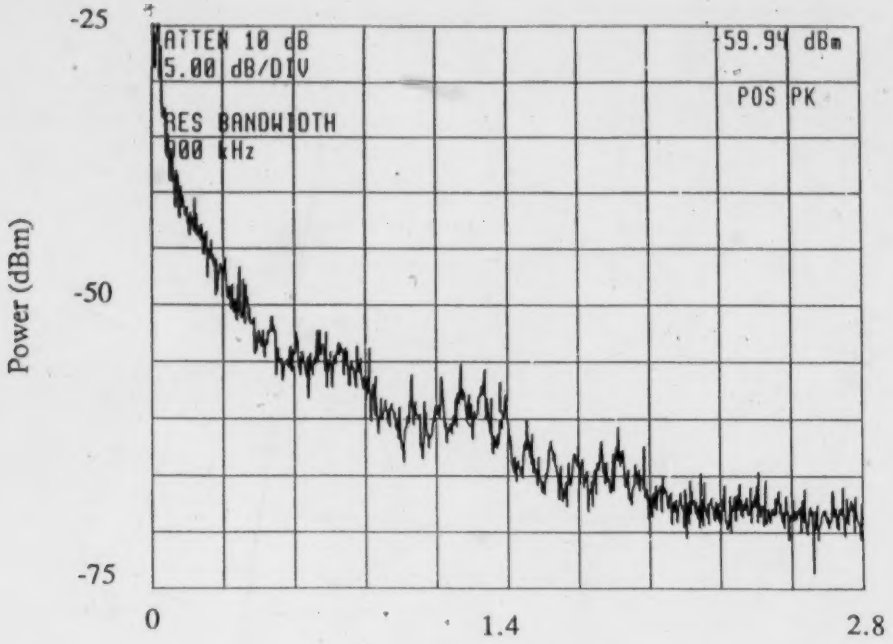

(a) wide spectrum trace

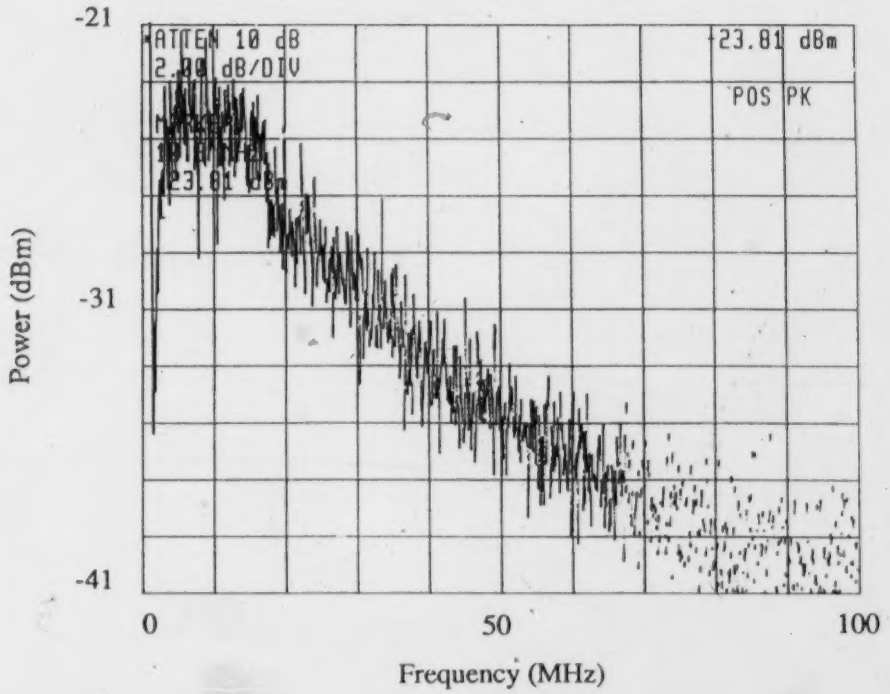

(b) zoom-in trace

Figure 4.11. Linewidth of Sharp LTO15MF laser, with isolator.

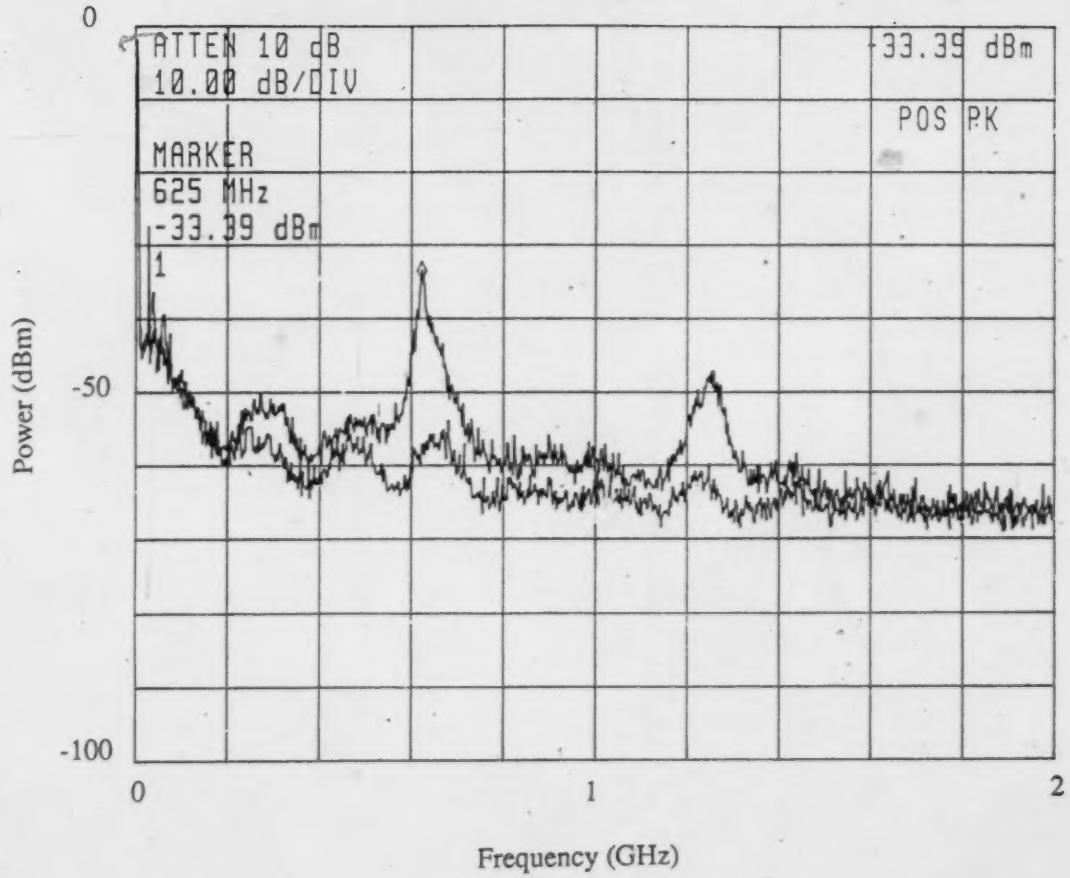

Figure 4.12. Effect of index matching fluid on external cavity modes.

The external cavity modes were eliminated by two techniques. First, a drop of index matching fluid was placed between the second GRIN lens and the fibre end. The effect of this is apparent in the lower trace of Figure 4.12, where the modes are all but gone. The second technique used a 'twisted' fibre cleave. To obtain a twisted cleave, a nick was made in the fibre with a diamond bit, and instead of pulling the fibre straight to get a 90 degree cleave, a slight twist was imparted. When the fibre was pulled, the resulting cleave was smooth and slightly spiral. This kind of cleave directs the reflection off the optical axis so that reflected light is not coupled back into the laser, yet allows efficient coupling of light into the fibre. The external modes were thus eliminated quite effectively.

4.1.2 Frequency Modulation Efficiency

The final laser characteristic investigated was the laser frequency modulation efficiency. The self-heterodyne setup of Figure 4.9 was employed to find the frequency deviation constant, k_f (in MHz/mA or GHz/mA), of the Sharp LT015MF laser. This involved frequency modulating the laser with either a square wave or a triangle wave, and observing the resultant IF spectrum.

In the square wave case, the delay path was a fibre of length 1.15 kilometers and the modulation was an 87 kHz, 50% duty cycle square wave added to the laser bias current. As shown in Figure 4.13, the square wave frequency was chosen so that its period was approximately twice the delay time, Δt, of the fibre path, so that the high level frequency, f_2, of one path is combined with the low level frequency, f_1, of the other path.

Interference and detection at the receiver produces an IF of $f_{IF}=f_2-f_1$. Knowing the peak-to-peak current amplitude, Δi, of the square wave, and observing the value of f_{IF} on a spectrum analyser, k_f can be calculated as

$$k_f = \frac{f_{IF}}{\Delta i} . \qquad (4.1)$$

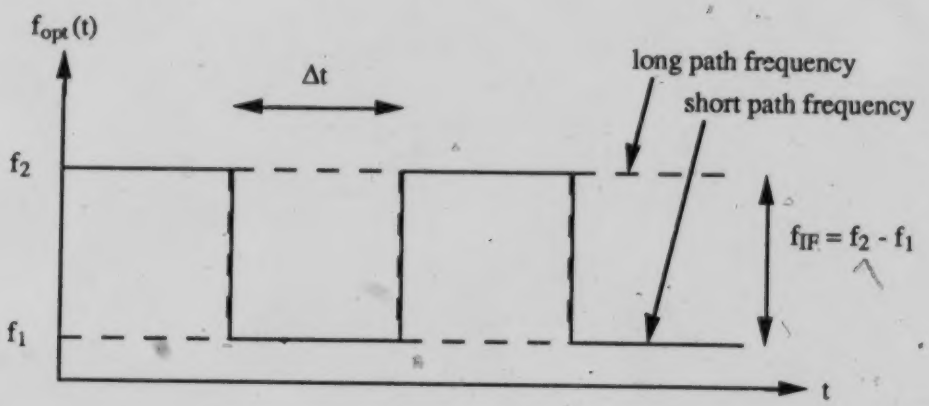

Figure 4.13. Self-heterodyne optical signals, square wave modulation.

Figure 4.14 contains the IF spectrum resulting from square wave modulation with a Δi of 0.76 mA. Here, f_{IF} is approximately 1.2 GHz, which gives a k_f of 1.6 GHz/mA. By changing the delay path, k_f was determined at 5 MHz and 10 MHz, as 850 MHz/mA and 524 MHz/mA, respectively.

The problem with the square wave technique is that different lengths of fibre are required for each modulating frequency. In order to find k_f easily at many different frequencies, the triangle modulation technique was employed. When the laser frequency is modulated with a triangle wave, the received IF is given by equation (2.13). Knowing the path length, and frequency and amplitude of the signal, and observing the value of f_{IF} on the spectrum analyser, one can calculate k_f with (2.13) and

$$\Delta f = k_f \Delta i \quad . \tag{4.2}$$

The k_f constant was found using this technique for frequencies of 10 MHz, 20 MHz and 50 MHz. The results were 700 MHz/mA, 620 MHz/mA, and 340 MHz/mA, respectively.

Upon comparison of the 10 MHz square wave and triangle wave results, there is found a 14% error, which can be accredited to two factors. First, the IF spectrum is very wide, and thus the choice of the value of f_{IF} is subjective. Second, the value of Δi was calculated from the voltage amplitude and the assumed input impedance of the laser circuit. This impedance was always assumed to be 50Ω (referring to the laser circuit in Figure C.2, the impedance is due to the 47Ω resistor in series with the dynamic laser impedance, which

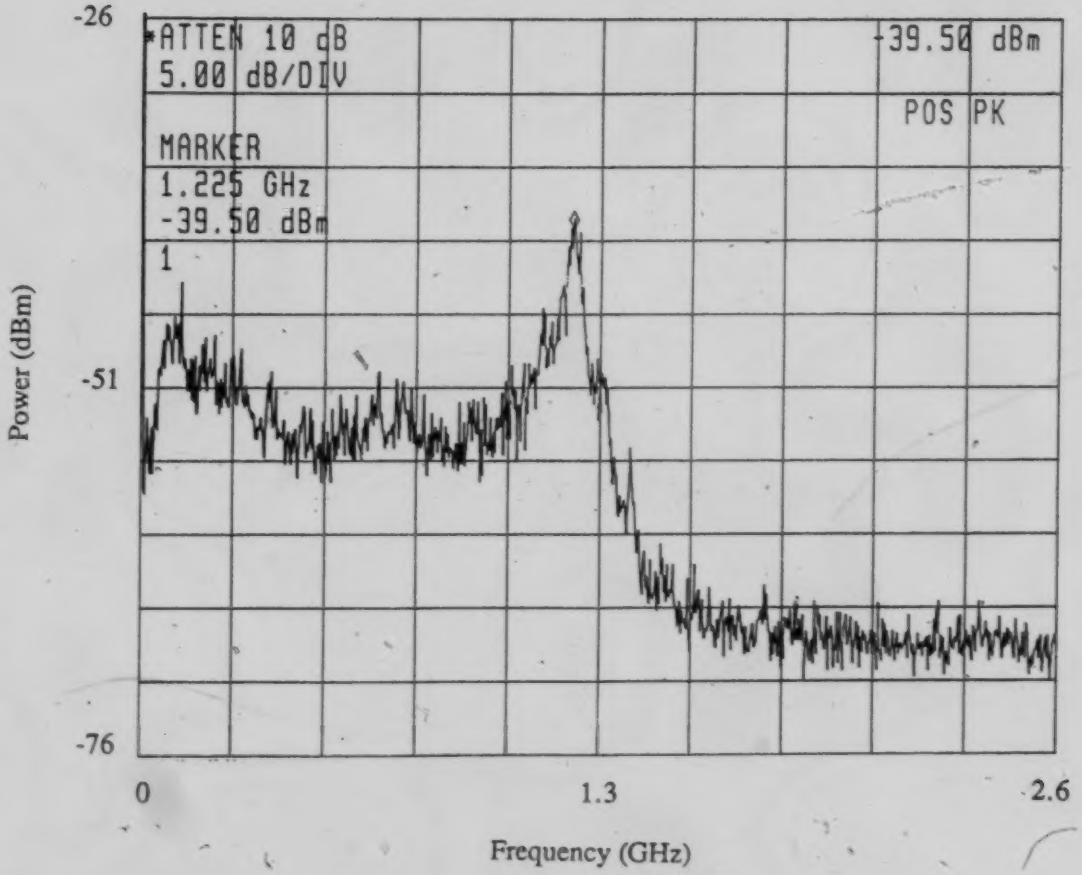

Figure 4.14. Self-heterodyne IF spectrum.

was measured to be approximately 3Ω), but in fact may change with frequency and bias current.

4.2 Data Transmission Experiment

Once the lasers were characterised and the Sharp LTO15MF laser selected, an experimental system using the OTFM principle was set up to transmit data at a rate of 10 Mb/s.

4.2.1 Experimental Configuration

The configuration of the system is shown in Figure 4.15. The triangle sweep is supplied by the HP 8116A Pulse/Function Generator and the data by the HP 3780A Pattern Generator/Error Detector. A 10 MHz clock for the 3780A is provided by the HP 3325A Synthesizer/Function Generator. The triangle sweep is switched off for a logical '1', and on for a '0' by the FET switch, whose circuit diagram appears in Figure C.1 in Appendix C. The voltage extinction ratio[2] of the switch was found to be 0.24. The switched sweep signal is sent to the laser circuit, the details of which appear in Figure C.2 in Appendix C.

Light from the laser is collimated with a GRIN lens, directed through an Optics For Research IO-5-NIR tunable optical isolator, and focussed into one input of a Canstar SF4-G-850-B fibre coupler. The other coupler input is immersed in index matching oil to avoid any reflections from the fibre end.

Optical connections between sections of fibre are made with Norland's reusable splices so that the delay line may be easily changed. The fibre is Corning Flexcor-850 whose mode field diameter is estimated to be 4 to 6 μm, and which has a cutoff wavelength of approximately 750 nm.

The cladding mode stripper was constructed by removing the jacket from a length of fibre and immersing the slightly bent fibre in index matching oil. This is necessary as the fibres are not long enough to fully attenuate modes that may be coupled into the cladding of the fibre.

---

2 Since the 'on' channel resistance of the FET in Figure C.1 is not zero, the amplitude of the triangle wave cannot be brought fully to zero. The voltage extinction ratio is therefore defined as the ratio of the amplitude of the 'off' triangle to the amplitude of the 'on' triangle. The impact of this (as will be demonstrated in Section 4.2.2) is the appearance of a second IF signal during the logical '1'.

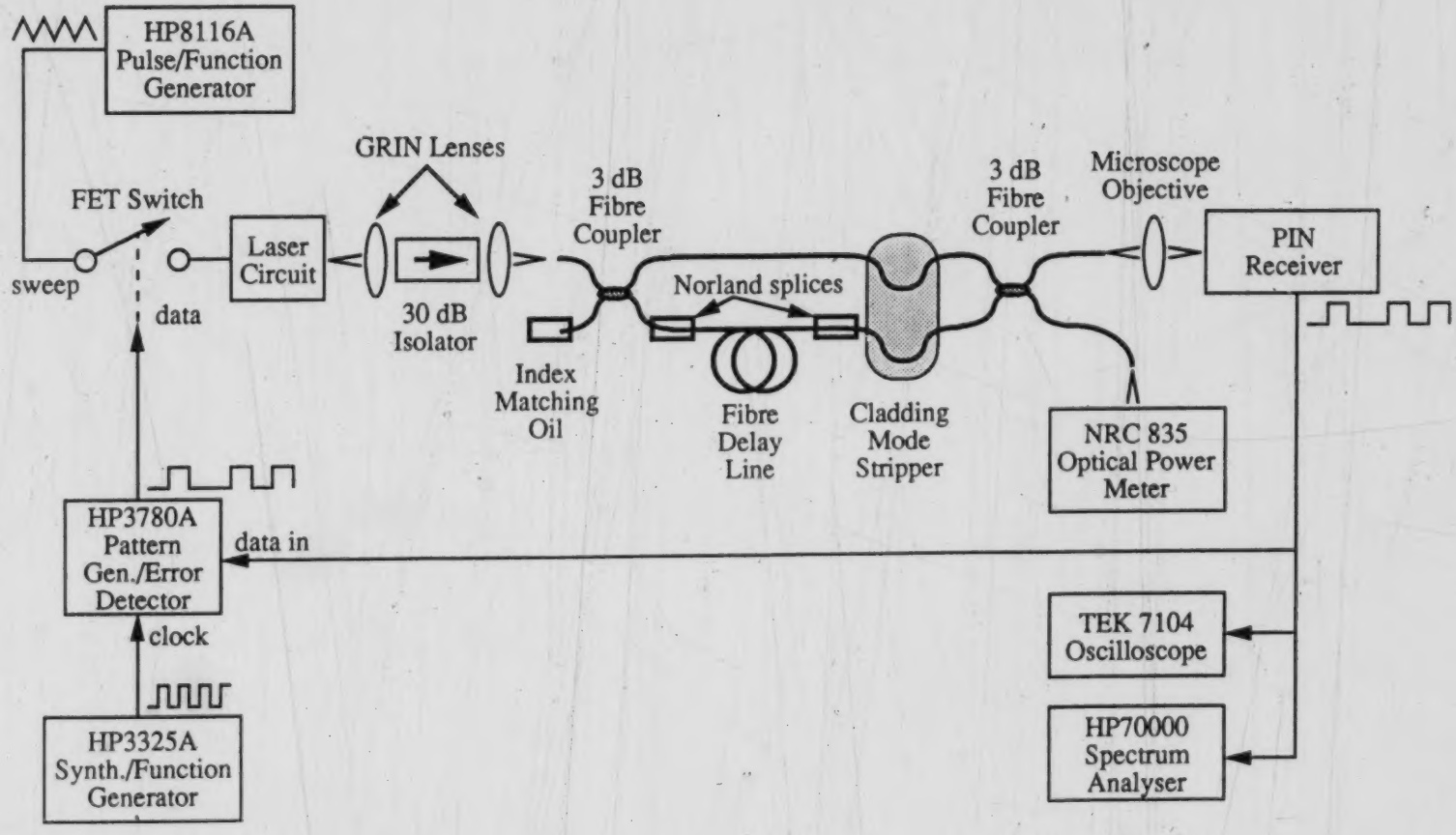

Figure 4.15. Data transmission experimental configuration.

A second 3 dB coupler combines the light from the two paths, and the light is subsequently focussed by a Newport FLA-40 objective lens onto the PIN diode of the receiver. The signal from the receiver is sent to an oscilloscope, spectrum analyser, and also to the receiver of the HP 3780A to monitor bit errors. The second output of the coupler is directed onto a Newport 835 Optical Power Meter in order to monitor the received optical power.

The block diagram of the receiver appears in Figure 4.16, with details of the blocks in Figures C.3 to C.11, in Appendix C.

In the receiver, light is transformed into an electrical signal by the PIN diode, and the IF signal is amplified to a level that the demodulator can handle. The bandpass filter, BP1, is required to select only the IF signal, and the highpass filter, HP2, is added to provide extra reduction of the low frequency noise due to laser linewidth. The demodulator downconverts the IF signal to baseband using a Schottky diode as a square law detector, and also provides some gain with a built-in high-input-impedance FET amplifier. Data is filtered by a low pass filter, LP1 or LP2, to remove high frequency components generated in the demodulator, and is amplified with an automatic gain control (AGC) circuit. There is a dc bias level control at the output of the AGC amplifier so that the signal may be shifted to a position that is optimum with respect to the threshold of error detector.

4.2.2 Data Transmission

The system described above was used to transmit data at a rate of 10 Mb/s. An IF of between 650 and 800 MHz was chosen to give a high IF-to-bit rate ratio while maintaining an easily handled frequency. The bandpass filter was designed with a centre frequency of 688 MHz and a bandwidth of 580 MHz.

The upper trace in Figure 4.17 shows the IF obtained at the output of amplifier 3 (point I in Figure 4.16) when a 20 MHz, 4.4 mA peak-to-peak triangle wave was applied to the laser, a path imbalance of 1.87 meters was in place, and 10 Mb/s data in NRZ format was superimposed. The lower trace was obtained by disabling the triangle sweep, and represents the received noise level due to laser linewidth. The centre of the IF spectrum was estimated at 750 MHz, which, using expressions (2.13) and (4.1), gives a k_f of 455 MHz/mA. Note the peak near 1.3 GHz due to the external cavity, which was still present despite the use of a twisted cleave. Note also that an IF signal appeared at about 200 MHz because of the presence of the lower amplitude triangle due to the FET switch's non-zero

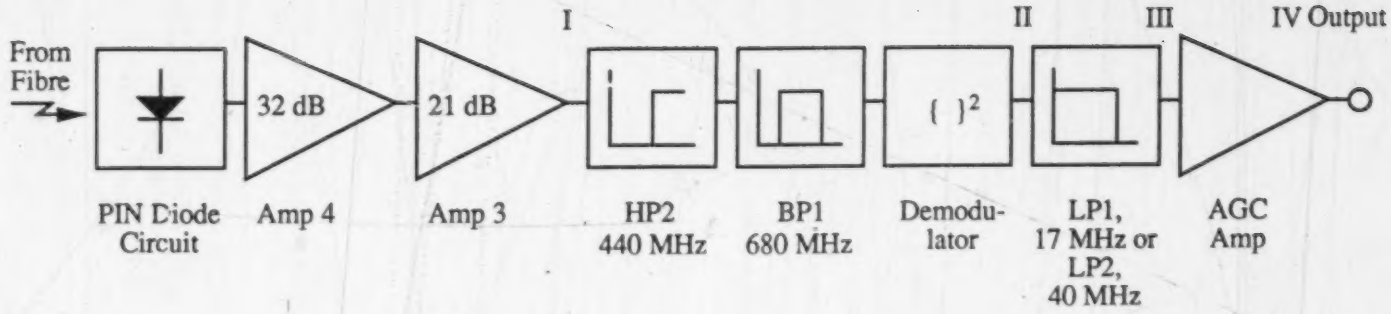

Figure 4.16. PIN receiver.

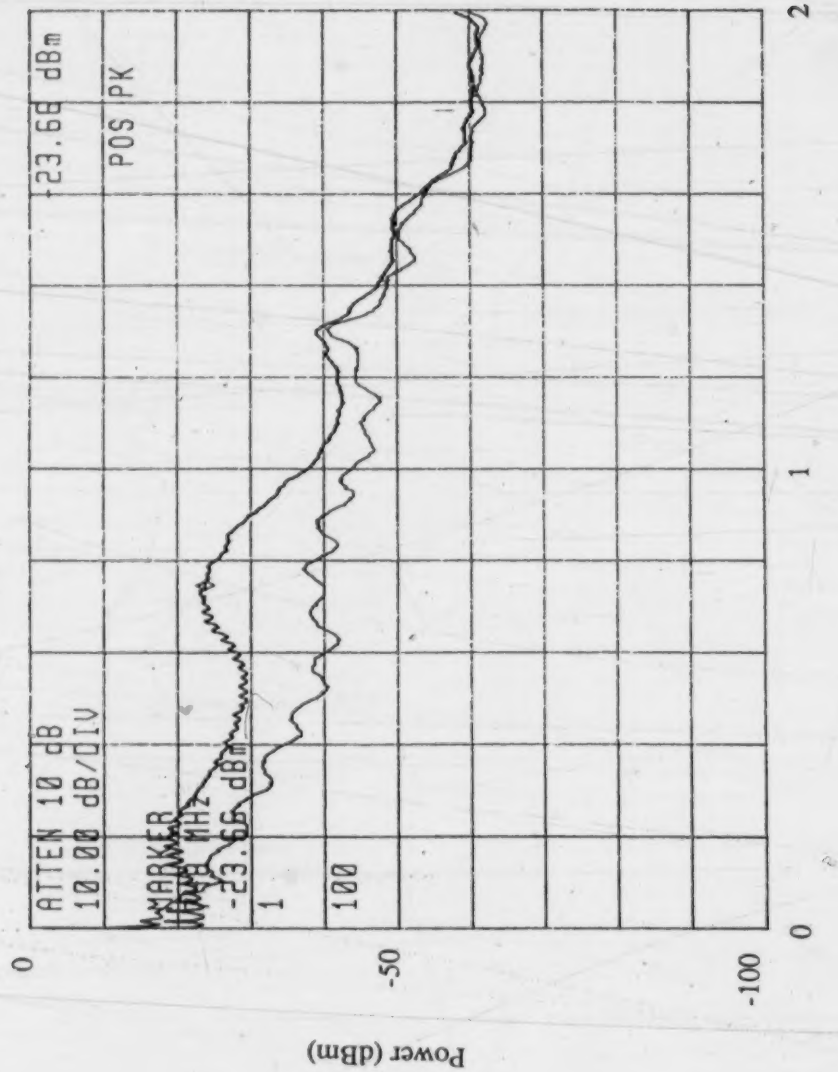

Figure 4.17. Received IF spectrum.

extinction ratio. The ratio of the lower to higher IFs is roughly 200 MHz/750 MHz=0.27, which is close to the 0.24 extinction ratio obtained in Section 4.2.1.

The width of IF signal was approximately 200 MHz. It is believed that this width was mainly due to three factors: the linewidth of the laser, nonlinearity of the triangle wave, and a nonlinear relationship between laser drive current and optical frequency.

The oscilloscope signal at point I in Figure 4.16 appears at the bottom of Figure 4.18, the top signal being the transmitted data signal of bit sequence '1010... .' A different IF of similar amplitude appears for each of the bits '1' and '0.' When this signal is filtered, only the data-carrying IF remains, as shown in Figure 4.19.

Data is recovered by the demodulator, which follows the envelope of the filtered IF signal, and subsequent low pass filtering rejects the high frequency components. Two different low pass filters were tried in order to observe the effect of cutoff frequency. Figure 4.20(a) shows the oscilloscope trace at point III in Figure 4.16 when a filter with a cutoff frequency of 40.9 MHz was in place, and Figure 4.20(b) is that with a 17.5 MHz filter. To understand why the '0' in trace (a) is noisier, refer back to Figure 2.3. In this figure, it is obvious that the signal disappears for the delay time, Δt, twice per triangle period. This results in a signal added to the '0' having a frequency twice that of the triangle. The 17.5 MHz filter is able to remove this signal while the 40.9 MHz filter is not, hence the trace in (b) is cleaner. Figure 4.21 shows the unfiltered 'chop-out' signal more clearly. Here, the triangle frequency is 40 MHz, giving a chop-out signal of 80 MHz.

The amplified data at point IV (in Figure 4.16) appears in Figure 4.22. An estimate can be made of the received signal-to-noise ratio (SNR) by estimating the signal and noise amplitudes in this oscilloscope trace. The signal amplitude, v_{signal}, is approximately 700 mV peak-to-peak, and the noise amplitude, v_{noise}, is about 160 mV peak-to-peak. This gives a SNR of approximately 13 dB. Using the expression [32]

$$BER = \frac{1}{2} \cdot \operatorname{erfc}\left(\frac{v_{signal}/v_{noise}}{\sqrt{2}}\right) \tag{4.3}$$

which relates signal and noise voltages to bit error rate (BER) for fibre systems, a BER of 6.1×10^{-6} is obtained In fact, the BER measured for the data pattern, '1010... ,' was as low as 2.7×10^{-7}. This rough calculation is thus reasonably close to the actual BER.

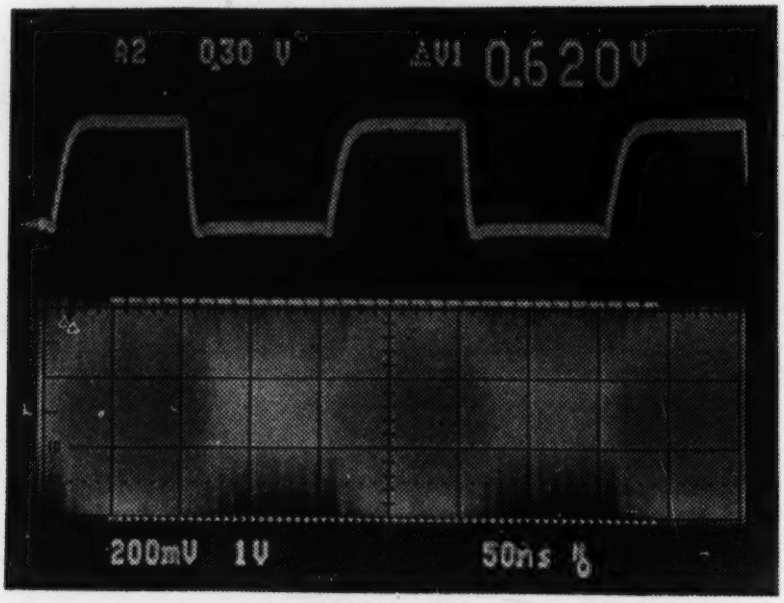

Figure 4.18. Transmitted and received IF oscilloscope signals, unfiltered (horizontal scale: 50 ns/div., vertical scales: 1 V/div. upper trace, 200 mV/div. lower trace).

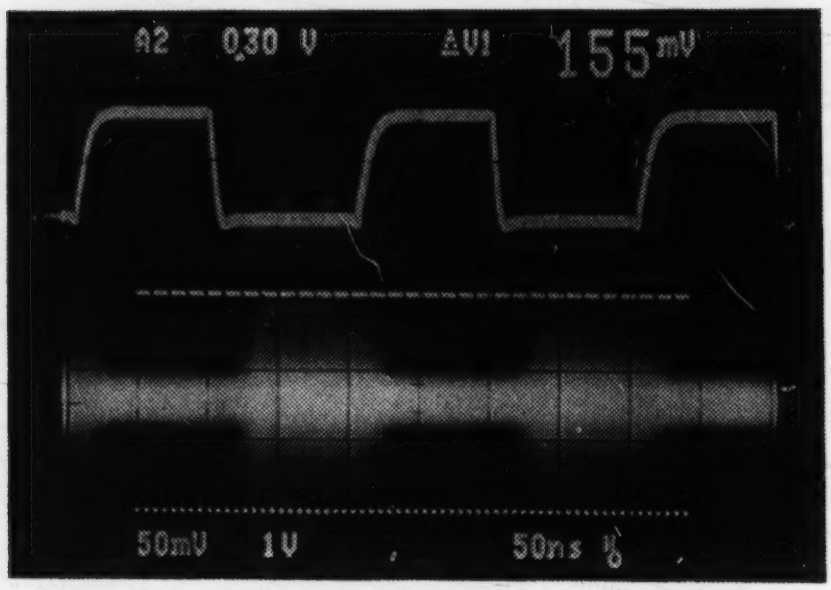

Figure 4.19. Transmitted and received IF oscilloscope signals, filtered with bandpass filter (horizontal scale: 50 ns/div., vertical scales: 1 V/div. upper trace, 50 mV/div. lower trace).

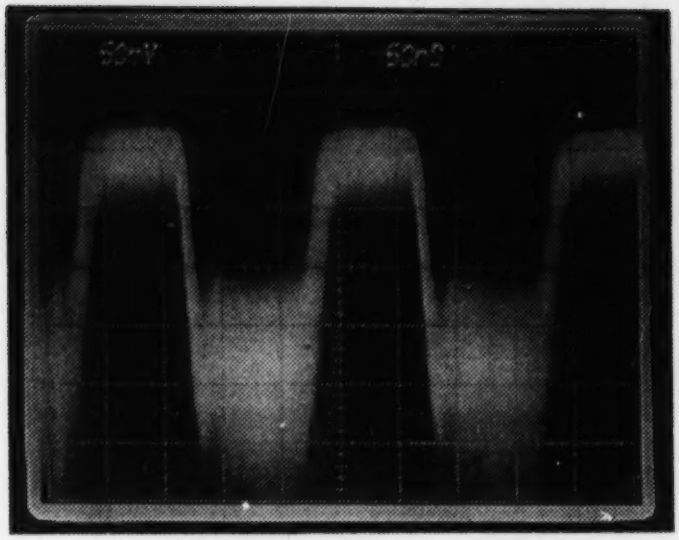

(a) using lowpass filter with 40.9 MHz cutoff frequency

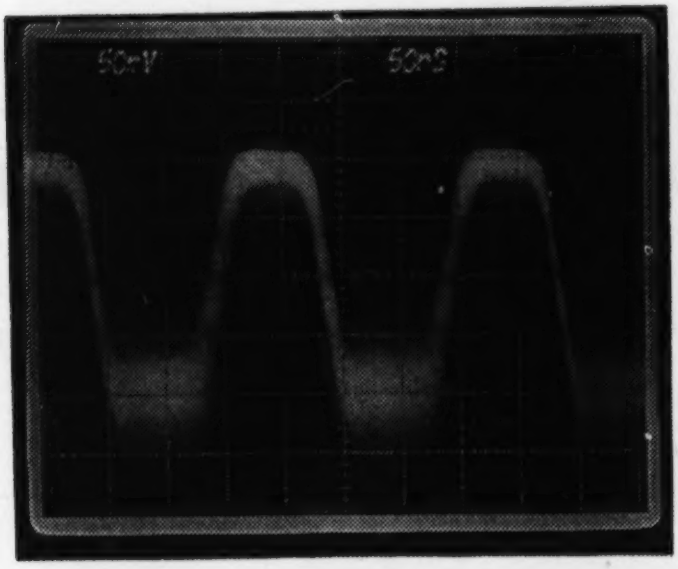

(b) using lowpass filter with 17.5 MHz cutoff frequency

Figure 4.20. Demodulated data 1010... (horizontal scale: 50 ns/div., vertical scale: 50 mV/div.).

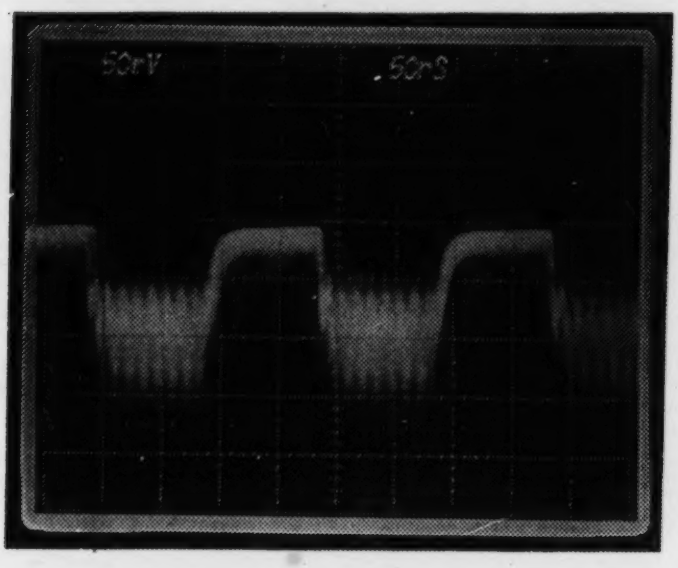

Figure 4.21. Demodulated data 1010... , using 40 MHz sweep, unfiltered (horizontal scale: 50 ns/div., vertical scale: 50 mV/div.).

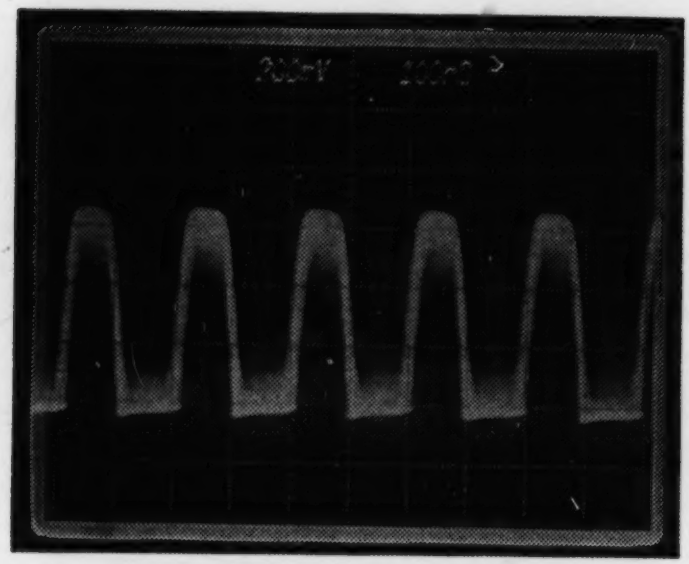

Figure 4.22. Demodulated data 1010... , after amplification (horizontal scale: 100 ns/div., vertical scale: 200 mV/div.).

The SNR ratio can also be inferred from the IF spectrum of Figure 4.17. If the area under each of the two curves within the bandpass filter extremes is estimated, a SNR of approximately 14 dB is obtained. This is close to the above estimate.

The eye diagram obtained with a pseudo-random bit sequence (PRBS) of length 2^{20}-1 is shown in Figure 4.23. The BER obtained for this sequence was 6.0×10^{-6}. The degradation of BER from the '1010...' pattern to the above PRBS can be explained by inspecting Figure 4.24. This is the received signal for the pattern, '1010,' followed by ten additional '0's. The noise is significantly higher, and this is because of the AGC amplifier. When many '0's occur in a row, the amplitude detection circuit of the AGC amplifier detects a lower level signal , and thus boosts the gain. This serves to amplify the noise, which degrades the SNR, and thus raises the BER.

It was shown that optical feedback into the laser was still at a level which affected the BER performance by adjusting the laser-to-fibre coupling. When the coupling efficiency was adjusted to its optimum, giving a received light power of approximately 1 mW, the received data stream was so noisy that the eye was completely closed. The level of optical feedback was lowered gradually by axially misaligning the fibre with respect to the focus of the laser light, and in doing so, the eye slowly opened. One can conclude from this that the noise was primarily due to optical feedback. The results described above were obtained when the coupling efficiency was approximately 6 dB worse than the best obtainable efficiency. This particular alignment, giving a received light power of about 230 μW, afforded the best BER. Further misalignment lowered the signal to a level below the thermal noise limit of the amplifier, and thus the BER was degraded.

An attempt was made to assess the level of crosstalk that would appear if there were a second transmission adjacent in frequency. This was done in two ways. First, the width of the frequency sweep was doubled by doubling the amplitude of the triangle wave. This resulted in a doubling of the IF. The effect of this was to place the secondary IF signal (that signal due to the non-extinguished sweep) very near the 650 MHz cavity mode. Thus, the cavity mode seemed to become noisy, and while no data could be recovered, the noise level within the receiver's bandpass filter was increased by a few dB. Also, the primary IF was still partially inband due to its large width, and therefore also contributed to the noise level. Second, the 1.87 m optical path was replaced by one of length 10 m, to simulate addressing by delay insertion. There was very little additional noise since the IF

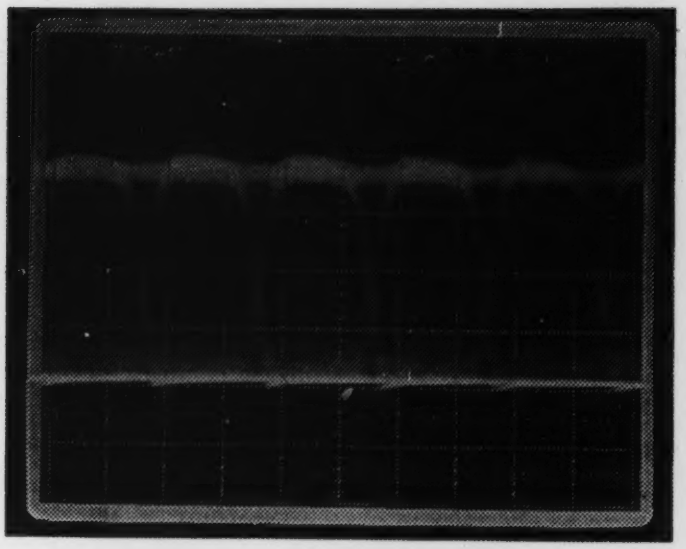

Figure 4.23. Received eye diagram, PRBS sequence of length 2^{20}-1 (horizontal scale: 50 ns/div., vertical scale: 200 mV/div.).

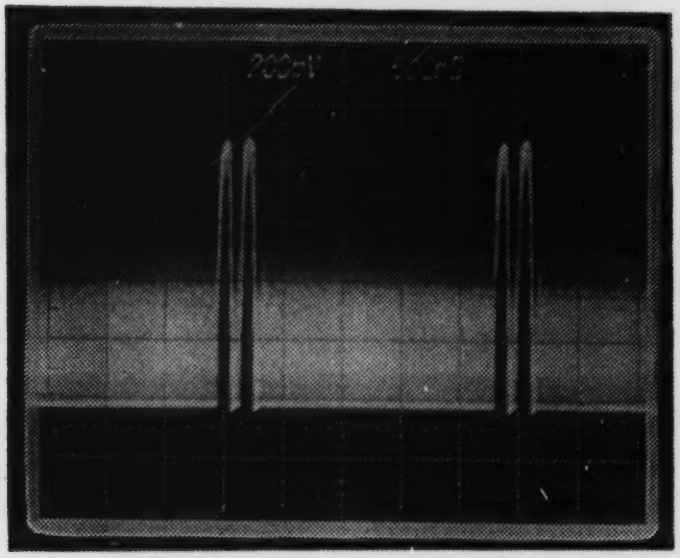

Figure 4.24. Received data, 1010000000000... (horizontal scale: 500 ns/div., vertical scale: 200 mV/div.).

was shifted up by a factor more than 5. From this it may be concluded that the cross-channel interference was at a level below that of the phase noise.

4.2.3 Receiver Noise Discussions

From the experimental data obtained in the previous section, some general statements about the noise in the system can be made.

It was stated in Section 2.4.2 that a linewidth-to-bit-rate ratio of 0.17 is theoretically required to achieve a BER of 10^{-10}. By way of an indirect comparison to this system, it is noted that a BER of 10^{-7} was achieved with a ratio of 1.

The dominant noise in this system is that which arises from the laser linewidth. In Figure 4.17, one may assume that the noise is constant with frequency within the passband of the filter at a level of -40 dBm. Using the resolution bandwidth of 300 kHz, a noise power spectral density of 3.3×10^{-10} mW/Hz is obtained. Thus the total noise power in the filter bandwidth of 580 MHz is 0.19 mW, or -7.2 dBm. This power level is at the output of the amplifier, Amp 3. To refer this noise to the input of the first amplifier, the 53 dB of gain and the 7 dB cumulative amplifier noise figure is subtracted from -7.2 dBm, giving a noise level of -67.2 dBm at the detector. To show that this is in fact the dominant noise, the thermal and detector shot noise contributions are calculated from standard equations. Thermal noise with the above filter bandwidth is -86 dBm, and shot noise for a typical detector current of 220 μA is -104 dBm. These noise powers are much less than the linewidth noise.

The receiver sensitivity may be defined in this instance as that signal level which gives a BER of 10^{-7}. From expression (4.3), the required SNR is 14.3 dB. With the measured noise level of -67.2 dBm, a signal level of -52.9 dBm out of the detector is required.

Knowing that linewidth noise is dominant, there are two things that may be done to improve the BER. First, since the linewidth noise decreases with increasing frequency, one may shift the IF up in frequency to where the noise is lower. This, however, requires higher frequency receiver components, which is more costly. Second, linewidth noise may be reduced by increasing the optical isolation.

CHAPTER 5

SUMMARY AND CONCLUSIONS

This thesis has discussed the Optical Time-of-Flight Multiplexing (OTFM) technique, which is a method for addressing and multiplexing signals in an optical local area network. This coherent, self-heterodyne technique promises fuller utilisation of the immense bandwidth that optical fibre provides. The thesis attempted to assess some of the problems and options in the implementation of a network utilising OTFM, and to prove the concept by transmitting data between two nodes.

OTFM is based on a network which provides two signal paths between nodes. The difference in propagation times in the two paths is used as an address. By appropriate design of the network, propagation time differences may be arranged to be unique, and thus there exist unique addresses. To make use of these addresses, a technique called Frequency Modulated Continuous Wave (FMCW) ranging is used, in which the optical frequency of a laser is linearly swept. This technique transforms unique time differences into unique radio frequency carriers upon which messages may be placed.

There are several schemes of addressing possible in an OTFM system. These include bandpass filter tuning, frequency shifting by external modulator, frequency sweep parameter adjustment, and optical delay insertion. It was shown that optical delay insertion is the most desirable scheme at high bit rates, since the other techniques impose severe network size constraints at high bit rates.

Numerous frequency domain effects arise from the use of FMCW in an OTFM system, some of which are: the signal 'chop-out effect,' in which the message drops out for short periods of time, carrier frequency broadening due to linewidth of the laser, and broadening due to laser intensity modulation. It was shown that the chop-out and intensity modulation effects could be controlled with careful system design. The effect due to laser linewidth was, on the other hand, more severe. Results from the literature [31] suggest that linewidth-to-bit-rate ratios of 0.17 are required for a bit error rate of 10^{-10}.

There exist a number of topologies that provide the dual paths that OTFM requires. The topologies reviewed in this thesis were the central loop, bus, double star, folded ring, and ladder networks, from the points of view of network size maximisation, constant received power, robustness, and freedom from addressing ambiguities and signal

repropagation. It was suggested that the double star and bus networks were the most desirable topologies.

An experimental system was set up in which digital data at a rate of 10 Mb/s was transmitted between two mock-up nodes. The system used a readily available and inexpensive single mode laser, similar to the type found in compact disk players. The best bit error rate obtained was 10^{-7}, and was believed to be limited by laser linewidth and optical frequency instability due to optical feedback into the laser. The linewidth-to-bit-rate ratio for the system was 1. The three dB width of the received IF spectrum was found to be approximately 200 MHz.

Much more research could be done on the OTFM technique. Some possible avenues that may be explored are outlined in the following paragraphs.

A more thorough study of the effect of linewidth on the breadth of the received spectrum is desirable. This would involve an approach similar to that taken in [21], but with the consideration of a swept frequency optical signal. From this theory, channel separation rules could be derived which are specifically applicable to OTFM.

The bit error rate for data transmission could be improved by increasing the level of optical isolation. The 30 dB of isolation used in this research was shown to be insufficient, and was believed to be the factor limiting the bit error rate performance.

Another avenue of potential research is the construction of a system utilising the external modulator addressing scheme. Only the delay insertion and frequency width addressing schemes were tried in this research.

Furthermore, a multi-node experimental system could be built to assess the effect of the buildup of cross-channel interference due to several active nodes.

To conclude, the OTFM principle may be a feasible data transmission technique for use in an optical local area network. It was found that are several problems to be considered in designing a system using OTFM, but it was shown that there are solutions to these problems. Further, the construction of an experimental system proved that the technique does indeed work.

REFERENCES

[1] Y. Yamamoto and T. Kimura, "Coherent optical fiber transmission systems," *IEEE J. Quantum Electron.*, vol. QE-17, pp. 919-935, June 1981.

[2] T. Okoshi, "Recent advances in coherent optical fiber communication systems," *IEEE J. Lightwave Technol.*, vol. LT-5, pp. 44-52, Jan. 1987.

[3] R.A. Linke and P.S. Henry, "Coherent optical detection: a thousand calls on one circuit," *IEEE Spectrum*, vol. 24, pp. 52-57, Feb. 1987.

[4] T. Kimura, "Coherent optical fiber transmission," *IEEE J. Lightwave Technol.*, vol. LT-5, pp. 414-428, April 1987.

[5] L.G. Kazovsky, "Multichannel coherent optical communications systems," *IEEE J. Lightwave Technol.*, vol. LT-5, pp. 1095-1102, Aug. 1987.

[6] L.G. Kazovsky and R.E. Wagner, "Multichannel coherent lightwave technology," *Proc. of ICC*, pp.1210-1218, June 1987.

[7] Y. Yoshikuni and G. Motosugi, "Multielectrode distributed feedback laser for pure frequency modulation and chirping suppressed amplitude modulation," *IEEE J. of Lightwave Technol.*, vol. LT-5, pp. 516-522, April 1987.

[8] A.H. Cherin, *An Introduction to Optical Fibers*, McGraw-Hill Book Company, New York, 1983.

[9] T. Okoshi, "Polarization-state control schemes for heterodyne or homodyne optical fiber communications," *IEEE J. Lightwave Technol.*, vol. LT-3, pp. 1232-1236, Dec. 1985.

[10] R. Noe, H. Heidrich, and D. Hoffmann, "Endless polarization control systems for coherent optics," *IEEE J. Lightwave Technol.*, vol. 6, pp. 1199-1208, July 1988.

[11] K. Kobayashi and I. Mito, "Single frequency and tunable laser diodes," *IEEE J. Lightwave Technol.*, vol. 6, pp. 1623-1633, Nov. 1988.

[12] Y.F. Chan and G.D. Cormack, "Singlemode operation and linewidth reduction of a GRECC multimode semiconductor laser," *Proc. of Wescanex 88*, 11-12 May, 1988, pp. 119-121.

[13] A. Yariv, *Optical Electronics, 3rd edition*, Holt, Rhinehart and Winston, USA, 1985.

[14] D.R. Scifres, R.D. Burnham, and W. Striefer, "Single longitudinal mode operation of diode lasers," *Appl. Phys. Lett.*, vol. 31, pp. 112-114, July 1977.

[15] W. Streifer, R.D. Burnham, and D.R. Scifres, "Dependence of longitudinal mode structure on injected carrier diffusion in diode lasers," *IEEE J. Quantum Electron.*, vol. QE-13, pp. 403-404, June 1977.

[16] R.F. Kazarinov, C.H. Henry, and R.A. Logan, "Longitudinal mode self-stabilization in semiconductor lasers," *J. Appl. Phys.*, vol. 53, pp. 4631-4644, July 1982.

[17] K.E. Stubkjaer and M.B. Small, "Noise properties of semiconductor lasers due to optical feedback," *IEEE J. Quantum Electron.*, vol. QE-20, pp. 472-478, May 1984.

[18] C.H. Henry and R.F. Kazarinov, "Instability of semiconductor lasers due to optical feedback from distant reflectors," *IEEE J. Quantum Electron.*, vol. QE-22, pp. 294-301, Feb. 1986.

[19] McPherson Model 270 Scanning Monochromator Instruction Manual.

[20] T. Okoshi, K. Kikuchi, and A. Nakayama, "Novel method for high resolution measurement of laser output spectrum," *Electron. Lett.*, vol. 16, pp.630-631, 1980.

[21] K. Kikuchi and T. Okoshi, "High resolution measurement of the spectrum of semiconductor lasers," *Japan. Annual Review on Electronics, Comp.,*

Telecomm., Opt. Devices and Fibres, 1982. Published by Ohmsha Ltd., Tokyo, Japan and North Holland Publishing Co., Amsterdam, Netherlands, pp. 51-59, 1982.

[22] R.I. MacDonald, "Optical Time-of-Flight Multiplexing," ATRC internal report, 1987.

[23] D. Uttam, I.P. Giles, B. Culshaw, and D.E.N. Davies, "Remote interferometric sensors using frequency modulated laser sources," *Proc. of First International Conference on Optical Fibre Sensors*, 26-28 April, 1983, pp. 182-184.

[24] I. Sakai, "Frequency-division multiplexing of optical-fibre sensors using a frequency-modulated source," *J. of Optical and Quantum Electronics*, vol. 18, pp. 279-289, 1986.

[25] H. Hattori and T. Takeo, "Optical fiber position sensor using a frequency modulated semiconductor laser," *Fiber Optic and Laser Sensors V*, SPIE vol. 838, pp. 288-291, 1987.

[26] D.W. Smith, P. Healy, G.P. Fry, K. and Clayton, "A frequency chirped heterodyne spread spectrum optical fibre multiple access technique," *Proc. of 14th European Conference on Optical Communication*, 11-15 September, 1988, pp. 82-85.

[27] W. Elsässer and E.O. Göbel, "Multimode effects in the spectral linewidth of semiconductor lasers," *IEEE J. Quantum Electron.*, vol. QE-21, pp. 687-691, June 1985.

[28] A.J. Hymans, and J. Lait, "Analysis of a frequency-modulated continuous-wave ranging system," *Proc. IEE*, vol. 107B, pp. 365-372, 1960.

[29] British Telecom and DuPont Preliminary Data Sheets, *IOC1500 KTP phase modulator, IOC250 KTP Mach-Zehnder modulator*, Dec. 1988.

[30] B. Swekla, ATRC private communication.

[31] L.G. Kazovsky, "Impact of laser phase noise on optical heterodyne communication systems," *J. Optical Communications*, vol. 7, pp. 66-78, 1986.

[32] G. Keiser, *Optical Fiber Communications*, McGraw-Hill Book Company, New York, 1983.

APPENDIX A

APL FUNCTION LISTINGS

This appendix contains the APL functions which were written for this thesis. The first function, LS2, uses the algorithm described in Section 3.2 to generate an asymmetric ladder network. The second function, FINDS, uses LS2 with different patterns of slot-skipping. The third function, LSQ, is able to generate one specific pattern of an asymmetric ladder very quickly.

```
NAME OF WORKSPACE:
1 wsdoc
LISTED ON 1989 10 3 AT 22:22


FUNCTIONS:
LS2         1


LISTING OF ALL FUNCTIONS:
[00]  LS2
[01]  ⍝ THIS FUNCTION WILL CREATE A LADDER NETWORK OF A GIVEN SIZE WITH
[02]  ⍝ NO SYMMETRIES.  THE SKIP VECTOR, S, IS USED TO CREATE DIFFERENT
[03]  ⍝ NETWORKS BY SKIPPING STATION OPPORTUNITES.  THIS VERSION IS TO
[04]  ⍝ BE USED WHEN LOOPING WITH FUNCTION FINDS, AS IT IS STREAMLINED
[05]  ⍝ TO FIND THE OPTIMUM S ONLY.
[06]  START←⎕TS
[07]  SS←S
[08]  P←1,(N-1)/2
[09]  NONES←1
[10]  PO←1
[11]  L←1
[12]  I←1
[13]  LP3:I←I+1 ⍝                    'CREATE' LOOP
[14]  →(I=N+1)/END
[15]  →(P[I]<2)/LP3 ⍝                CHECK IF STATION ALLOWED HERE
[16]  →(SS[L]=1)/JMP1 ⍝              SHOULD THIS OPEN SPOT BE SKIPPED?
[17]  SS[L]←SS[L]-1
[18]  →LP3
[19]  JMP1:L←L+1
[20]  NONES←NONES+1
[21]  PO←PO,I ⍝                      STORE POSITION OF NEW STATION
[22]  P[I]←1 ⍝                       ADD IN NEW STATION
[23]  J←0
[24]  LP2:J←J+1 ⍝                    'X OUT' LOOP
[25]  →(J=NONES)/LP3
[26]  X←I+I-PO[J] ⍝                  X IS THE SYMMETRY TO RIGHT OF I TO BE X-ED
[27]  →(X>N)/JMP2 ⍝                  IF X IS TOO BIG, FORGET IT
[28]  P[X]←0 ⍝                       X IT OUT (BY SETTING TO 0)
[29]  JMP2:X←0.5×I+PO[J] ⍝           X IS THE SYMMETRY TO LEFT OF PO[J]
[30]  Y←PO[J]+PO[J]-1 ⍝              Y IS THE BISECTOR OF I AND PO[J]
[31]  →(X≠⌊X)/JMP3 ⍝                 SKIP IF DIFFERENCE OF I AND PO[J] IS ODD
[32]  P[X]←0 ⍝                       X OUT THIS SPOT
[33]  JMP3:→(Y<2)/LP2
[34]  P[Y]←0 ⍝                       X OUT  THIS SPOT
[35]  →LP2
[36]  END:
[37]  I←1 ⍝                          FINAL STEP
[38]  LP5:→(I=N)/END2
[39]  I←I+1
[40]  →(P[I]≠2)/LP5 ⍝                CHECK IF THIS SPOT IS OPEN
[41]  P[I]←1 ⍝                       PUT IN A STATION
[42]  PO←PO,I ⍝                      STORE ITS POSITION
[43]  NONES←NONES+1
[44]  J←0
[45]  LP4:J←J+1
[46]  →(J=NONES)/LP5
[47]  →(PO[J]≥I)/LP4
[48]  X←I+I-PO[J] ⍝                  X OUT SYMMETRY TO LEFT
[49]  →(X>N)/LP4
```

A.1. APL function: LS2.

```
[50]  P[X]←0
[51]  Y←0.5×I+PO[J] ⍬                X OUT BISECTION
[52]  →(Y≠⌊Y)/LP4
[53]  P[Y]←0
[54]  →LP4
[55]  END2:PO←PO[⍋PO] ⍬              SORT PO IN ASCENDING ORDER
[56]  P←PO[NONES]↓P ⍬                CHOP OFF ZEROES AT THE END
[57]  N1←⍴P ⍬                         COUNT THE NUMBER OF INTERVALS LEFT
[58]  UT←100×NONES÷N1 ⍬               CALCULATE THE NETWORK EFFICIENCY
[59]  FINISH←⎕TS
[60]  TIME←FINISH-START
[61]  'TIME TAKEN:  ';TIME
-------------------------------------  1


VARIABLES:


GROUPS:
essentials
```

```
        WORKSPACE DOCUMENTATION

NAME OF WORKSPACE:
1 wsdoc
LISTED ON 1989 10 3 AT 22:45


FUNCTIONS:
FINDS       1


LISTING OF ALL FUNCTIONS:
[00]  FINDS
[01]  ⍝ THIS FUNCTION CREATES ASYMMETRIC NETWORKS GENERATED BY NUMEROUS
[02]  ⍝ SKIP VECTORS (THE NUMBER OF WHICH IS ENTERED BY THE USER), AND
[03]  ⍝ WRITES THE SKIP VECTOR ID NUMBER, NUMBER OF ADDRESSABLE NODES,
[04]  ⍝ NUMBER OF POTENTIALLY ADDRESSABLE NODES, AND NETWORK (OR PACKING)
[05]  ⍝ EFFICIENCY TO THE FILE SPECIFIED.  THE FUNCTION CALLS LS2 TO
[06]  ⍝ CALCULATE THE NETWORKS.
[07]  Z←⎕L,⎕R
[08]  'INPUT SIZE OF LADDER:'
[09]  N←⎕ ⍝                              THIS IS THE SIZE OF THE NETWORK
[10]  'MAXIMUM SKIP SIZE:'
[11]  SMAX←⎕ ⍝                           THIS IS THE MAXIMUM NUMBER OF AVAILABLE NODES
[12]  ⍝                                    THAT WILL BE SKIPPED
[13]  'HOW FAR TO GO WITH S (MUCH LESS THAN SMAX*(N÷2)):'
[14]  Q←⎕ ⍝                              THIS IS THE NUMBER OF SKIP VECTORS TO TRY
[15]  'FILE TO WRITE TO (MUST ALREADY EXIST):'
[16]  FILE←⎕
[17]  START←⎕TS
[18]  'TIME STARTED:  ';START
[19]  1 STTIE PATH,FILE
[20]  R←((⍕N,Q,SMAX),Z)STWRITE 1
[21]  N2←⌊N÷4
[22]  C←¯1+⍳Q
[23]  SMAT←1+⍉⍉(N2/SMAX)⊤C ⍝             CREATE A MATRIX OF SKIP VECTORS
[24]  C←1
[25]  'PROGRAM RUNNING ........ AND RUNNING ............ AND RUNNING ...'
[26]  LP:→(C>Q)/END ⍝                    LOOP THROUGH THE SKIP VECTORS
[27]  S←SMAT[C;]
[28]  LS2
[29]  R←((⍕C,NONES,N1,UT),Z)STWRITE 1 ⍝   WRITE TO FILE
[30]  C←C+1
[31]  →LP ⍝                              LOOP BACK
[32]  END:FINISH←⎕TS
[33]  TIME←FINISH-START ⍝                CALCULATE TIME TAKEN
[34]  R←((⍕TIME),Z)STWRITE 1
[35]  STUNTIE 1
[36]  'DONE.  DATA STORED IN FILE: ',PATH,FILE
[37]  'TIME TAKEN:                 ';TIME
------------------------------------  1


VARIABLES:


GROUPS:
```

A.2. APL function: FINDS.

```
        WORKSPACE DOCUMENTATION

NAME OF WORKSPACE:
1 wsdoc
LISTED ON 1989 10 3 AT 23:5


FUNCTIONS:
LSQ         1


LISTING OF ALL FUNCTIONS:
[00]  LSQ
[01]  ⍝ THIS FUNCTION CREATES AN ASYMMETRIC LADDER FUNCTION QUICKLY BY
[02]  ⍝ CALCULATING THE APPROPRIATE SERIES NUMBERS.
[03]  'HOW MANY SERIES NUMBERS DO YOU WANT TO DO ?'
[04]  SN←⍞
[05]  SER←⍳SN
[06]  SER[1]←1
[07]  K←2
[08]  LP1:SER[K]←¯1+3×SER[K-1] ⍝     CALCULATE SERIES NUMBERS
[09]  K←K+1
[10]  →(K≤SN)/LP1
[11]  K←2
[12]  A←1
[13]  LP2:A←A,SER[K],A ⍝             CREATE NETWORK VECTOR
[14]  K←K+1
[15]  →(K≤SN)/LP2
------------------------------------  1


VARIABLES:


GROUPS:
essentials
```

A.3. APL function: LSQ.

APPENDIX B

DEVICE DATA SHEETS

This appendix contains the data sheets for the two Ortel SL300-H lasers, and the Sharp LTO15MF laser, as well as for the Ortel PD050-OM PIN photodiode.

ORTEL CORPORATION

LDS10-H
LASER DIODE

NOTE: The SL 300H is an improved version of the LDS10-H

SINGLE LONGITUDINAL MODE GaAlAs LASER

FEATURES

- 10mW Output Power
- Single Spatial Mode
- Single Longitudinal Mode
- No Astigmatism
- 150ps Rise Time
- 25mA Threshold Current

DESCRIPTION

Ortel Corporation's Model LDS10-H consists of a very low threshold, highly efficient, single spatial mode GaAlAs laser diode mounted on an open heatsink. The model LDS10-H emits up to 10mw and has a direct modulation bandwidth of 3 GHz. Light-current characteristics are highly linear and kink-free.

The output facets of the Model LDS10-H laser are passivated to assure long operating lifetime. The laser chip is mounted junction side up on the heatsink. The mount is designed to allow complete access to the front facet of the laser. Light from the rear facet of the laser can be used to monitor the laser output power.

The high speed performance of Model LDS10-H allows modulation of the laser at frequencies as high as 3 GHz with typical rise and fall times of 150 picoseconds. The output wavelength (840 nm) is well matched to most optical fibers and to both GaAs and Si photodiodes. The absence of astigmatism and the nearly circular far field pattern allow the output beam to be easily collimated or focused to a diffraction limited spot.

The Model LDS10-H laser diode is well suited to a variety of applications, including:

- Free Space Communication
- Fiberoptic Communication
- Optical Disc Systems
- Optical Distance Measurement
- High Speed Instrumentation

The LDS10-series laser is also available in a high speed optical mount with a monitor photodiode (Model LDS10-OM) and with a fiber pigtail (Model LDS10-PM). Other versions based on a special high frequency laser cavity design have modulation bandwidths to 6 GHz (Models LDS10-OMF/PMF). Consult the factory for complete information.

ORTEL CORPORATION 2015 W. Chestnut St. • Alhambra, CA 91803 • (818) 281-3636 • TLX 752434

B.1. Data sheets for Ortel SL 300H laser.

ORTEL CORPORATION

LDS10-H
LASER DIODE

SINGLE LONGITUDINAL MODE GaAlAs LASER

DIMENSIONAL DRAWING

ABSOLUTE MAXIMUM RATINGS

PARAMETER	SYMBOL	RATING	UNITS
Laser Reverse Voltage	V_{rl}	3.0	V
Output Power	P_o	10.0	mW
Operating Temperature	T_{op}	0 to +50	°C
Storage Temperature	T_{st}	0 to +70	°C
Photodiode Reverse Voltage	V_{rp}	50	V

OPERATIONAL CHARACTERISTICS (@ 22°C)

PARAMETER		SYMBOL	MIN	TYP	MAX	UNITS
CW Optical Power①		P	5.6	7		mW
Threshold Current		I_{th}		25	50	mA
Peak Wavelength		λ_p	820	840	860	nm
Forward Voltage②		V_f		1.β	2.5	V
3dB Modulation Bandwidth③		B	2.5	3.0		GHz
Beam Diver-gence (FWHM)	Parallel	$\Theta_{\parallel}$		25		Degrees
	Perpen-dicular	$\Theta_{\perp}$		35		Degrees

NOTES: ① $I_f = I_{th} + 18mA$ (I_f = Forward Current)
② $I_f = 38mA$
③ $P_o = 7$ mW

ORTEL CORPORATION 2015 W. Chestnut St. • Alhambra, CA 91803 • (818) 281-3636 • TLX 752434

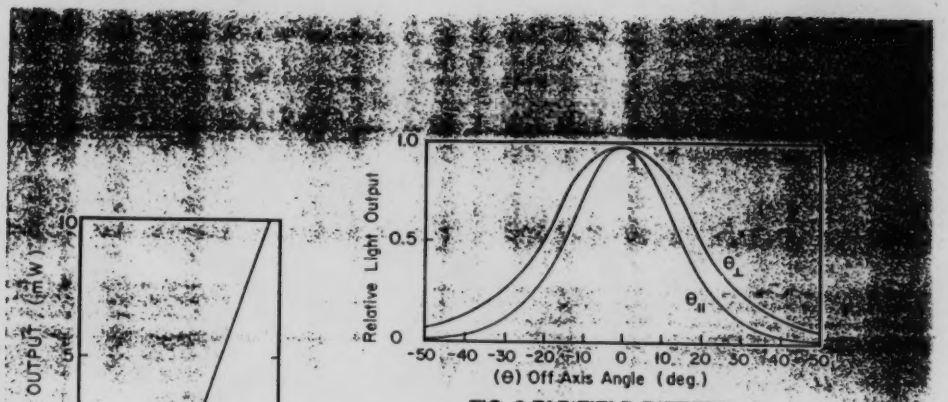

FIG. 3 FAR FIELD PATTERN

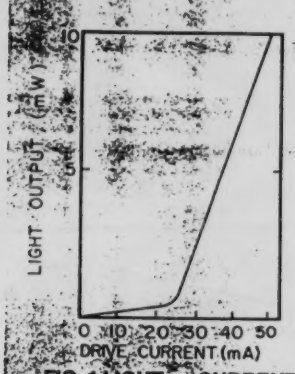

FIG. 1 LIGHT vs CURRENT

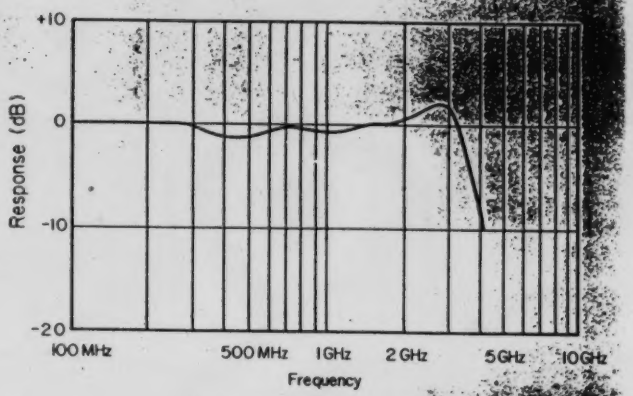

FIG. 4 FREQUENCY RESPONSE

(Measurement made with ORTEL CORPORATION Model PD050-OM GaAlAs/GaAs High Speed PIN Photodiode.)

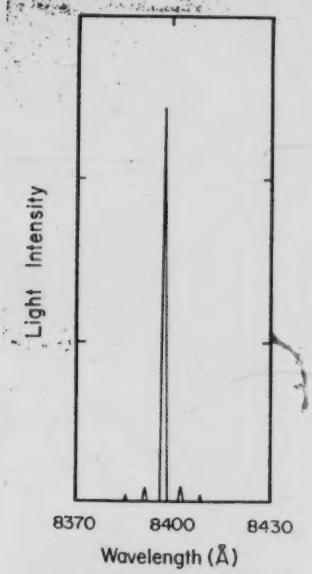

FIG. 2 EMISSION SPECTRUM

ORTEL CORPORATION

LDS10-H
LASER DIODE

SINGLE LONGITUDINAL MODE GaAlAs LASER

SAFETY CONSIDERATIONS

The laser light emitted from this laser diode is invisible and may be harmful to the human eye. Avoid looking directly into the laser diode or into the collimated beam along its optical axis when the device is in operation.

Operating the laser diode outside of its maximum ratings may cause device failure or a safety hazard.

OPERATION & HANDLING CONSIDERATIONS

The Ortel Model LDS10-H laser diode is a very low threshold, highly efficient device and is therefore susceptible to excesssive drive current. When using a power supply, a suitable current-limiting resistor should be placed in series with the laser diode. The laser diode should be connected or disconnected from the power supply only while the main power is on and the output voltage is set at zero. The current should be increased or decreased slowly while monitoring the laser optical output power.

The semiconductor laser chip on this device is mounted directly to an open heatsink. Proper care should be exercised to insure that no physicial contact is made with the laser chip or the bonding wires.

LABELING

Because of the small size of these devices, each of the labels shown below are attached to the individual shipping container. They are illustrated here to comply with DHEW standards under the Radiation Control for Health and Safety Act of 1968.

Warning Label

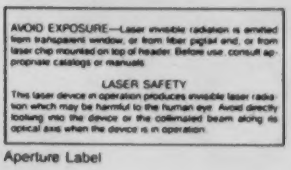
AVOID EXPOSURE—Laser invisible radiation is emitted from transparent window, or from fiber pigtail end, or from laser chip mounted on top of header. Before use, consult appropriate catalogs or manuals.
LASER SAFETY
This laser device in operation produces invisible laser radiation which may be harmful to the human eye. Avoid directly looking into the device or the collimated beam along its optical axis when the device is in operation.

Aperture Label

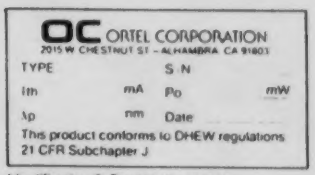

Identification & Certification Label.

Information contained herein is deemed to be reliable and accurate. No responsibility is assumed for its use, nor for any infringements on the rights of others. Ortel Corporation reserves the right to change the design, specifications, etc., of the product at any time without notice.

ORTEL CORPORATION 2015 W. Chestnut St. • Alhambra, CA 91803 • (818) 281-3636 • TLX 752434

ORTEL CORPORATION
2015 W. Chestnut St. Alhambra, CA 91803 Tel: (818) 281-3636 Telex: 752 434 Fax: (818) 281-8231

Serial No. W10509

Date 10-08-88

GaAlAs Laser Certificate

Laser Model: SL 300 - H

Threshold Current: 22 mA

Burn-in Test: ✓

Peak Wavelength: 838.7 nm

Absence of Self Pulsation: ✓

Forward Voltage: 2.22 Volts at 10mW output power

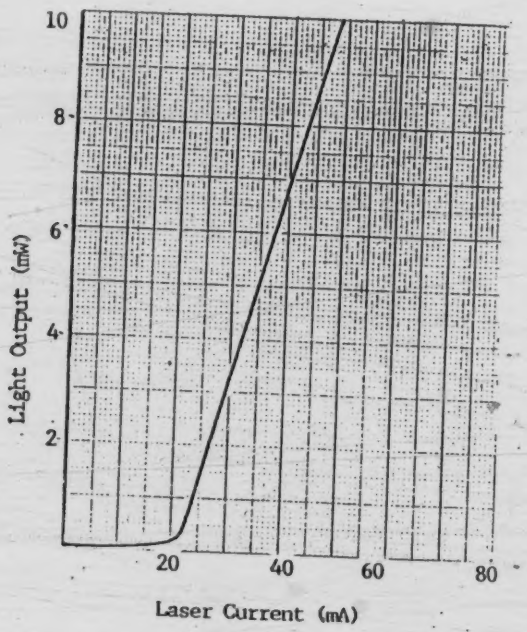

Stephanie N. Lee

Test Technician

OC ORTEL CORPORATION
2015 W. Chestnut St. Alhambra, CA 91803 Tel: (818) 281-3636 Telex: 752 434 Fax: (818) 281-8231

Serial No. W10511

Date 10.08.88

GaAlAs Laser Certificate

Laser Model: SL 300 - H

Threshold Current: 27 mA

Burn-in Test: ✓

Peak Wavelength: 834.0 nm

Absence of Self Pulsation: ✓

Forward Voltage: 2.28 Volts at 10mW output power

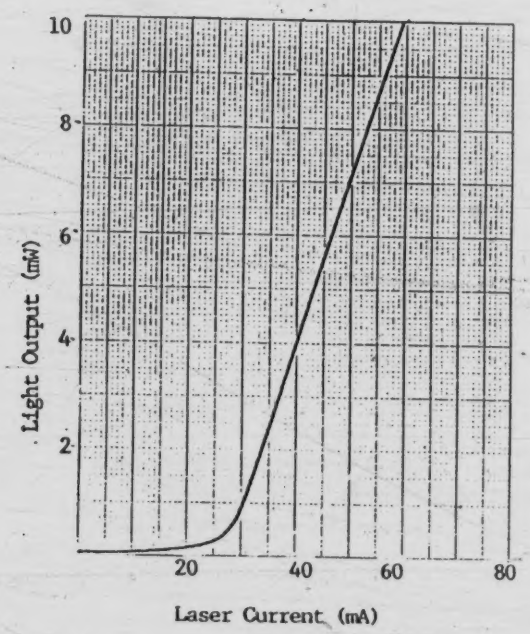

Stephanie N. Wu

Test Technician

ORTEL CORPORATION

MODEL PD050-OM PHOTODIODE

HIGH SPEED GaAlAs/GaAs PIN PHOTODIODE

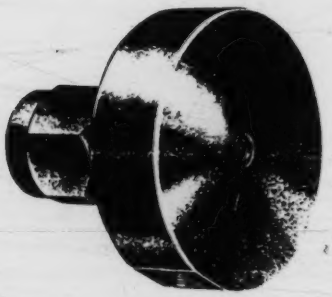

FEATURES

- 10db Bandwidth of 7.0 GHz
- Responsivity of 0.45 A/W
- 700 to 900 nm Response
- Rise Time of 50 ps
- Optical Mount
- Semi-Insulating Substrate

DESCRIPTION

The Ortel Corporation Model PD050-OM is a photodetector consisting of a very high speed, highly efficient GaAlAs/GaAs p-i-n photodiode mounted in a high speed package with an integral SMA type electrical connector. The photodiode has a typical rise time of 50 ps, 10dB bandwidth of greater than 7.0 GHz, and quantum efficiency of 65%. The Model PD050-OM also features extremely low capacitance and dark current.

The photodiode structure consists of a photosensitive GaAs layer, overlayed by a transparent GaAlAs window layer, grown on a semi-insulating substrate. The use of a semi-insulating GaAs substrate in the Model PD050-OM significantly reduces parasitic capacitance. The photodiode chip is passivated with a dielectric coating to assure high reby a sapphire window. An SMA-type connector is incorporated into the diode for ease in coupling to 50Ω systems.

The wavelength response of the Model PD050-OM (700-900 nm) is well matched to the output spectrum of GaAlAs lasers. To construct a high speed optical link with our photodiode, we recommend our semiconductor laser sources, Models LDM3-H or LDS3-H, which have transmission bandwidths in excess of 3.0 GHz, or LDS3-OMF, which has a transmission bandwidth in excess of 6.0 GHz.

The Model PD050-OM p-i-n photodiode is well suited to a variety of applications, including:

- Optical Communications
- Picosecond Pulse Detection

B.2. Data sheets for Ortel PD050-OM PIN photodiode.

ORTEL CORPORATION

MODEL PD050-OM PHOTODIODE

HIGH SPEED GaAlAs/GaAs PIN PHOTODIODE

ABSOLUTE MAXIMUM RATINGS

PARAMETER	SYMBOL	RATING	UNITS
Forward Current	I_F	10	mA
Reverse Voltage	V_R	25	V
Power Dissipation	P_T	100	mW
Operating Temperature	T_{op}	0 → + 70	°C
Storage Temperature	T_{st}	0 → + 70	°C

OPERATIONAL CHARACTERISTICS (@ 22°C)

PARAMETER	SYMBOL	MIN	TYP	MAX	UNITS
Dark Current[1]	I_D		200		pA
Capacitance[1]	C_J		1.0		pf
Quantum Efficiency[2]	η		65		%
Rise Time[3]	t_r		50		ps
Pulse Response (FWHM)[3]			100		ps
Recommended Operating Voltage	V_R	5	10-20	25	V
Responsivity[2]	R		0.45		A/W
Noise Equivalent Power[1]	NEP		2.1×10^{-14}		$W/\sqrt{Hz}$
Diameter of Photosensitive Area			50		μm

NOTES:
(1) V_R = 20 V
(2) λ = 840 nm
(3) V_R = 20 V; R_L = 50Ω

DIMENSIONAL DRAWING

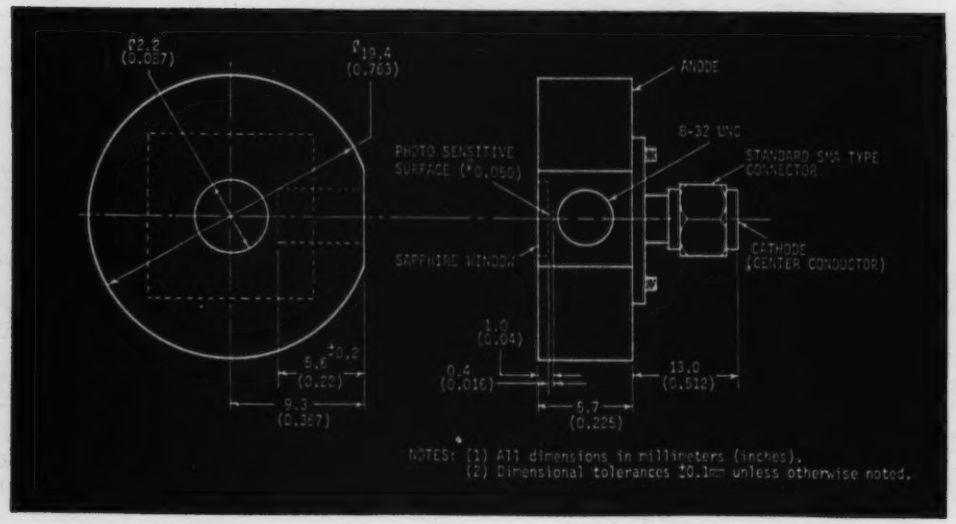

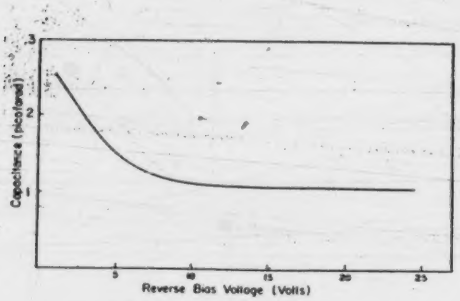

FIG. 1 Capacitance vs Reverse Voltage

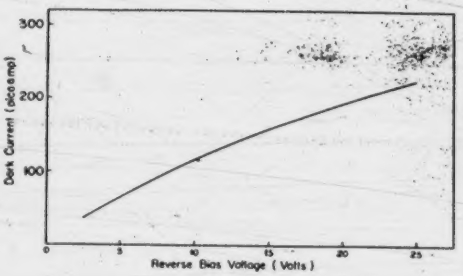

FIG. 2 Dark Current vs Reverse Voltage

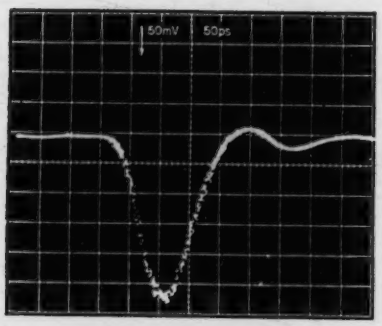

FIG. 3 Pulse Response

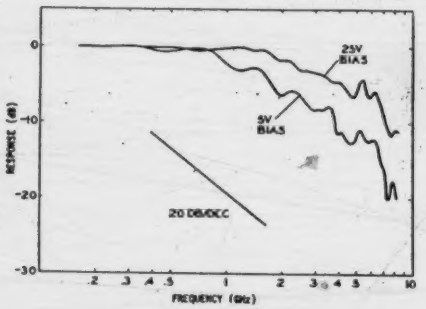

FIG. 4 Frequency Response

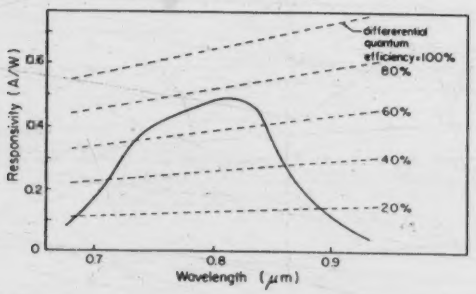

FIG. 5 Spectral Responsivity

ORTEL CORPORATION

MODEL PD050-OM PHOTODIODE

HIGH SPEED GaAlAs/GaAs PIN PHOTODIODE

OPERATING CONSIDERATIONS

The Model PD050-OM p-i-n photodiode can be operated in either an AC or DC coupled mode.

A circuit for AC coupling the Model PD050-OM is shown in Fig. 6. The DC and AC photocurrents are decoupled using a microwave bias-T. The amount of CW incident optical power can be determined by measuring the current along the DC bias path. The AC coupled signal appears at the rf output of the bias T.

A circuit for DC coupling the Model PD050-OM is shown in Fig. 7. A load must be present at the photodiode output to complete the DC bias path. The amount of CW incident optical power can be determined by measuring the current delivered by the bias supply. In the DC biasing mode, the case of the photodetector will be at the bias voltage, and should therefore be insulated.

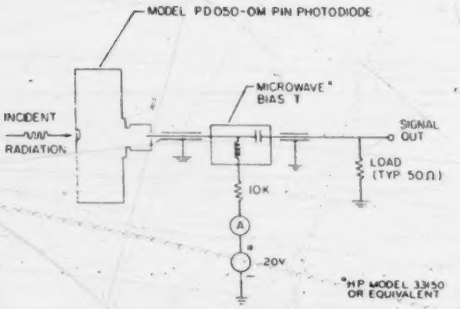

FIG. 6 AC Coupled Circuit

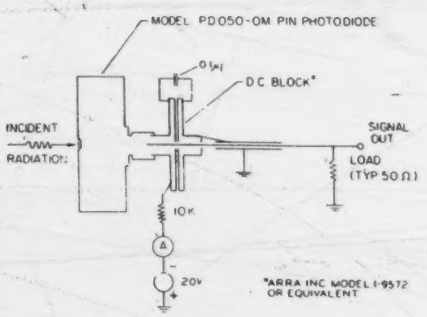

FIG. 7 DC Coupled Circuit

Information contained herein is deemed to be reliable and accurate. No responsibility is assumed for its use, nor for any infringement on the rights of others. Ortel Corporation reserves the right to change the design, specifications, etc., of the product at any time without notice.

ORTEL CORPORATION 2015 West Chestnut Street • Alhambra, CA 91803 • (213) 281-3636

LITHO IN U.S.A. 8309

LT015MD/MF

Features

- High output (maximum optical power output: 40 mW)
- Wavelength: 830nm
- Single transverse mode

Application

- Optical disk memories
- Medical apparatus
- Optical floppy disks
- Optical memory cards
- Light source for optical information processing

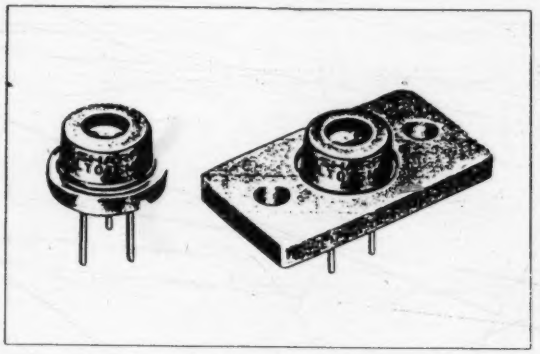

Absolute Maximum Ratings

(Tc=25°C)

Parameter		Symbol	Ratings	Units
Optical power output		Po	40	mW
Reverse voltage	Laser	V_R	2	V
	PIN		30	
Operating temperature *1		Topr	−10~+50	°C
Storage temperature *1		Tstg	−40~+85	°C
Soldering temperature *2		Tsol	260 (less than 5 seconds)	°C

*1 Case temperature *2 At point 1.6 mm from lead base

Electro-Opitical Characteristics *1

(Tc=25°C)

Parameter			Symbol	Condition	Ratings MIN.	Ratings TYP.	Ratings MAX.	Units
Threshold current			Ith	—	—	60	80	mA
Operating current			Iop_1	Po=30mW	—	95	130	mA
Operating voltage			Vop	Po=30mW	—	1.75	2.2	V
Wavelength *2			λp	Po=30mW	815	830	845	nm
Monitor current			Im	Po=30mW, V_R=15V	75	250	750	μA
Radiation characteristics	Angle *3	Parallel to junction	θ∥	Po=30mW	8	9.5	14	deg
		Perpendicular to junction	θ⊥	Po=30mW	20	27	38	deg
	Ripple			Po=30mW	—	—	±20	%
Emission point accuracy	Angle		Δφ∥	Po=30mW	—	—	±2	deg
			Δφ⊥	Po=30mW	—	—	±3	deg
	Position *4		Δx, Δy, Δz	—	—	—	±80	μm
Differential efficiency			η	20mW / I(30mW)−I(10mW)	0.5	0.8	1.1	mW/mA

*1 Initial value *3 Angle at 50% peak intensity (full width at half-maximum)
*2 Single transvevse mode *4 Not specified for LT015MF

Electrical Characteristics of Photodiode

(Tc=25°C)

Parameter	Symbol	Condition	Ratings MIN.	Ratings TYP.	Ratings MAX.	Units
Sensitivity	S	V_R=15V	—	8.3	—	μA/mW
Dark current	I_D	V_R=15V	—	—	150	nA
Terminal capacitance	Ct	V_R=15V	—	8	20	pF

B.3. Data sheets for Sharp LTO15MF laser.

Fig. 130 Forward Current vs. Forward Voltage

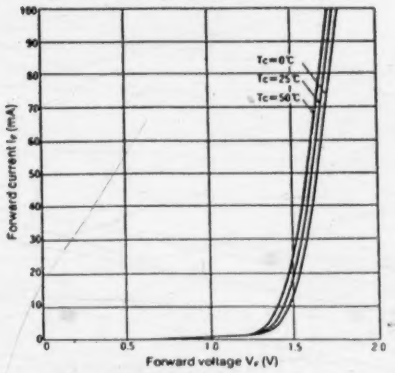

Fig. 131 Optical Power Output vs. Forward Current and Monitor Current

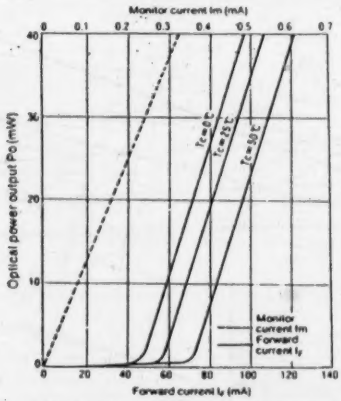

Fig. 132 Threshold Current vs. Temperature

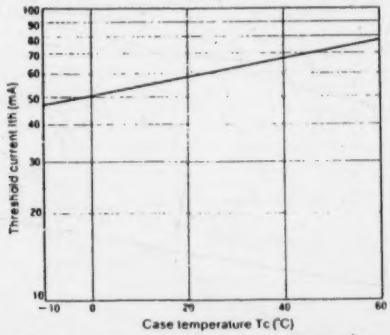

Fig. 133 Wavelength vs. Temperature

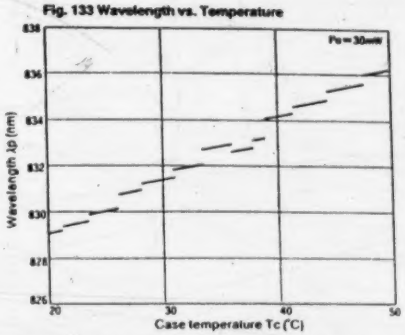

Fig. 134 Optical Power Output Dependence of Wavelength

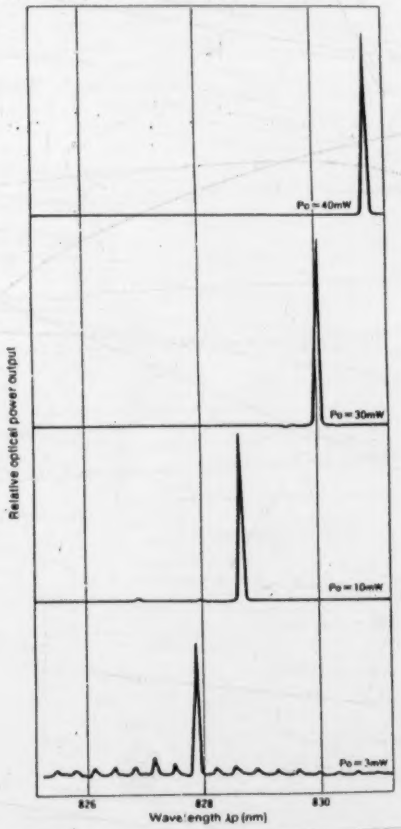

Note All data on this page is typical only, and is not intended as a specification. The shapes of these curves can be used as a general reference, but the actual characteristics will vary from device to device.

APPENDIX C

CIRCUIT DIAGRAMS

This appendix contains the circuit diagrams for each section of the laser transmitter and PIN receiver.

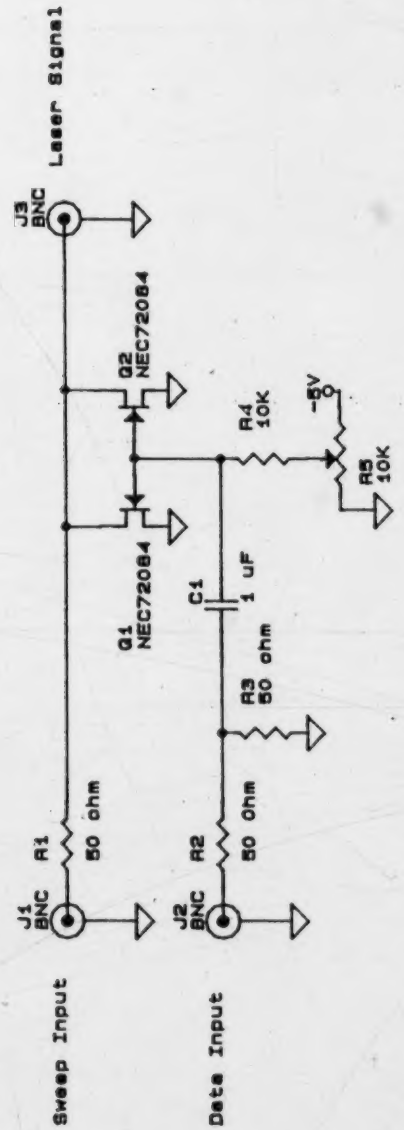

Figure C.1. FET Switch.

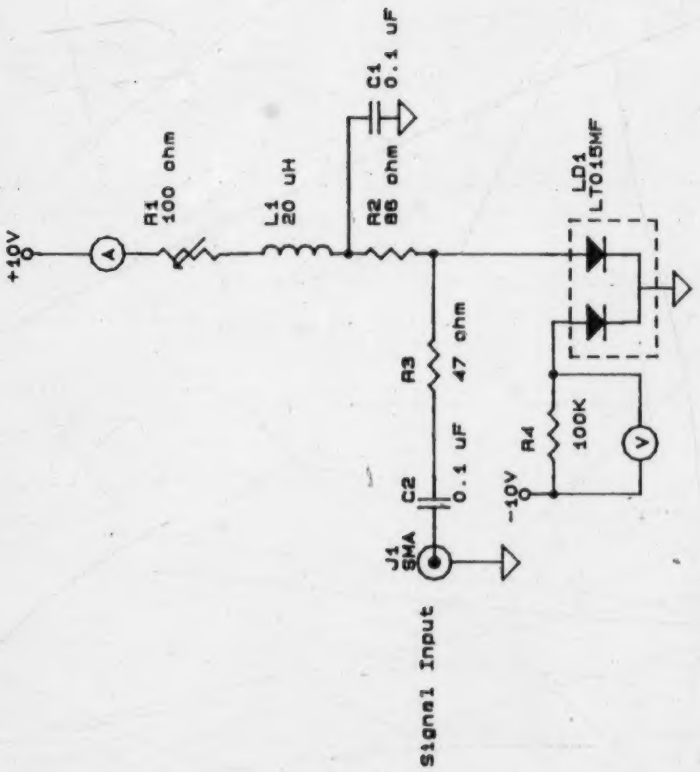

Figure C.2. Laser bias circuit.

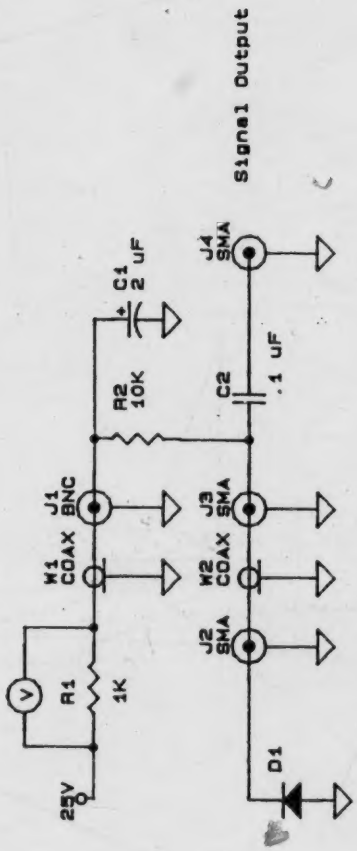

Figure C.3. PIN diode circuit.

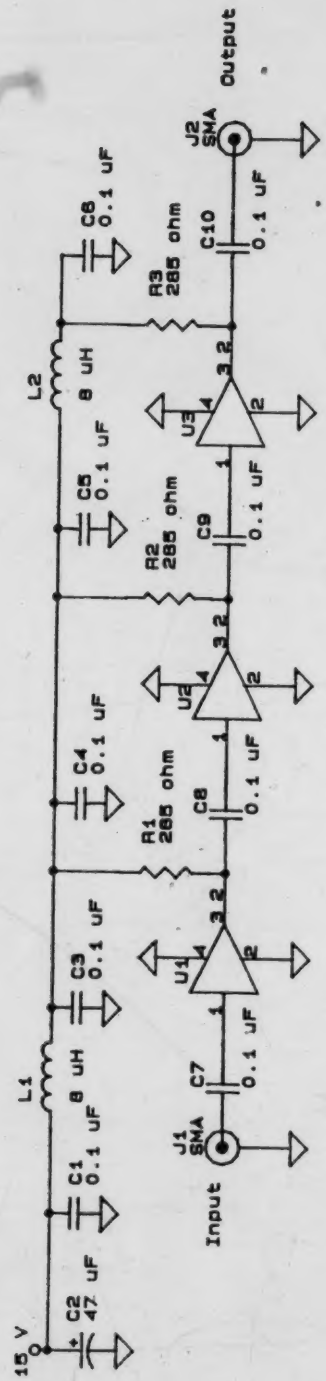

Amps U1, U2, U3 are Avantek MSA-0335

Figure C.1. Amp 4: Wideband amplifier.

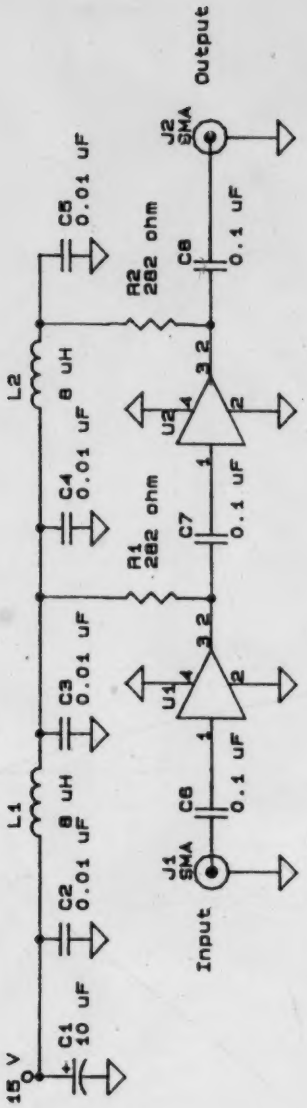

Amps U1, U2, are Avantek MSA-0335

Figure C.5. Amp 3: Wideband amplifier.

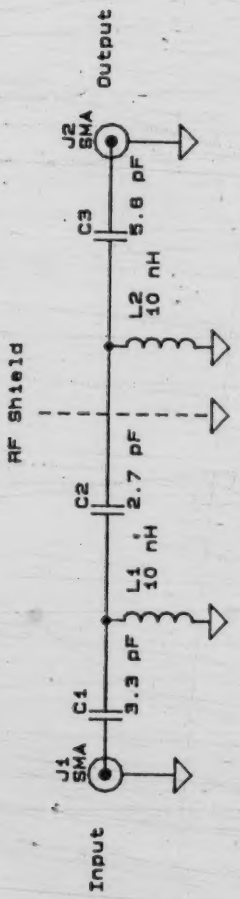

Figure C.8. HP2: high pass filter, 440 MHz cutoff.

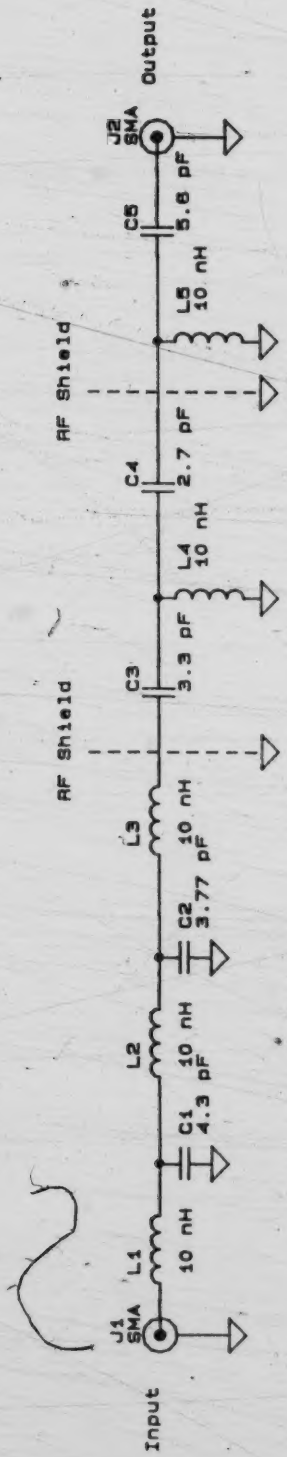

Figure C.7. BP1: bandpass filter.

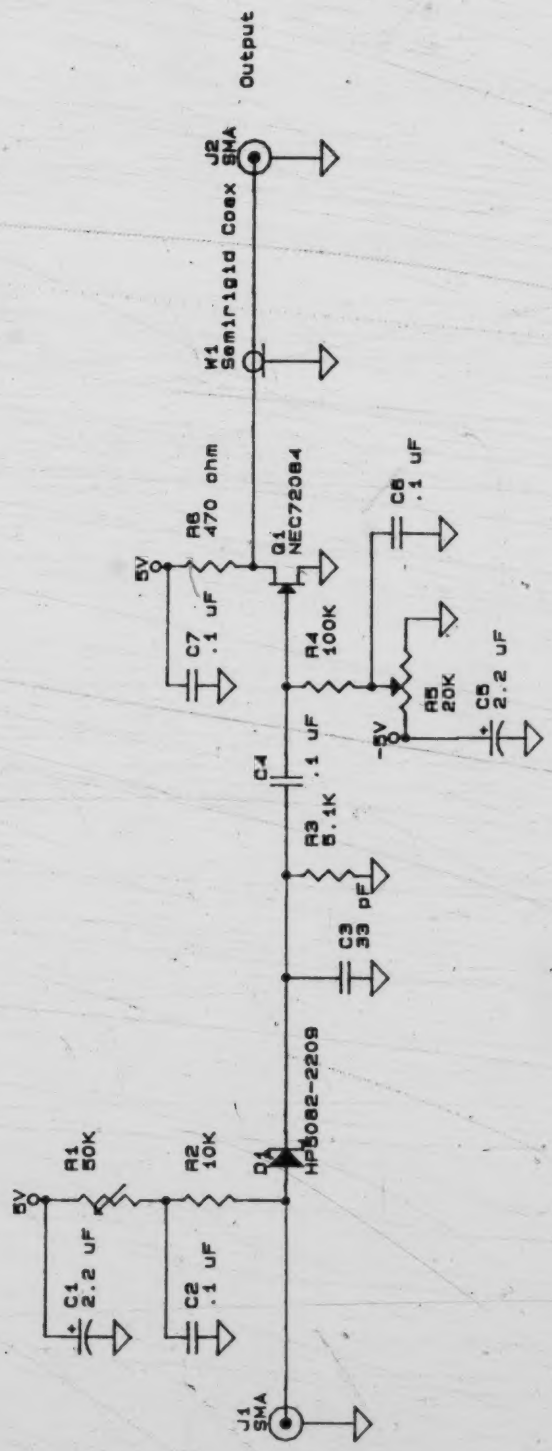

Figure C.8. Demodulator.

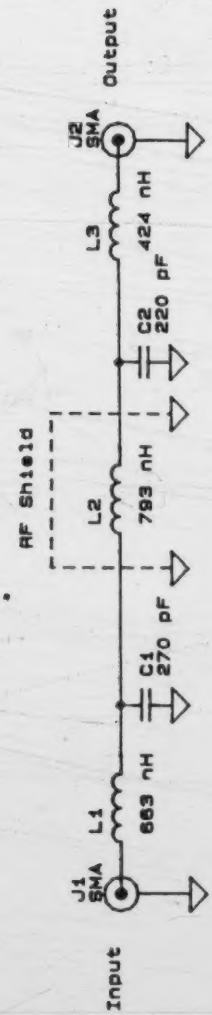

Figure C.9. LP1: lowpass filter, 17.5 MHz cutoff.

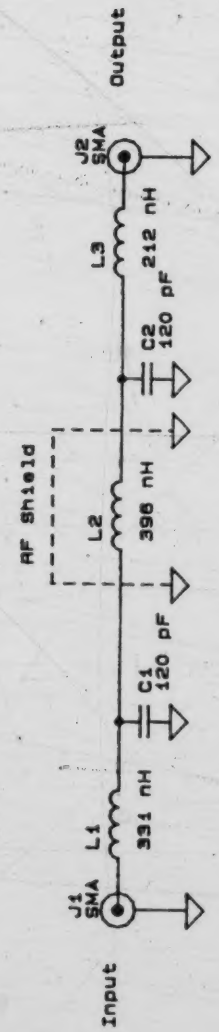

Figure C.10. LP2: lowpass filter, 40.9 MHz cutoff.

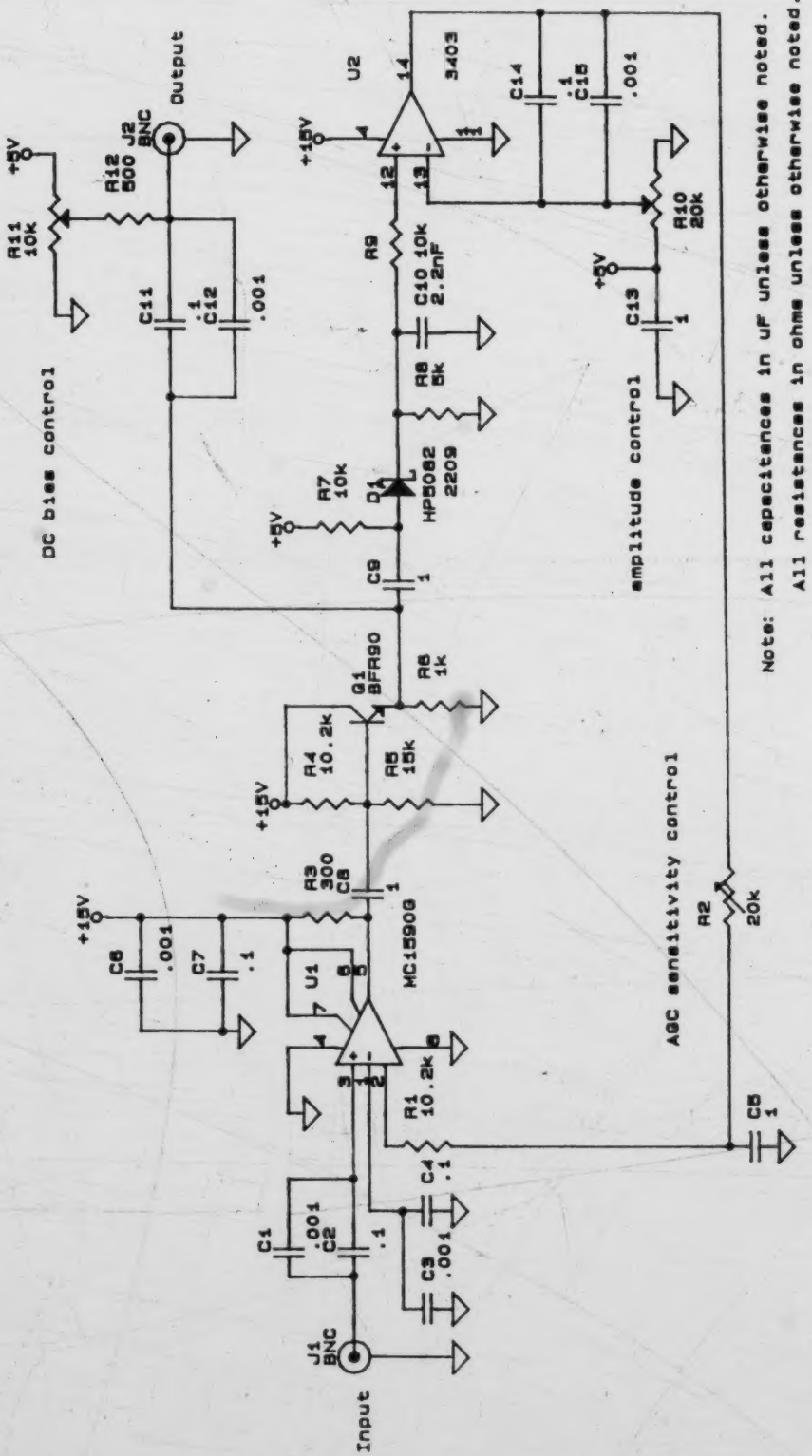

Note: All capacitances in uF unless otherwise noted.
All resistances in ohms unless otherwise noted.

Figure C.11. AGC amplifier.